NAVAL POSTGRADUATE SCHOOL
Monterey, California

DTIC
ELECTE
JUL 2 8 1993
S
A
D

THESIS

THEORETICAL STUDY OF LAMINAR FILM
CONDENSATION ON HORIZONTAL ELLIPTICAL TUBES
UNDER CONDITIONS OF FREE AND FORCED CONVECTION

by

Vance Hiro Adams

March 1993

Thesis Advisor: Paul J. Marto
Co-Advisor: Steven B. Memory

Approved for public release; distribution is unlimited

REPORT DOCUMENTATION PAGE

Public reporting burden for this collection of information is estimated to average 1 hour per response, including the time for reviewing instructions, searching existing data sources, gathering and maintaining the data needed, and completing and reviewing the collection of information. Send comments regarding this burden estimate or any other aspect of this collection of information, including suggestions for reducing this burden, to Washington Headquarters Services, Directorate for Information Operations and Reports, 1215 Jefferson Davis Highway, Suite 1204, Arlington, VA 22202-4302, and to the Office of Management and Budget, Paperwork Reduction Project (0704-0188), Washington, DC 20503.

1. AGENCY USE ONLY (Leave blank)	2. REPORT DATE	3. REPORT TYPE AND DATES COVERED
	March 1993	Master's Thesis March 1993

4. TITLE AND SUBTITLE

Theoretical Study of Laminar Film Condensation on Horizontal Elliptical Tubes Under Conditions of Free and Forced Convection

5. FUNDING NUMBERS

6. AUTHOR(S)

Vance Hiro Adams

7. PERFORMING ORGANIZATION NAME(S) AND ADDRESS(ES)

Naval Postgraduate School
Monterey, CA 93943-5000

8. PERFORMING ORGANIZATION REPORT NUMBER

9. SPONSORING / MONITORING AGENCY NAME(S) AND ADDRESS(ES)

Naval Postgraduate School
Monterey, CA 93943-5000

10. SPONSORING / MONITORING AGENCY REPORT NUMBER

11. SUPPLEMENTARY NOTES

The views expressed are those of the author and do not reflect the official policy or position of the Department of Defense or the U.S. Government

12a. DISTRIBUTION / AVAILABILITY STATEMENT

Approved for public release: distribution is unlimited

12b. DISTRIBUTION CODE

13. ABSTRACT (Maximum 200 words)

Analytical studies have been made of laminar film condensation on a horizontal elliptical cylinder in a pure saturated vapor under conditions of free and forced convection. Estimation of interfacial shear stress was made in two ways: the first involving an asymptotic value of the shear stress under conditions of infinite condensation rate and the second based on simultaneously solving the two-phase vapor boundary layer and condensate equations. The latter approach enables the determination of the vapor boundary layer separation point. For the assumption of asymptotic shear stress, effects of surface tension and pressure gradient in the condensate film have been included. At the extremes of eccentricity, corresponding to a circular tube and a vertical plate, the results are compared with theoretical and experimental work of others. Improvement in the condensation heat transfer coefficient was found for elliptical tubes under both free and forced convection conditions when compared to circular tubes of the same surface area. In the latter case, this improvement was due mainly to the reduced drag of the elliptical tube providing a higher vapor velocity for the same pressure drop as that across a circular tube.

14. SUBJECT TERMS

Laminar Film Condensation, Horizontal Elliptical Tube, Free and Forced Convection

15. NUMBER OF PAGES

124

16. PRICE CODE

17. SECURITY CLASSIFICATION OF REPORT	18. SECURITY CLASSIFICATION OF THIS PAGE	19. SECURITY CLASSIFICATION OF ABSTRACT	20. LIMITATION OF ABSTRACT
unclassified	unclassified	unclassified	SAR

Approved for public release, distribution unlimited

THEORETICAL STUDY OF LAMINAR FILM CONDENSATION ON HORIZONTAL ELLIPTICAL TUBES UNDER CONDITIONS OF FREE AND FORCED CONVECTION

by

Vance Hiro Adams
Lieutenant Commander, United States Navy
B.S., United States Naval Academy, 1978

Submitted in partial fulfillment of the
requirements for the degrees of
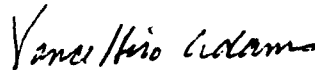
MASTER OF SCIENCE IN MECHANICAL ENGINEERING

and the degree of
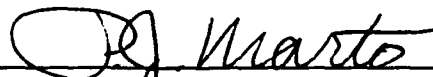
MECHANICAL ENGINEER

from the

NAVAL POSTGRADUATE SCHOOL
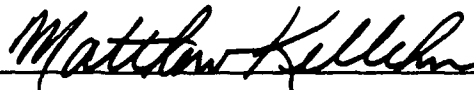March 1993

Author: _____

Vance Hiro Adams

Approved By: _____

Paul J. Marto, Thesis Advisor

_____

Stephen B. Memory, Thesis Co-Advisor

_____

Matthew D. Kelleher, Chairman
Department of Mechanical Engineering

_____

Richard S. Elster, Dean of Instruction

ii

ABSTRACT

Analytical studies have been made of laminar film condensation on a horizontal elliptical cylinder in a pure saturated vapor under conditions of free and forced convection. Estimation of interfacial shear stress was made in two ways: the first involving an asymptotic value of the shear stress under conditions of infinite condensation rate and the second based on simultaneously solving the two-phase vapor boundary layer and condensate equations. The latter approach enables the determination of the vapor boundary layer separation point. For the assumption of asymptotic shear stress, effects of surface tension and pressure gradient in the condensate film have also been included. At the extremes of eccentricity, corresponding to a circular tube and a vertical flat plate, the results are compared with theoretical and experimental work of others. Improvement in the condensation heat transfer coefficient was found for elliptical tubes under both free and forced convection conditions when compared to circular tubes of the same surface area. In the latter case, this improvement was due mainly to the reduced drag of the elliptical tube providing a higher vapor velocity for the same pressure drop as that across a circular tube.

Accesion For		
NTIS CRA&I		☑
DTIC TAB		☐
Unannounced		☐
Justification		
By		
Distribution /		
Availability Codes		
Dist	Avail and / or Special	
A-1		

TABLE OF CONTENTS

LIST OF FIGURES

NOMENCLATURE

a	semi-major axis dimension
A_C	tube cross-sectional area
b	semi-minor axis dimension
B_1	as defined by Equation (II-35)
B_2	as defined by Equation (II-52)
Bo	Bond number $(\rho_l g D_e^2 / \sigma)$
D_e	effective diameter defined by Equation (II-16)
$f(\kappa, \kappa_1)$	shear function defined by Equation (II-104)
F	dimensionless parameter defined by Equation (II-64)
$f_1(\phi)$	gravity function defined by Equation (II-21)
$f_2(\phi)$	potential velocity function defined by Equation (II-47)
$f_3(\phi)$	pressure gradient function defined by Equation (II-76)
$f_4(\phi)$	surface tension function defined by Equation (II-80)
g	gravitational constant
G	dimensionless parameter defined by Equation (II-111)
$H(\kappa, \kappa_1)$	shape function defined by Equation (II-104)
h_{fg}	latent heat of evaporation
k	elliptical tube eccentricity (b/a)
m	condensate mass flux rate
Nu	Nusselt number $(\alpha D_e / \lambda_l)$
p	fluid pressure
p_ϕ	fluid pressure due to potential flow
p_σ	fluid pressure due to surface tension
P	dimensionless parameter defined by Equation (II-85)
r	radial dimension, cylindical coordinate system

$R(\phi)$	radius of curvature
$\widetilde{Re}$	two-phase Reynolds number $(\rho_l U_\infty D_e / \eta_l)$
Re_v	vapor Reynolds number $(\rho_v U_\infty D_e / \eta_v)$
T_{wall}	tube wall temperature
T_{sat}	vapor saturation temperature
u	condensate film streamwise velocity
U	vapor boundary-layer streamwise velocity
u_m	mean condensate film streamwise velocity
U_ϕ	vapor potential velocity outside boundary-layer
$\bar{U}_\phi$	dimensionless vapor potential velocity defined by Equation (II-108)
U_∞	vapor free-stream velocity
v	condensate film normal velocity
V	vapor boundary-layer normal velocity
V_δ	vapor interfacial normal velocity
$\bar{V}_\delta$	dimensionless vapor interfacial velocity defined by Equation (II-108)
x	streamwise length dimension, curvilinear coordinate system
x_1	coordinate, cartesian coordinate system
$x^\bullet$	dimensionless streamwise length defined by Equation (II-17)
$x_S^\bullet$	dimensionless streamwise vapor boundary-layer separation location
y	normal length dimension, curvilinear coordinate system
y_1	coordinate, cartesian coordinate system
Z	dimensionless parameter defined by Equation (II-105)
Z_1	dimensionless parameter defined by Equation (II-34)
Z_2	dimensionless parameter defined by Equation (II-51)
α	heat transfer coefficient
Δ	vapor boundary-layer thickness

Δ_1	vapor boundary-layer displacement thickness
Δ_2	vapor boundary-layer momentum thickness
δ	condensate film thickness
δ^*	dimensionless condensate film thickness defined by Equation (II-64)
η	dynamic viscosity
θ	angular coordinate, cylindrical coordinate system
κ	pressure gradient parameter defined by Equation (II-103)
κ_1	suction parameter defined by Equation (II-103)
κ_A	parameter defined by Equation (II-118)
λ	thermal conductivity
ρ	fluid mass density
σ	fluid surface tension
τ	fluid shear stress
τ_δ	condensate/vapor interfacial shear stress
$\bar{\tau}_\delta$	dimensionless interfacial shear stress defined by Equation (II-119,120)
ϕ	parametric angle
$\chi(\phi)$	parametric radius defined by Equation (II-15)

SUBSCRIPTS

δ	vapor/condensate interface
l	condensate
v	vapor

ACKNOWLEDGEMENTS

I. INTRODUCTION

A. MOTIVATION FOR INVESTIGATION OF ELLIPTICAL TUBES

For many years, condenser design in the United States has been based on the Heat Exchange Institute (H.E.I.) or Tubular Exchange Manufacturers Association (T.E.M.A.) standards [1,2] which rely on tube-side empirical relations and averaged data to predict heat transfer parameters. Since there is a large degree of uncertainty in the accuracy of the prediction, the condensers are over designed to ensure sufficient margin of reliability. The result is an excessively large, expensive condenser for the desired thermal duty rating requirements. The majority of condensers currently used in the Navy were designed under these standards.

Within the last two decades, computer modeling has been used to more accurately predict the heat-transfer coefficients of condensers. There are two basic approaches to computer modelling, an integrated and a differential approach, of which the former is most commonly used in condenser design (Walker [3]). Integrated approaches divide the condenser into zones with associated mean heat transfer and fluid properties which are typically determined from semi-empirical relations. These zones are integrated over the whole condenser and provide overall performance predictions with respect to shell side pressure drop and duty rating. Though easy to use, integrated methods are restrictive when used in conditions which are outside of the fluid parameter and geometry constraints of the empirical relations employed in the approach. Differential approaches solve the basic equations of fluid mechanics and heat transfer and provide an understanding of local variations within the condenser, but are too complex for use in condenser design. The improvements in accuracy as a rsult of computer design

1

methods are a function of the empirical or theoretical models used in their development. Marto [4] provides a comprehensive overview of the state of computer design methods.

The purpose of empirical and theoretical research into condenser performance is to more accurately predict condenser characteristics such that the designer can develop reliable, smaller, and hence less costly condensers which meet the same thermal duty requirements. Analyses of single tubes allow isolation of individual factors which affect condensation without the complexities which result from vapor flow over tube bundles or condensate inundation. Since the pioneering work of Nusselt [5], a significant amount of theoretical work has been done analyzing laminar film condensation on horizontal circular tubes (see Rose [6]), the results of which have greatly contributed to the ability to reasonably predict single tube heat transfer performance.

Over the last two decades, major effort has been expended to study effects which enhance laminar film condensation heat transfer over that obtained from a plain circular tube. The majority of these techniques have focussed on controlling the thickness of the condensate film as this is the major resistance to heat transfer. The condensate film thickness generally increases with streamwise distance from the top of the tube and is dependent on both the rate of condensation and the interfacial shear between the vapor boundary-layer and condensate film. Additionally, at high vapor velocities, vapor boundary-layer separation occurs which results in a rapid thickening of the condensate film downstream of the separation point. Enhancement techniques include, but are not limited to, extended surfaces (fins), profiled tube surfaces (roped or corrugated tubes), and non-circular tube geometries. Marto [7], Bergles et al. [8] and Webb [9] provide comprehensive reviews on such enhancement techniques. These techniques enhance heat transfer through an increase in surface area to volume ratio and/or the use of surface tension to thin the condensate film.

2

Non-circular geometries contribute to a thinning of the condensate film by placing more of the surface in line with the direction of gravity; thus, making the average streamwise gravity component in the momentum balance of the condensate film larger than that obtained from a circular geometry. Dhir and Lienhard [10] applied a simple Nusselt type analysis to an arbitrary plane or axisymmetric body in which the streamwise gravity component varied with streamwise length. The results of this analysis gave expressions for condensate film thickness and Nusselt number which were identical to those derived by Nusselt except that the gravitational constant, g, is replaced by an effective constant, g_{eff}, which is defined by

$$g_{eff} = \frac{x \, (g \, R)^{4/3}}{\int_0^x g^{1/3} R^{4/3} dx} \tag{I-1}$$

where x is the streamwise distance from the leading edge of the surface and R is the radius of curvature of the axisymmetric body. These expressions can only be applied to systems for which curvilinear coordinates are applicable, i.e., for bodies in which the radii of curvature are much greater than the film thickness.

Shklover and co-workers [11,12] analyzed a horizontal cylinder with a logarithmic spiral type of surface curvature (see Figure I-1) such that more of the body surface is aligned in the direction of gravity and the radius of curvature is continuously increasing along the streamwise direction. They manufactured this tube by "mechanical deformation of a circular tube." The effect of this profile was to increase the streamwise effective gravity component over that found for a circular cylinders and to utilize surface tension effects on the pressure gradient to increase the mean film velocity, $u(x,y)$, in the streamwise direction. Their analysis considered viscous, gravity and surface tension forces in the momentum balance of the condensate film and neglected vapor shear at the condensate/vapor interface. These effects resulted in a

3
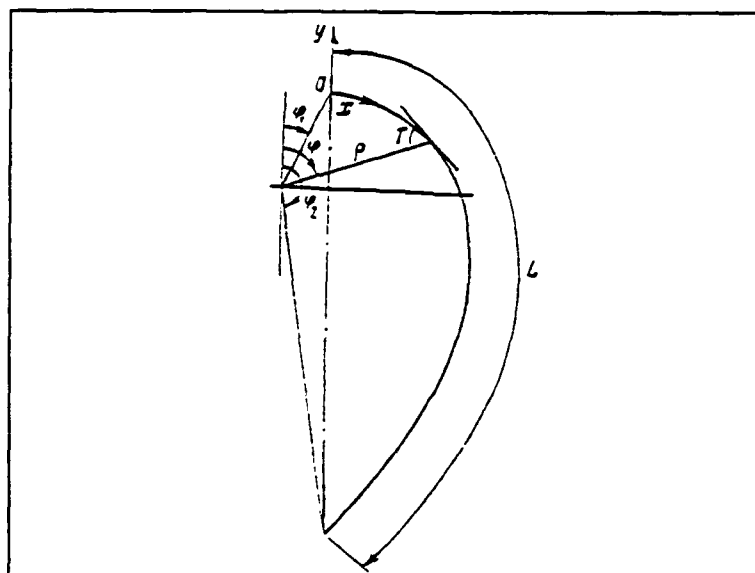
Figure I-1. Logarithmic Spiral Tube from Reference [12].

thinning of the condensate film and an increase of 20-30% in the overall heat-transfer coefficient when compared to a circular tube of the same surface area. These results agreed with experimental data. In analyzing the individual effects of gravity and surface tension, it was determined that surface tension was most significant over the top portion of the tube where dR/dx is largest and accounted for 10-15% of this increase.

An elliptical tube with major axis aligned with the direction of gravity has a larger effective gravity than a circular cylinder, as well as an increasing radius of curvature over the top half of the tube. In addition, they are more practical from a manufacturing standpoint than the non-circular tubes analyzed above. Vapor boundary-layer separation should also occur at a point further downstream as compared to a circular tube and thus the rapid thickening of the condensate film would be delayed. Methods of manufacturing elliptical tubes, and associated problems will be discussed in Chapters IV and VI.

4

Wallis [13] conducted flow visualizations (Figure I-2)of water around circular and elliptical tube bundles. These photographs provide a qualitative feel for the flow
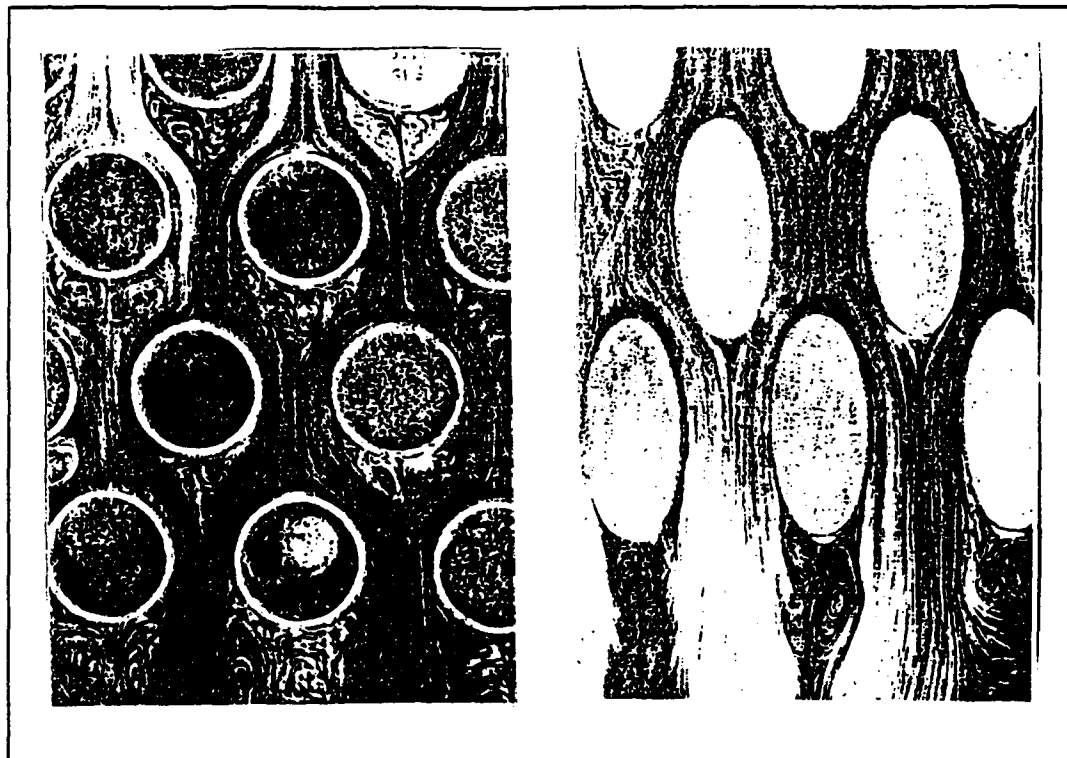
Figure I-2. Flow Visualization, Water over Circular and Elliptical Tube Banks, from Reference [13].

characteristics around each type of tube bundle. In examining the photographs, it can be concluded that the separation point for the elliptical tube bank shifts downstream compared to the circular tube bank and results in smaller wake regions behind individual tubes. These effects should contribute to better heat transfer performance for the elliptical tube bank. Experimental studies by Joyner and Palmer [14] show that single phase flow resistance and pressure drop are significantly smaller for elliptical tube bundles as compared to circular tube bundles. In power condensers, shell-side (vapor) pressure drop has an effect on the overall efficiency of the power plant and on the thermal driving force for condensation $(T_{sat} - T_{wall})$. Minimizing the vapor pressure drop improves power plant efficiency and maintains a relatively constant T_{sat} (for a

large pressure drop, T_{sat} is reduced as vapor flows through the condenser resulting in less thermal driving force).

Studies involving single-phase heat exchangers and condenser-evaporators indicate that elliptical tube heat transfer performance is superior to a circular tube of comparable surface area. Ota and Nishiyama [15] conducted an experimental investigation of single phase forced convection heat transfer of air over an elliptical cylinder of minor-to-major axis ratio of 1:3 at various angles of attack. They concluded that elliptical cylinders gave improved heat transfer performance over circular cylinders at all angles of attack (as a result of fluid turbulence) in the range of Reynolds numbers studied (8000 - 79000). Moalem and Sideman [16] conducted a theoretical analysis of a horizontal elliptical tube in a condenser-evaporator used in desalinization plants. Their study showed a 10-20% enhancement for elliptical tubes as compared to circular tubes with the maximum enhancement achieved at a minor-to-major axis ratio (aspect ratio) of 1:4 where the major axis is aligned with the vertical. Huang and Mayinger [17] conducted an experimental free convection heat transfer study around elliptical tubes and found optimum improvement in heat exchanger performance for tubes with major axis aligned vertically and with an aspect ratio of 1:2. Merker and Bähr [18] used an analogy between momentum and heat transport to derive a semi-empirical relation from which to determine mass transfer rate from the fluid boundary-layer into the free stream. The results of their study showed improved heat transfer performance for heat exchangers in which the elliptical tubes were spaced wider in the longitudinal direction and more compact in the transverse direction. In all these studies it appears that an elliptical geometry improves the heat transfer performance of a heat exchanger.

B. SIGNIFICANT THEORETICAL STUDIES ON HORIZONTAL CIRCULAR TUBES

The purpose of this survey is to provide a historical perspective to the understanding of laminar film condensation on a horizontal circular cylinder. Only those works which have made significant advances in this understanding are considered. The methods of some of these analyses will later be applied to formulate and solve the governing equations for the case of the horizontal elliptical cylinder. Figure I-3 provides the geometrical layout and coordinate systems used in these analyses.
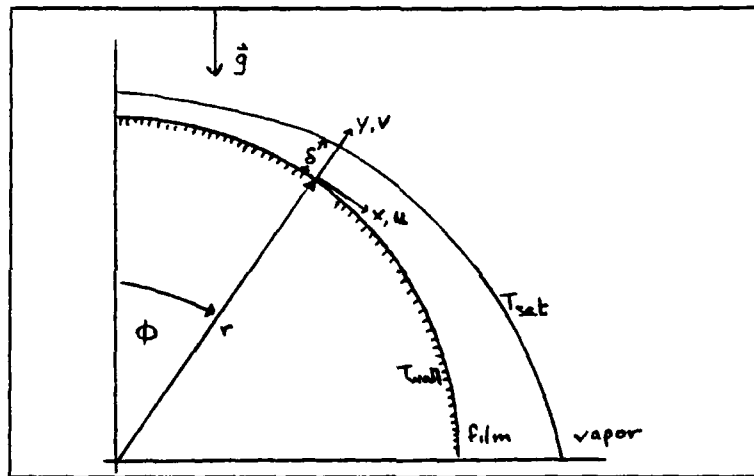
Figure I-3. Geometry for Film Condensation on a Horizontal Circular Cylinder.

Nusselt [5] used a simple momentum and energy balance to determine the heat transfer properties for condensation on flat plates and horizontal circular cylinders. In simplifying these physical laws for solution, he made the following assumptions:

(1) The tube wall temperature is constant.
(2) The thermophysical properties of the fluid are constant.
(3) The temperature at the film/vapor interface is T_{sat}.
(4) The condensate film thickness is small compared to the radius of the tube.
(5) Heat transfer in the condensate film is one dimensional in the radial direction which implies a linear temperature distribution when the film is very thin. Convection in the condensate film is neglected.
(6) The only forces acting on the condensate element are due to viscosity and gravity. Inertial forces are neglected.

7

(7) Flow in the condensate film is laminar.

(8) The vapor is quiescent with no interfacial shear.

The governing equations for this system become

$$\eta_l \frac{d^2 u}{dx^2} + \rho_l \, g \, \sin\phi = 0$$

$$m \, h_{fg} = \frac{\lambda_l}{\delta}(T_{sat} - T_{wall})$$

(I-2)

where m is the condensate mass flux rate across the interface. The mean heat transfer is given by

$$\bar{\alpha}_{Nu} = 0.943 \left[\frac{\lambda_l^3 \, g \, h_{fg} \, \rho_l^2 \, \sin\phi}{\eta_l \, L \, \Delta T} \right]^{1/4}$$

(I-3a)

for a flat plate at angle ϕ to the horizontal (not valid at $\phi = 0$) and

$$\bar{\alpha}_{Nu} = 0.728 \left[\frac{\lambda_l^3 \, g \cdot h_{fg} \, \rho_l^2}{\eta_l \, D \, \Delta T} \right]^{1/4}$$

(I-3b)

for a horizontal circular cylinder.

Sparrow and Gregg [19,20] extended the Nusselt [5] analysis by applying boundary layer theory to the condensate film. This study incorporated convection and inertia in the energy and momentum balance while continuing to neglect interfacial shear. They determined that for practical engineering fluids, inertia and convection had negligible effect.

Shekriladze and Gomelauri [21] included interfacial shear by considering momentum transfer across the interface due to the condensation process. They used an asymptotic expression for the interfacial shear based on an infinite condensation rate given by

$$\tau_\delta = m(U_\phi - u_\delta)$$

(I-4)

where U_ϕ is the streamwise velocity of the vapor at the outer edge of the boundary-layer. It was also assumed that $U_\phi \gg u_\delta$ such that the film velocity may be neglected and

that inertia and convection effects in the condensate film could also be neglected. As noted by Rose [6], the validity of neglecting u_δ requires that $\lambda_l \Delta T / \eta_l h_{fg}$ be small (large Prandtl number). For forced convection heat transfer on a horizontal circular tube, Shekriladze and Gomelauri determined the following expression:

$$\bar{Nu} = 0.9\sqrt{\bar{Re}} \tag{I-5}$$

where

$$\bar{Re} = \frac{\rho_l \, U_\infty \, D}{\eta_l} \tag{I-6}$$

is the two-phase Reynolds number. When the effect of gravity cannot be neglected (mixed convection) the mean heat-transfer coefficient is given by

$$\bar{Nu} = 0.64\sqrt{\bar{Re}}\sqrt{1 + \sqrt{1 + 1.69 \, F}} \tag{I-7}$$

where

$$F = \frac{\eta_l \, h_{fg} \, g \, D}{\lambda_l \, \Delta T \, U_\infty^2} \tag{I-8}$$

and measures the relative effects of vapor velocity and gravity. It should be noted that based on potential flow outside the vapor boundary layer, the interfacial shear will always be positive and therefore this method does not predict vapor separation as would occur in reality. Based on a minimum separation angle of 82° for single phase flow over a circular cylinder without suction and no heat transfer after separation, Shekriladze and Gomelauri conservatively estimated that the heat-transfer coefficient would be reduced by about 35%. Actual separation occurs at a point further downstream and results in a heat-transfer coefficient between the result for separation at 82° and no separation. These expressions have been found to be reasonably accurate for cases of high condensation rate and are useful for their simplicity.

Fujii et al. [22] conducted an analysis of mixed convection condensation on horizontal cylinders using the two-phase boundary-layer equations. Their formulation

9

neglected inertia, convection and pressure gradient effects in the condensate film. The governing equations for the model are given by

$$\frac{\partial U}{\partial x} + \frac{\partial V}{\partial y} = 0$$

$$U\frac{\partial U}{\partial x} + V\frac{\partial U}{\partial y} = U_\phi \frac{dU_\phi}{dx} + \frac{\eta_v}{\rho_v}\frac{\partial^2 U}{\partial y^2}$$

(I-9a)

for the vapor boundary-layer and

$$\frac{\partial u}{\partial x} + \frac{\partial v}{\partial y} = 0$$

$$0 = \eta_l \frac{\partial^2 u}{\partial y^2} + \rho_l \, g \, \sin\phi$$

(I-9b)

$$m = \rho_l \frac{d}{dx}\int_0^\delta u\,dy = \frac{\lambda_l \Delta T}{\delta \, h_{fg}}$$

for the condensate film. The compatibility equations at the interface are given by

$$U_\delta = 0$$

$$\eta_l \left(\frac{\partial u}{\partial y}\right)_{y=\delta} = \eta_v \left(\frac{\partial U}{\partial y}\right)_{y=\delta} = \tau_\delta$$

(I-9c)

$$\rho_l \left(u\frac{\partial \delta}{\partial x} - v\right)_{y=\delta} = -\rho_v V_{y=\delta}$$

An approximate integral solution of the momentum equation for flow over a cylinder, with suction by Truckenbrodt [23], was modified to more closely agree with the numerical solutions of Terril [24]. This method enabled the determination of the interfacial shear and subsequent solution of the governing equations for the condensate film. This technique also predicted the point of vapor separation and subsequently, a more accurate heat-transfer coefficient. For locations downstream of the vapor boundary-layer separation point, the interfacial shear was assumed to be negligible and simple Nusselt theory used to determine the heat transfer. Local and mean Nusselt numbers were numerically determined for boundary conditions of uniform wall temperature and uniform wall heat flux. Their results were in fair agreement with

10

with experimental data. In addition to the dimensionless parameter, F, a new dimensionless parameter, G, was defined as

$$G = \frac{\Delta T \, \lambda_l}{\eta_l \, h_{fg}} \sqrt{\frac{\rho_l \, \eta_l}{\rho_v \, \eta_v}} \tag{I-10}$$

which is a measure of the condensation rate. As $G \to \infty$, the results of Fujii et al. [22] agreed with the previous results of Shekriladze and Gomelauri [21]. Lee and Rose [25] noted an error in the formulation of Fujii et al. [22] in that the interfacial shear terms in the condensate film momentum equation should have been divided by 2. They re-analyzed the system of equations using both the modified and unmodified method of Truckenbrodt [23] and found little difference whether one used the modified or unmodified method of Truckenbrodt.

To date, Gaddis [26] has conducted the most comprehensive study of condensation on horizontal circular tubes using the two-phase boundary-layer equations. His analysis neglected surface tension in the momentum equation as well as viscous dissipation and pressure in the energy equation of the condensate film. He determined that inertia effects were negligible for most media (with the exception of liquid metals) and that convection effects were somewhat significant for viscous liquids with $Pr \gg 1$, similar to the conclusions of the simpler analyses of Sparrow and Gregg [19, 20]. He identified three regimes of behavior for flowing vapors. For low vapor Reynolds numbers, Re_v, gravity effects dominate the heat transfer and Nusselt's analysis adequately represents the heat transfer behavior. For high Re_v, condensation was shear controlled and the Nusselt number is proportional to the square root of Re_v as found by Shekriladze and Gomelauri [21]. The intermediate region, in which gravity and vapor shear are both significant, results in no simple relation. Gaddis also analyzed several cases of flow separation (vapor boundary-layer and/or condensate film separation). For low Re_v ($\approx$

11

10^2), vapor boundary-layer separation occurred with no flow reversal in the liquid film. This result is expected as the pressure gradient effect on the condensate film, which tends to slow the condensate flow over the rear half of the tube, is a function of the vapor potential velocity. At moderate Re_v ($\approx 10^3$) vapor boundary-layer separation and condensate flow reversal near the interface occurred with a resulting decrease in the mean fluid velocity and rapid thickening of the condensate film. At high Re_v ($\approx 10^5$), no vapor boundary-layer separation occurred but the condensate film separated at the wall causing a sharp reduction in mean condensate velocity with a rapid thickening of the film as a result of a significant, adverse pressure gradient. Fluid separation at their respective boundaries is defined as the condition at which the shear is less than or equal to zero.

diMarzo and Casarella [27] conducted a similar analysis using a more general solution technique and arrived at the same results as Gaddis [26]. In their analysis of the flow separation phenomenon, they provided guidance on determining heat transfer performance once separation had occurred. At low Re_v, gravity effects dominate and no flow reversals or thickening of the condensate film occurred. The use of a Nusselt type analysis with no interfacial shear would seem prudent in the region beyond vapor separation. At moderate to large Re_v, pressure gradient effects dominate. The adverse pressure gradient over the back half of the tube causes flow reversal and a rapid thickening of the condensate film. In this case, it would be prudent to neglect heat transfer completely beyond the separation point of the vapor-boundary layer or condensate film.

Rose [28] studied the effects of pressure gradient in the condensate film. In this case, the pressure gradient on the condensate film is due to the pressure gradient of the vapor, as determined by potential theory, which is impressed on the condensate film.

He simplified the analysis by using the Shekriladze-Gomelauri model [21] which ignores inertia and convection in the condensate film and uses the asymptotic expression for the interfacial shear. As a result of this analysis, a dimensionless parameter, P, was defined by

$$P = \frac{\rho_v \, h_{fg} \, \eta_l}{\rho_l \, \lambda_i \, \Delta T} \qquad (I-11)$$

which represents the pressure gradient effect (Gaddis [26] had a similar combination of dimensionless parameters which were equivalent to P). When $P = 0$, the governing equations reduce to those of Shekriladze and Gomelauri [21]. He concluded that the effect of including pressure gradient was to improve heat transfer over the forward half of the tube since the pressure gradient over this region is favorable (tends to increase the mean film velocity which reduces the condensate film thickness). As a result of the formulation, he found that for cases where $P > F/8$, a critical angle at some point on the rear of the tube was reached where $d\delta^*/d\phi \to \infty$. In this case, it was not possible to obtain a solution over the entire tube. It was postulated that this critical angle might indicate some instability followed by some degree of waviness or turbulence. It was noted that this critical point was reached prior to the point at which the condensate film separated. For conditions which permitted solution over the entire tube (i.e. $P < F/8$), any increase in heat transfer achieved over the forward part of the tube was balanced by a decrease in heat transfer as a result of the adverse pressure gradient over the back half of the tube such that there was little change in the mean heat-transfer coefficient. Since the pressure gradient due to potential flow of vapor just outside the vapor boundary-layer is given by

$$\frac{dP}{dx} = -\rho_v U_\phi \frac{dU_\phi}{dx} \qquad (I-12)$$

13

which is symmetric around the surface of the tube from front to back, the favorable effect over the front half of the tube is exactly offset by the adverse effect over the back half of the tube. Referring to the studies conducted by Gaddis [26] and diMarzo-Casarella [27], in the region of moderate Re_v, condensate film separation from the tube wall does not occur but the pressure gradient sufficiently retards the film such that flow reversals occur and the film still rapidly thickens. In the present study, the effects of pressure gradient using the analysis of Rose [28] resulted in a condensate velocity distribution which approached zero as the critical angle was reached. This phenomenon may be a result of the model used in formulating the problem. Since Shekriladze and Gomelauri [21] used an asymptotic expression for the interfacial shear, negative velocities cannot exist in the velocity profile. The positive velocity distribution is retarded by the adverse pressure gradient. In the case of $P > F / 8$, the pressure gradient is large enough to cause complete stoppage of film flow at ϕ_c and the film thickness increases rapidly.

Krupiczka [29] examined the effects of surface tension due to film curvature on condensation on circular cylinders. He used a simple Nusselt type model but included surface tension in the momentum equation. In his development he did not assume the film thickness was much less than the radius of the cylinder until after the inclusion of the surface tension term to account for the curvature of the film. The resulting equation was a second order ordinary differential equation which required two initial conditions. The first condition was given by the symmetry of the problem. However, the initial thickness was not obvious and was arbitrarily chosen to be that obtained from the Nusselt model. He concluded that the effect of surface tension was small on the forward part of the tube and increases in significance over the back part of the tube due to the rapidly changing film thickness. This significance was dependent on the

14

magnitude of dimensionless parameter, A, given by

$$A = \frac{1}{4} We \left[\frac{3\eta_l^2 Ja}{\rho_l^2 \, g \, r^3 \, Pr} \right]^{1/4} \qquad (I\text{-}13)$$

which is dependent on the surface tension of the fluid through a "modified" Weber number ($We = \sigma/(\rho g r^2)$) and the radius of the cylinder, r. The conclusion was that surface tension can be significant for small diameter tubes and wires where, as r becomes smaller, the film thickness becomes relatively significant and hence the film curvature cannot be neglected. For most practical cases, $r \gg \delta$ and therefore the surface tension effect due to film curvature can be neglected. The effect of assuming the initial film thickness to be that given by Nusselt [5] was checked and verified to have minimal effect on the mean heat-transfer coefficient.

C. SIGNIFICANT THEORETICAL STUDIES ON HORIZONTAL ELLIPTICAL TUBES

Some theoretical work has been done on horizontal elliptical cylinders in a quiescent pure vapor using a Nusselt type model. The physical orientation and coordinate system is shown in Figure I-4.

Cheng and Tao [30] approximated the surface of an ellipse by several circular arcs. They analyzed condensation on these arcs using the same assumptions as Nusselt. The ellipse was aligned such that the major axis, a, was aligned with the direction of gravity. From their numerical results they determined that the heat-transfer coefficient decreased with increasing eccentricity, k (defined as the ratio of the minor to major axis). Values of k were varied from that of a vertical flat plate ($k = 0$) to that for a horizontal circular cylinder ($k = 1$). The mean Nusselt number was determined by a surface area weighted average of the mean Nusselt number for each circular arc and

15
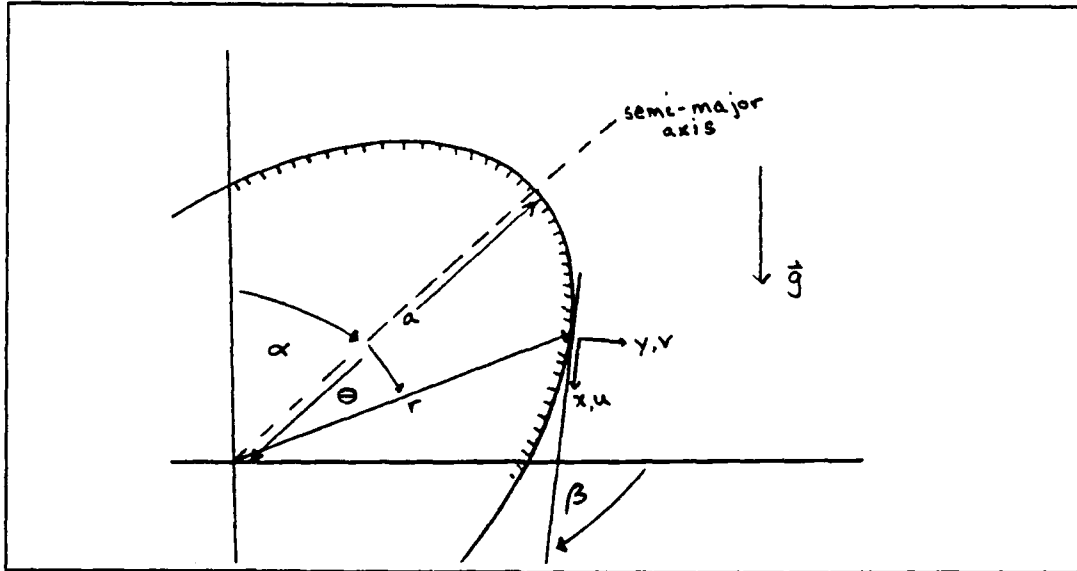
Figure I-4. Geometry for Film Condensation on a Horizontal Elliptical Cylinder.

is given by

$$\bar{Nu} = 0.2876 \left[\frac{Pr}{Ja}\right]^{1/4} \sum_i \left\{\frac{\rho^2 \, d_i^3 \, g}{\eta_l^2} \int_{\theta_{l,i}}^{\theta_{l,2}} Z_i(\theta)^{1/4} d\theta \right\} \qquad \text{(I-14)}$$

where

$$Z_i(\phi) = \frac{4}{3}(\sin\theta)^{-4/3} \int_{\theta_{l,i}}^{\theta} (\sin\theta)^{1/3} d\theta + C_i \qquad . \qquad \text{(I-15)}$$

C_i is an integral constant which links each arc and i is the number of arcs used in the approximation. In the practical range of eccentricity (0.3 – 0.6), the mean heat transfer coefficient was increased by 10 to 18% over that of a circular tube with the same surface area. Ali and McDonald [31] conducted a similar type analysis as Cheng and Tao without the circular arc approximation as a first estimate for condensation on inclined circular tubes.

Wang et al. [32] used the Nusselt assumptions to analyze condensation on horizontal elliptical tube for which the major axis is oriented at an angle, α, with respect to the vertical axis. They obtained an expression for the mean heat-transfer

coefficient given by

$$\bar{\alpha} = \left[\frac{1}{4}\frac{h_{fg}\,\rho_l^2\,g\,\lambda_l^3}{\eta_l\,\Delta T}\frac{1}{\sqrt{ab}}\right]^{1/4}\frac{1}{2\pi}\left(\int_0^{\pi}Z(\beta)^{-1/4}\,d\beta + \int_0^{-\pi}Z((\beta)^{-1/4}\,d\beta\right)\qquad\text{(I-16)}$$

where

$$Z(\beta) = \sin^{-4/3}\beta\int_0^{\beta}\left[\frac{ab}{a^2\sin^2(\beta-\alpha) + b^2\sin^2(\beta-\alpha)}\right]^{3/2}\sin^{1/3}\beta\;d\beta\;.\qquad\text{(I-17)}$$

The results of this study showed that the maximum mean heat-transfer coefficient is obtained when the major axis is aligned with the vertical ($\alpha = 0^{\circ}$). These theoretical results were validated with experimental data for an elliptical tube with semi-minor axis of 8 mm and semi-major axis of 22 mm. Sheng and Cha'o [33] noted that the mean heat-transfer coefficient was incorrectly determined since the heat-transfer coefficient is averaged over the surface area and the radial distance, r, is not constant for an ellipse. In the course of this current study, the problem formulation of Wang et al. [32] was rerun with the correct expression for the mean heat-transfer coefficient (as later derived in Chapter II). The corrected mean heat-transfer coefficient of the elliptical tube analyzed by Wang et al. is 11.3% larger then a circular tube with the same surface area. Additionally, it should be noted that the heat transfer performance of this elliptical cylinder was better than the circular cylinder for angular orientations up to $\alpha \approx 50^{\circ}$. The corrected theoretical results are approximately 5% lower than those determined by Wang et al. and more closely agree with their experimental data. Figure (I-5) shows the heat transfer enhancement for elliptical tubes of varying eccentricity and orientation angle.

Sheng and Cha'o [33] studied the effects of surface tension and variable wall temperature on condensation on a horizontal elliptical tube. The remaining assumptions of the analysis were the same as those above. For the wall temperature, a cosine

17
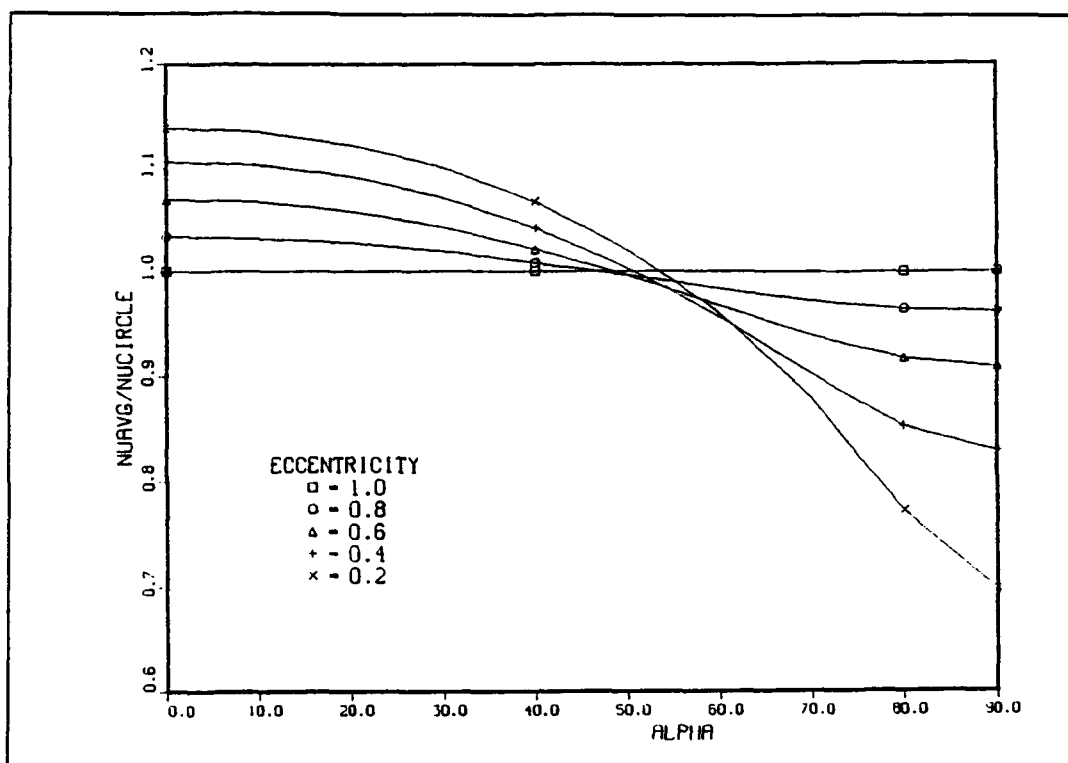
Figure (I-3). Elliptical Tube Mean Nu Compared to Circular Tube Mean Nu for varying Eccentricity and Orientation Angle.

distribution of the form

$$\Delta T = (T_{sat} - \bar{T}_{wall})(1 - A \cos\theta) \qquad (I-18)$$

was used (which has been shown (Memory and Rose [34]) to be in good agreement with experimental data) where the value of A depends on the ratio of the outside to inside heat-transfer coefficient. They determined that variable wall temperature affected local values but not the mean values of the heat-transfer coefficient. For the surface tension effect, it was assumed that the film thickness was much smaller than the radius of curvature of the elliptical surface and thus the surface tension effect was due solely to the curvature of the tube wall. This is in contrast to the study of Krupiczka [29] for a circular tube where the surface tension was due to the curvature of the condensate film. Over the back half of the tube the radius of curvature decreases with streamwise

18

distance resulting in a retarding effect on film flow. As the flow is slowed, the film thickness increases rapidly and at some critical angle becomes infinite in magnitude. This phenomenon is similar to that described by Rose [28] for the pressure gradient effect. The surface tension effect was determined to be significant for $k < 0.6$. In comparison to a circular tube, surface tension causes a favorable pressure gradient over the front half of the tube resulting in a greater film velocity, thinner film thickness and improved heat transfer. It has an opposite effect on the back half of the tube which tends to negates this improvement. The gravity component of the momentum balance is the driving force behind the enhancement in elliptical tubes. Consideration of surface tension results in a slight decrease in the mean Nusselt number as compared to the situation in which the surface tension is neglected.

A potential advantage of an elliptical tube compared to a circular tube is the difference in vapor flow characteristics as a result of a better streamlined shape. Panday [35] developed an explicit numerical method for two dimensional film condensation and applied it to the case of downward flowing vapor over elliptical cylinders. Convection and inertia were included in the condensate film as well as surface tension and pressure gradient (as a result of potential flow of vapor outside the vapor boundary-layer). The interfacial shear was approximated using the asymptotic expression for infinite condensation rate. Several errors were found in the expressions for surface tension and pressure gradient as a result of an incorrect analysis of the differential streamwise length, dx. The first error is the result of assuming that $dx = rd\phi$. This relationship assumes that the radial distance from the centroid of the ellipse is constant over the interval of the parametric angle. This fact is not true (as will be shown in Chapter II) and results in an error whose magnitude is dependent on the step size used in the numerical procedure. The second error involves the expression for r.

19

If the parametric angle is measured from the vertical axis of the ellipse (as appears to be the case in Panday's expression for vapor velocity potential), then r should be given by

$$x = b \sin\phi$$
$$y = a \cos\phi \qquad (I\text{-}18)$$
$$r = \sqrt{x^2 + y^2} = a\sqrt{\cos^2\phi + k^2\sin^2\phi} \quad .$$

Panday used an expression for radial distance given by

$$r = a\sqrt{\sin^2\phi + k^2\cos^2\phi} \quad . \qquad (I\text{-}19)$$

The magnitude of the resulting error is dependent on the eccentricity of the ellipse. Additionally, there appears to be an error in the gravity component of the momentum equation. Panday uses a body force given by $\rho g \sin\theta$, which is true only for circular geometries but is untrue for elliptical geometries. His results will therefore not account for the improved performance which are obtained by placing more of the surface in line with the direction of gravity. Panday's conclusions were that the overall heat transfer was reduced for elliptical tubes at low velocities (as compared to a similar circular tube) due to a rapid thickening of the film at the stagnation point and the overall heat transfer is increased for high velocities due to increased interfacial shear. These conclusions are opposite to what one may expect. At low velocities, the film thickness near the stagnation point for elliptical cylinders is thinner than the equivalent circular tube as a result of increased effective gravity. This effect results in improved heat transfer. Pressure gradient effects due to potential flow and interfacial shear should be negligible since the velocity is small. At high velocities, the streamlined geometry of elliptical cylinders results in lower interfacial shear and pressure gradient effects as compared to circular cylinders. These effects should result in a thickening

of the condensate film as compared to circular cylinders and hence reduced heat transfer for the same effective diameter and free stream vapor velocity.

D.   OBJECTIVES OF THIS THEORETICAL STUDY

The results of previous studies indicate that elliptical tubes can be used to increase condensation heat transfer in low vapor velocity condensers as compared to circular tubes with the same surface area. The present investigation examines the effects of vapor shear, pressure gradient and surface tension in laminar film condensation on a single horizontal elliptical tube with its major axis aligned with gravity and the free stream velocity. Interfacial shear is estimated using both the simple assumptions of Shekriladze and Gomelauri [21] and the more complex technique of Fujii et al. [22]. The latter case calculates the angle at which the vapor boundary-layer separates such that the effect of reduced drag on the mean heat-transfer coefficient can be evaluated.

II. THEORETICAL DEVELOPMENT

Following the theoretical developments used for the case of laminar film condensation on a horizontal circular tube, theoretical models are developed for laminar film condensation on a horizontal elliptical tube of eccentricity, k. This development starts with a Nusselt [5] type model in a quiescent vapor, and then adds forced and mixed convection as in the models of Shedkriladze and Gomelauri [21] and pressure gradient as considered by Rose [28]. The pressure gradient takes into account the effects of potential flow outside the vapor boundary-layer as well as surface tension. Finally, a model is developed which analyzes the vapor boundary-layer and boundary-layer separation following Fujii et al. [22]. Pressure gradient and surface tension are not considered in this model due to the complexities introduced by the use of the two-phase boundary-layer equation. Where possible these elliptical models are checked against existing theories for the "limiting" eccentricities of a circular cylinder (k=0), vertical flat plate (k=1) and horizontal flat plate ($k \rightarrow \infty$).

A. FACTORS RELATED TO ELLIPSE GEOMETRY

Consider an elliptical cylinder whose cross-section is oriented such that the major-axis is aligned with the vertical as shown in Figure II-1. The eccentricity, k, of the ellipse is defined by

$$k = \frac{b}{a} . \tag{II-1}$$

where a and b are the semi-major and semi-minor lengths, respectively. Functions related to the geometry of the ellipse are initially developed in a cartesian coordinate system (x_1, y_1) whose origin coincides with the centroid of the ellipse. This is then transformed into a cylindrical coordinate system (r, θ) where r is the radial distance

from the ellipse centroid to a point on the ellipse surface and θ is the angle measured from the vertical. The transformation equations are

$$x_1 = r \sin\theta$$
$$y_1 = r \cos\theta \ .$$

<div align="right">(II-2)</div>

The elliptical surface can also be defined by a parametric angle, ϕ, measured from the upper semi-major axis, such that the y_1 coordinate on a circle of radius a translates

Figure II-1. Geometry for Film Condensation on a Horizontal Elliptical Cylinder with Major Axis Parallel to Gravity.

to the y_1 coordinate on the ellipse and the x_1 coordinate on a circle of radius b translates to the x_1 coordinate on the ellipse. The transformation equations are given by

$$x_1 = b \sin\phi$$
$$y_1 = a \cos\phi \ .$$

<div align="right">(II-3)</div>

Combining Equations (I-2) and (I-3) results in a relationship between r, θ and ϕ:

$$\sin\phi = \frac{r}{b} \sin\theta \qquad (a)$$

$$\cos\phi = \frac{r}{a} \cos\theta \qquad (b) \qquad\qquad \text{(II-4)}$$

$$\tan\phi = \frac{\tan\theta}{k} \qquad (c) \; .$$

It is assumed that the condensate thickness, δ, is much smaller than the radius of the elliptical surface. Therefore, the equations for the condensate film and vapor boundary-layer are developed using an orthogonal, curvilinear coordinate system, (x,y), where x is the streamwise distance along the elliptical surface and y is the distance normal to the surface.

1. Radial Distance, r

In cartesian coordinates, the surface of an ellipse is given by

$$\frac{x_1^2}{b^2} + \frac{y_1^2}{a^2} = 1 \; . \qquad\qquad \text{(II-5)}$$

The radial distance, r, can be determined by

$$r(x_1,y_1) = \sqrt{x_1^2 + y_1^2} \; . \qquad\qquad \text{(II-6)}$$

Using the parametric transformation equations (Equation (II-3)), an equivalent expression for the radial distance is given in terms of ϕ by:

$$r(\phi) = a\sqrt{\cos^2\phi + k^2 \sin^2\phi} \; . \qquad\qquad \text{(II-7)}$$

24

2. Radius of Curvature of an Ellipse, R

The curvature, $\kappa(x_1)$, and the radius of curvature, $R(x_1)$, of a function, $f(x_1)$, is given by

$$\kappa(x_1) = \frac{|f''(x_1)|}{[1 + (f'(x_1))^2]^{3/2}} \qquad . \tag{II-8}$$

$$R(x_1) = 1/\kappa(x_1)$$

where the prime denotes differentiation with respect to x_1. Solving for y_1 as a function of x_1 using Equation (II-5), determining the radius of curvature using Equation (II-8) and transforming the results to parametric coordinates gives the radius of curvature as a function of ϕ:

$$R(\phi) = \frac{a}{k} \left[\sin^2\phi + k^2\cos^2\phi \right]^{3/2} \qquad . \tag{II-9}$$

3. Streamwise Length, x

Since the radial distance to a point on the elliptical surface is not constant, the streamwise length is not proportional to θ as it would be for a circle. Additionally, as eccentricity varies, the streamwise length for a given θ is not the same. To obtain an expression for x in terms of parametric angle ϕ, consider first a point on the ellipse surface as shown in Figure II-2. Moving a small distance, dx, results in incremental changes, $d\theta$ and dr. The resulting relationship between x,r and θ is given by.

$$(dx)^2 = (dr)^2 + (r \, d\theta)^2 \qquad . \tag{II-10}$$

Expressions are now needed for dr and $d\theta$ in terms of $d\phi$. For dr, this is simply achieved by differentiating Equation (II-7):

$$dr = \frac{1}{2} \frac{a \, (k^2-1) \, \sin 2\phi}{\sqrt{\cos^2\phi + k^2\sin^2\phi}} \, d\phi \qquad . \tag{II-11}$$

25
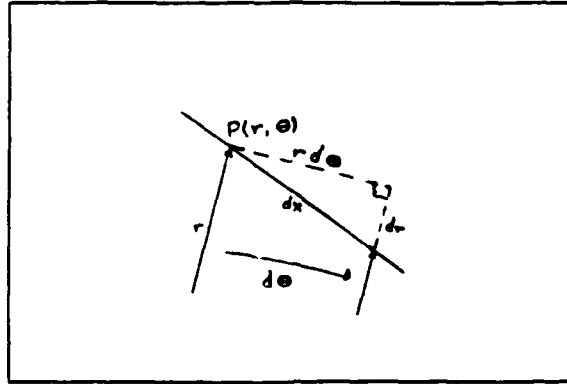
Figure II-2. Enlarged View of Point on Ellipse.

For $d\theta$, taking Equation (II-4a), substituting Equation (II-7) for r and differentiating the resultant expression results in:

$$\cos\theta \; d\theta = \frac{k \cos\phi}{[\cos^2\phi + k^2\sin^2\phi]^{3/2}} \quad . \tag{II-12}$$

Combining Equations (II-4b) and (II-7), and substituting for $\cos\theta$ in Equation (II-12) results in an expression for $d\theta$ in terms of $d\phi$:

$$d\theta = \frac{k}{\cos^2\phi + k^2\sin^2\phi} \; d\phi \quad . \tag{II-13}$$

Substituting Equations (II-11) and (II-13) into Equation (II-10) gives an expression for dx as a function of $d\phi$:

$$dx = a \sqrt{\frac{k^2 + \frac{1}{4}(k^2-1)^2\sin^2 2\phi}{\cos^2\phi + k^2\sin^2\phi}} \; d\phi \quad . \tag{II-14}$$

This may be integrated to obtain the streamwise length. For compactness, a function $\chi(\phi)$ is defined by

$$\chi(\phi) = a \sqrt{\frac{k^2 + \frac{1}{4}(k^2-1)^2\sin^2 2\phi}{\cos^2\phi + k^2\sin^2\phi}} \quad . \tag{II-15}$$

In later developments, a characteristic length is used to non-dimensionalize the heat transfer parameters in the model. An effective diameter, D_e, is defined as the diameter of a circular cylinder having the same surface area as an elliptical cylinder and will be used as a characteristic length. The effective diameter is given by

$$\pi D_e = 2\int_0^\pi \chi(\phi)d\phi \quad . \tag{II-16}$$

Streamwise length is non-dimensionalized by:

$$x^* = \frac{2x}{\pi D_e} \quad . \tag{II-17}$$

This enables direct comparison between elliptical and circular cylinders since it represents an equivalent surface area.

4. Streamwise Gravity Component, g_x

The component of gravity in the streamwise direction is tangent to the elliptical surface and is a function of streamwise location. A line tangent to the surface, defined by the slope of the surface, is obtained from Equation (II-5),

$$\frac{dy_1}{dx_1} = -\frac{a}{b}\frac{x_1}{\sqrt{b^2 - x_1^2}} \quad . \tag{II-18}$$

A unit vector in the streamwise direction is then given by

$$\hat{T} = \frac{1}{\sqrt{(b^2 - x_1^2) + \frac{a^2}{b^2}x_1^2}} \left[\sqrt{b^2 - x_1^2}\,\hat{\imath} - \frac{a}{b}x_1\,\hat{\jmath} \right] \quad . \tag{II-19}$$

The streamwise gravity component is given by the dot product of the gravity vector and the tangent vector,

$$g_x = \vec{g} \cdot \hat{T} = g\,\frac{a}{b}\,\frac{x_1}{\sqrt{(b^2 - x_1^2) + \frac{a^2}{b^2}x_1^2}} \quad . \tag{II-20}$$

27

Transforming Equation (II-20) into parametric coordinates results in the expression:

$$g_x = g\, f_1(\phi)$$

$$\textit{where} \quad f_1(\phi) = \frac{\sin\phi}{\sqrt{\sin^2\phi + k^2\cos^2\phi}} \quad . \tag{II-21}$$

5. Potential Flow at Ellipse Surface, U_ϕ

When considering forced convection due to the flow of vapor over the condensate film, the velocity of the vapor influences the condensate film thickness through the vapor shear at the film/vapor interface. The vapor velocity at the interface will be dependent on the vapor velocity outside the vapor boundary-layer. This velocity is determined from potential flow theory. Assuming that the film thickness, δ, and the vapor boundary-layer thickness, Δ, are much smaller than the radial distance, r, of the elliptical surface (and therefore may be neglected), the potential flow, U_ϕ, about an elliptical surface with major axis aligned with the vapor free stream velocity, U_∞, is given by

$$U_\phi = U_\infty \frac{(1+k)}{\sqrt{1 + k^2\cot^2\phi}} \quad . \tag{II-22}$$

Details of the derivation of this expression are provided in Appendix (A).

6. Ellipse with Major Axis Perpendicular to Gravity

For the case where the ellipse major axis is perpendicular to the vertical as shown in Figure II-3, the previously determined equation for streamwise component of gravity remains the same. For $0 < k < 1$, the major axis is aligned with gravity. For $1 < k < \infty$, the major axis is perpendicular to gravity.
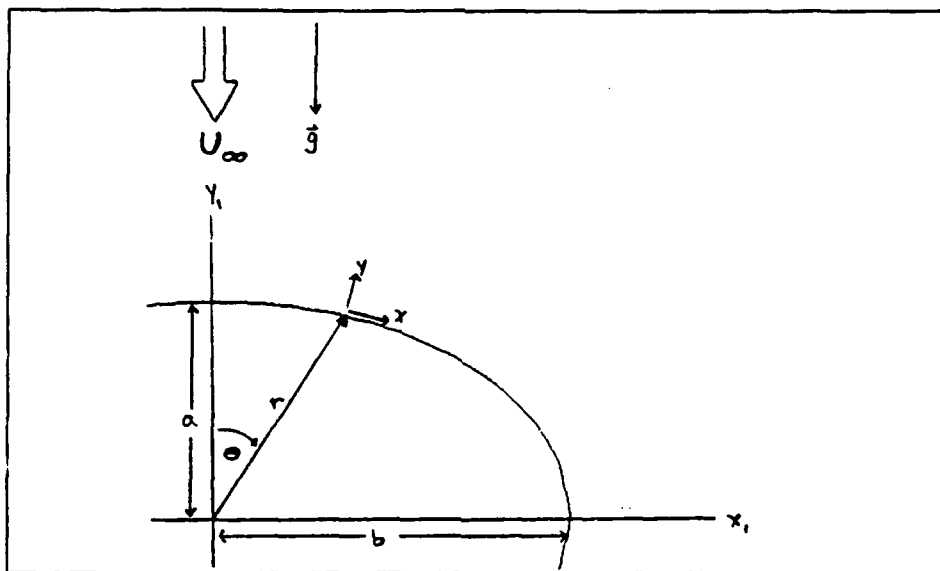
Figure II-3. Geometry for Condensation on Horizontal Elliptical Cylinder with Major Axis Perpendicular to Gravity.

B. FREE CONVECTION CONDENSATION ON AN ELLIPTICAL CYLINDER (NUSSELT [5] TYPE ANALYSIS)

Consider a quiescent, saturated vapor at a temperature T_{sat}, condensing on a horizontal elliptical cylinder of eccentricity, k, and semi-major axis, a, aligned with the direction of gravity as in Figure II-1. The same simplifying assumptions are made as proposed by Nusselt in his analysis of condensation on a horizontal circular cylinder. These assumptions are:

(1) The vapor is pure and quiescent.
(2) The tube wall temperature is uniform and constant.
(3) The thermophysical properties of the fluid are constant and evaluated at some given reference temperature.
(4) The temperature at the film/vapor interface is T_{sat}.
(5) The condensate film thickness is small compared to the radius of the ellipse.
(6) Heat transfer in the condensate film is one dimensional in the radial direction providing a linear temperature distribution across the film (based on $\delta \ll R$).
(7) The only forces acting on the condensate film are viscous and gravity forces.
(8) Flow in the liquid film is laminar with no waviness and no vapor boundary layer separation.

A fluid element of unit width is analyzed in detail and shown in Figure II-4.
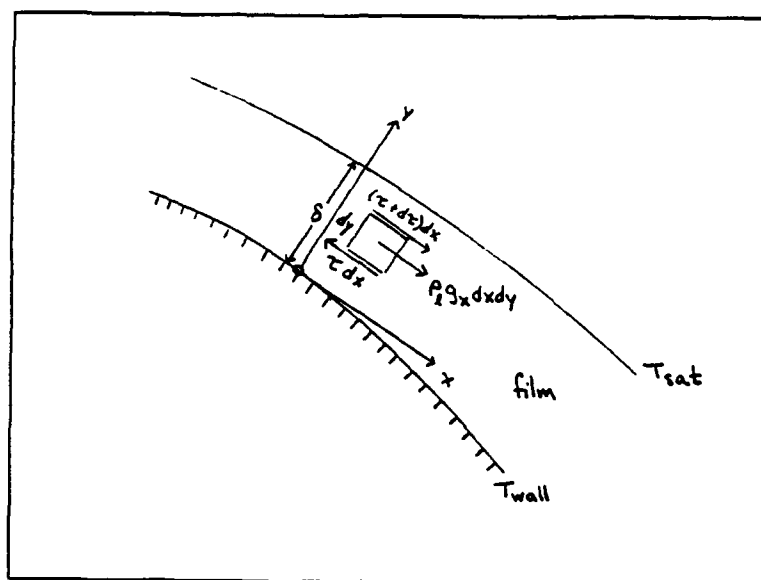
Figure II-4. Condensate Film Element for Free Convection.

Conservation of mass for the fluid element requires that,

$$\left[\rho_l \int_0^\delta u \, dy\right] dx - \left[\rho_l \int_0^\delta u \, dy + \frac{d}{dx}\left\{\rho_l \int_0^\delta u \, dy\right\}\right] dx + m \, dx = 0 \quad . \qquad \text{(II-23)}$$

where m is the local condensation mass flux rate.

Defining the mean film velocity as

$$u_m = \frac{1}{\delta}\int_0^\delta u \, dy \quad , \qquad \text{(II-24)}$$

Equation (II-23) simplifies to

$$m = \frac{d}{dx}\{\rho \mu_m \delta\} \quad . \qquad \text{(II-25)}$$

Conservation of momentum for the film element is a balance of viscous and body forces which reduces to

$$\eta_l \frac{d^2 u}{dy^2} + \rho_l \, g \, f_1(\phi) = 0 \quad . \qquad \text{(II-26)}$$

Here, an assumption is made that the fluid is Newtonian, i.e.,

$$\tau = \eta_l \frac{du}{dy} \quad . \tag{II-27}$$

Conservation of energy is a balance of latent heat from condensation and heat conduction through the condensate film which reduces to

$$h_{fg} m \ dx = \frac{\lambda_l}{\delta}(T_{sat} - T_{wall}) \ dx$$

$$m = \frac{\lambda_l \ (T_{sat} - T_{wall})}{h_{fg}\delta} \quad . \tag{II-28}$$

The boundary conditions for the momentum equation are

$$u_{y=0} = 0$$

$$\tau_\delta = \eta_l \left(\frac{du}{dy}\right)_{y=\delta} = 0 \quad . \tag{II-29}$$

Integrating the momentum equation subject to the boundary conditions results in a local film velocity of

$$u(y) = \frac{\rho_l g}{\eta_l} f_1(\phi) \left(\delta y - \frac{1}{2}y^2\right) \tag{II-30}$$

and a mean film velocity of

$$u_m = \frac{\rho_l g}{\eta_l} f_1(\phi) \frac{\delta^2}{3} \quad . \tag{II-31}$$

Combining the continuity equation, energy equation and expression for film mean velocity (Equations (II-25),(II-28) and (II-31)), results in

$$\frac{\lambda_l \ \Delta T}{h_{fg} \ \delta} = \frac{d}{dx}\left\{\frac{\rho_l^2 g}{3\eta_l} f_1(\phi) \ \delta^3\right\} \quad . \tag{II-32}$$

Using the relationship between dx and $d\phi$ from Equations (II-14) and (II-15) and

31

carrying out the differentiation results in

$$\frac{\lambda_l \Delta T}{h_{fg}} \frac{1}{\delta} = \frac{\rho_l^2 g}{3\eta_l} \frac{1}{\chi(\phi)} \left(\delta^3 f_1'(\phi) + 3 f_1(\phi) \delta^2 \frac{d\delta}{d\phi} \right) . \qquad \text{(II-33)}$$

A dimensionless parameter, Z_1, is defined by

$$Z_1 = \frac{\delta^4}{B_1} \qquad \text{(II-34)}$$

where B_1 is given by

$$B_1 = \frac{\lambda_l \eta_l \Delta T D_e}{\rho_l^2 h_{fg} g} . \qquad \text{(II-35)}$$

Note that the equivalent parameter used by Nusselt [3] multiplies Equation (II-35) by a factor of three and uses radius in place of effective diameter. Substituting Equations (II-34) and (II-35) into (II-33) results in a first order ordinary differential equation for Z_1:

$$\frac{dZ_1}{d\phi} + \frac{4 f_1'(\phi)}{3 f_1(\phi)} Z_1 = \frac{4 \chi(\phi)}{D_e f_1(\phi)} . \qquad \text{(II-36)}$$

This equation can be solved exactly by using an integrating factor which would require numerical integration or can be solved numerically using a forward stepping or propagation technique. The initial condition is determined based on the symmetry of the problem which requires that $(dZ_1/d\phi)_{\phi=0} = 0$. Solving Equation (II-36) at $\phi = 0$ results in the initial condition

$$Z_1 \big|_{\phi=0} = \frac{3 \chi(0)}{D_e f_1'(0)} = \frac{3 a k^2}{D_e} . \qquad \text{(II-37)}$$

The non-dimensional film thickness, δ^*, and film thickness, δ, are determined respectively by

$$\delta^*(\phi) = Z_1(\phi)^{1/4} \quad and$$

$$\delta(\phi) = \{\, Z_1(\phi)\; B_1\, \}^{1/4} \quad . \tag{II-38}$$

The local heat-transfer coefficient, α, and mean heat-transfer coefficient are given respectively by

$$\alpha(\phi) = \frac{\lambda_l}{\delta(\phi)} \quad and$$

$$\bar{\alpha} = \frac{\int_0^{2\pi} \alpha(\phi)\; dA_s}{\int_0^{2\pi} dA_s} = \frac{2}{\pi D_e}\int_0^{\pi} \alpha(\phi)\; \chi(\phi)\; d\phi \quad , \tag{II-39}$$

and the local Nusselt number and mean Nusselt number by

$$Nu(\phi) = \frac{\alpha(\phi)D_e}{\lambda_l} = \frac{D_e}{\delta(\phi)} \quad and$$

$$\bar{Nu} = \frac{\bar{\alpha}D_e}{\lambda_l} = \frac{2}{\pi}\int_0^{\pi} \frac{1}{\delta(\phi)}\; \chi(\phi)\; d\phi \quad . \tag{II-40}$$

For the case where $k = 1$ (circular tube); $f_1(\phi)=\sin\phi$, $f_1{}'(\phi)=\cos\phi$, $\chi(\phi)=a$ and $D_e = 2a$ and Equation (II-36) reduces to

$$\frac{dZ_1}{d\phi} + \frac{4}{3}\frac{\cos\phi}{\sin\phi}\; Z_1 = \frac{2}{\sin\phi} \quad , \tag{II-41}$$

which is the same as that found by Nusselt [5] except for a difference in the definition of B_1.

The above development can also be applied to a horizontal elliptical tube whose major axis is perpendicular to the direction of gravity as shown in Figure II-3. In this case, b is greater than a, i.e. $k > 1$.

33

C. FORCED CONVECTION CONDENSATION ON AN ELLIPTICAL CYLINDER (SHEKRILADZE-GOMELAURI [21] TYPE ANALYSIS)

Consider a saturated vapor at temperature T_{sat}, flowing downward over a horizontal elliptical cylinder with free stream vapor velocity, U_∞. The elliptical cylinder has eccentricity, k, and semi-major axis, a, parallel with the direction of gravity and vapor flow. The same assumptions as for the case of free convection are used here with the exceptions:

(1) The force of gravity is neglected.
(3) $U_\phi \gg u_{y=\delta}$.
(4) The interfacial shear stress is approximated by an asymptotic expression assuming an infinite condensation rate,

$$\tau_\delta = m(U_\phi - u_\delta) = mU_\phi \qquad \text{(II-42)}$$

Conservation of mass and energy are the same as previously derived (Equations (II-25) and (II-28)). The only forces acting on the fluid element are viscous forces. Thus, conservation of momentum reduces to

$$\eta_l \frac{d^2u}{dy^2} = 0 \quad , \qquad \text{(II-43)}$$

with the boundary conditions,

$$u_{y=0} = 0$$

$$\eta_l \left(\frac{du}{dy}\right)_{y=\delta} = \tau_\delta = m\,U_\phi \quad . \qquad \text{(II-44)}$$

Integrating the momentum equation subject to the boundary conditions results in a local velocity of

$$u(y) = \frac{m\,U_\phi}{\eta_l}\,y \qquad \text{(II-\,)}$$

34

and a mean film velocity

$$u_m = \frac{m \, U_\phi}{\eta_l} \frac{\delta}{2} \quad .$$ (II-46)

Using the expression for potential flow over an elliptical cylinder (Equation (II-22)) and defining a velocity function, $f_2(\phi)$, such that

$$f_2(\phi) = \frac{1+k}{\sqrt{1 + k^2 \cot^2\phi}} \quad ,$$ (II-47)

the mean film velocity can be expressed as

$$u_m = \frac{m \, U_\infty}{\eta_l} f_2(\phi) \frac{\delta}{2} \quad .$$ (II-48)

Combining the continuity equation, energy equation and expression for mean film velocity (Equations (II-25),(II-28) and (II-48)) results in

$$\frac{\lambda_l \, \Delta T}{h_{fg}} \frac{1}{\delta} = \frac{d}{dx}\left\{ \frac{\rho_l \, \lambda_l \, \Delta T \, U_\infty}{\eta_l \, h_{fg}} f_2(\phi) \frac{\delta}{2} \right\} \quad .$$ (II-49)

Using the relationship between dx and $d\phi$ from Equations (II-14) and (II-15), and carrying out the differentiation results in

$$\frac{\lambda_l \, \Delta T}{h_{fg}} \frac{1}{\delta} = \frac{\rho_l \, \lambda_l \, \Delta T \, U_\infty}{2\eta_l \, h_{fg}} \frac{1}{\chi(\phi)}\left(\delta \, f_2'(\phi) + f_2(\phi) \frac{d\delta}{d\phi} \right) \quad .$$ (II-50)

Defining a dimensionless parameter, Z_2, as

$$Z_2 = \frac{\delta^2}{B_2}$$ (II-51)

where

$$B_2 = \frac{\eta_l \, D_e}{\rho_l \, U_\infty} \quad ,$$ (II-52)

35

Equation (II-50) becomes

$$\frac{dZ_2}{d\phi} + 2\,\frac{f_2'(\phi)}{f_2(\phi)}\,Z_2 = \frac{4\,\chi(\phi)}{D_e\,f_2(\phi)} \quad . \tag{II-53}$$

This problem is a first order ordinary differential equation which can be solved using a forward stepping numerical integration technique. The initial condition for the problem is based on symmetry which requires that $(dZ_2/d\phi)_{\phi=0} = 0$. Solving Equation (II-53) at $\phi = 0$ results in the initial condition

$$Z_{2\,\phi\to 0} = \frac{2\,\chi(0)}{D_e\,f_2'(0)} = \frac{2ak^2}{D_e(1+k)} \quad . \tag{II-54}$$

The non-dimensional film thickness, δ^*, and film thickness, δ, are determined respectively by

$$\delta^* = \sqrt{Z_2(\phi)}$$

$$\delta = \sqrt{Z_2(\phi)\,B_2} \quad . \tag{II-55}$$

The heat-transfer coefficient for forced convection condensation can be considered in a different form. Combining Equations (II-40),(II-51), (II-52) and (II-55) results in

$$Nu\,\overline{Re}^{-1/2} = \frac{1}{\delta^*(\phi)} \quad , \quad and$$

$$\overline{Nu}\,\overline{Re}^{-1/2} = \frac{2}{\pi}\int_0^\pi \frac{1}{\delta^*(\phi)}\,\chi(\phi)\,d\phi \quad . \tag{II-56}$$

For the case where $k = 1$ (circular tube), $f_2(\phi) = 2\sin\phi$, $dx = a\,d\phi$ and Equation (II-49) reduces to

$$\frac{1}{\delta} = \frac{1}{a}\frac{d}{d\phi}\left\{\frac{\rho_l\,U_\infty}{\eta_l}\sin\phi\;\delta\right\} \quad . \tag{II-57}$$

which is the same as the Shekriladze-Gomelauri [21] governing equation for a circular cylinder with no body forces.

36

D. MIXED CONVECTION CONDENSATION ON AN ELLIPTICAL CYLINDER (SHEKRILADZE-GOMELAURI [21] TYPE ANALYSIS)

Consider a saturated vapor at temperature T_{sat}, flowing downward over a horizontal elliptical cylinder with free stream vapor velocity, U_∞. The elliptical cylinder has eccentricity, k, and semi-major axis, a, which is parallel with the direction of gravity and vapor flow. The forces acting on a film element are viscous and body forces. The interfacial shear is given by the Shekriladze-Gomelauri [21] model for infinite condensation rate as in the case of the forced convection model (Equation (II-42)).

Conservation of mass and energy are as previously derived. Conservation of momentum for the condensate film reduces to

$$\eta_l \frac{d^2 u}{dy^2} + \rho_l \, g \, f_1(\phi) = 0 \qquad\qquad \text{(II-58)}$$

with boundary conditions,

$$u_{y=0} = 0$$
$$\left(\frac{du}{dy}\right)_{y=\delta} = \frac{m \, U_\phi}{\eta_l} \, . \qquad\qquad \text{(II-59)}$$

Integrating the momentum equation, subject to the boundary conditions, results in the local film velocity

$$u(y) = \frac{\rho_l \, g}{\eta_l} f_1(\phi) \left(\delta y - \frac{y^2}{2}\right) + \frac{m \, U_\infty}{\eta_l} f_2(\phi) \, y \qquad\qquad \text{(II-60)}$$

and mean film velocity

$$u_m = \frac{\rho_l \, g}{\eta_l} f_1(\phi) \frac{\delta^2}{3} + \frac{m \, U_\infty}{\eta_l} f_2(\phi) \frac{\delta}{2} \, . \qquad\qquad \text{(II-61)}$$

where the expression for potential flow over an ellipse and its associated velocity function (Equations (II-22) and (II-47)) have been used.

37

Combining the continuity equation, energy equation and expression for mean film velocity (Equations (II-25), (II-28) and (II-61)) results in

$$\frac{\lambda_l \, \Delta T}{h_{fg}} \frac{1}{\delta} = \frac{d}{dx}\left\{ \frac{\rho_l^2 g}{\eta_l} f_1(\phi) \frac{\delta^3}{3} + \frac{\rho_l \, \lambda_l \, \Delta T \, U_\infty}{\eta_l \, h_{fg}} f_2(\phi) \frac{\delta}{2} \right\} \quad . \tag{II-62}$$

Using the relationship between dx and $d\phi$, and algebraically manipulating Equation (II-62) results in

$$\frac{1}{\delta^*} = \frac{D_e}{2 \, \chi(\phi)} \frac{d}{d\phi}\left\{ 2F \, f_1(\theta) \frac{\delta^{*2}}{3} + f_2(\phi) \, \delta^* \right\} \tag{II-63}$$

where F is a dimensionless parameter relating free and forced convection and δ^* is a dimensionless film thickness given respectively by

$$F = \frac{\eta_l \, D_e \, h_{fg} \, g}{U_\infty^2 \lambda_l \, \Delta T} \tag{II-64}$$

$$\delta^* = \delta \sqrt{\frac{\rho_l \, U_\infty}{\eta_l \, D_e}} = \frac{\delta}{D_e}\sqrt{Re} \quad .$$

Differentiating Equation (II-63) results in

$$\frac{1}{\delta^*} = \frac{D_e}{2 \, \chi(\phi)}\left\{ 2F \, f_1(\phi) \, \delta^{*2} \frac{d\delta^*}{d\phi} + 2F \, f_1'(\phi) \frac{\delta^{*3}}{3} + f_2(\phi) \frac{d\delta^*}{d\phi} + f_2'(\phi) \, \delta^* \right\} \quad . \tag{II-65}$$

Regrouping the terms shows that the equation is a first order ordinary differential equation:

$$\left\{ 2F \, f_1(\phi) \, \delta^{*3} + f_2(\phi) \, \delta^* \right\}\frac{d\delta^*}{d\phi} + \left\{ 2F \, f_1'(\phi) \frac{\delta^{*4}}{3} + f_2'(\phi) \right\} = \frac{2 \, \chi(\phi)}{D_e} \quad . \tag{II-66}$$

The initial condition for this problem is again based on symmetry, which requires that $d\delta^*/d\phi = 0$ at $\phi = 0$. Inserting this condition into Equation (II-66) results in a fourth order expression for δ^*

$$\frac{2}{3} F \, f_1'(0) \, \delta^{*4} + f_2'(0) \, \delta^{*2} - 2 \frac{\chi(0)}{D_e} = 0 \quad , \tag{II-67}$$

38

whose root of interest is given by

$$\delta^*(0) = \left[\frac{-f_2'(0) + \sqrt{(f_2'(0))^2 + 4\ \{2/3\ F f_1'(0)\}\ \{2\ \frac{\chi(0)}{D_e}\}}}{2\ \{2/3\ F f_1'(0)\}} \right]^{1/2} \tag{II-68}$$

$$= \left[\frac{3k}{4F} \left(\sqrt{\left(\frac{1+k}{k}\right)^2 + \frac{16\ F\ a}{3\ D_e}} - \frac{1+k}{k} \right) \right]^{1/2}$$

Equation (II-66) can be solved numerically to obtain the film thickness. The other heat transfer parameters are determined as before (Equations (II-39) and (II-56)).

For the case where $F=0$ and $k=1$ (forced convection over a circular tube), Equation (II-63) reduces to Equation (II-57) as expected. For the case where $F \to \infty$ and $k=1$ (free convection over a circular tube), Equation (II-63) becomes

$$\frac{1}{\delta^*} = \frac{D_e}{2\chi(\phi)} \frac{d}{d\phi} \left\{ \frac{2}{3} F f_1(\phi)\ \delta^{*3} \right\} \ . \tag{II-69}$$

Upon substitution for the parameters F and δ^* (Equation (II-64)), Equation (II-69) becomes

$$\frac{1}{\delta} = \frac{1}{a} \frac{\rho_l^2\ h_{fg}\ g}{\lambda_l\ \Delta T\ \eta_l} \frac{d}{d\phi} \left\{ \sin\phi\ \frac{\delta^3}{3} \right\} \ , \tag{II-70}$$

which is the same as Nusselt's governing equation [5] for laminar film condensation on a horizontal circular cylinder.

E. MIXED CONVECTION CONDENSATION ON AN ELLIPTICAL CYLINDER WITH SURFACE TENSION AND PRESSURE GRADIENT EFFECTS

Consider a pure saturated vapor at temperature T_{sat}, flowing downward over a horizontal elliptical cylinder with free stream vapor velocity, U_∞. The elliptical cylinder has eccentricity, k, and semi-major axis, a, parallel with the direction of gravity and vapor flow. In addition to the assumptions used for mixed convection in

39

the last section, pressure effects in the condensate film are considered in the development of the governing equations. The pressure on a condensate film element will be a combination of that impressed upon the element by the potential flow of the vapor as well as that due to surface tension. A fluid element is shown in detail in Figure II-5.
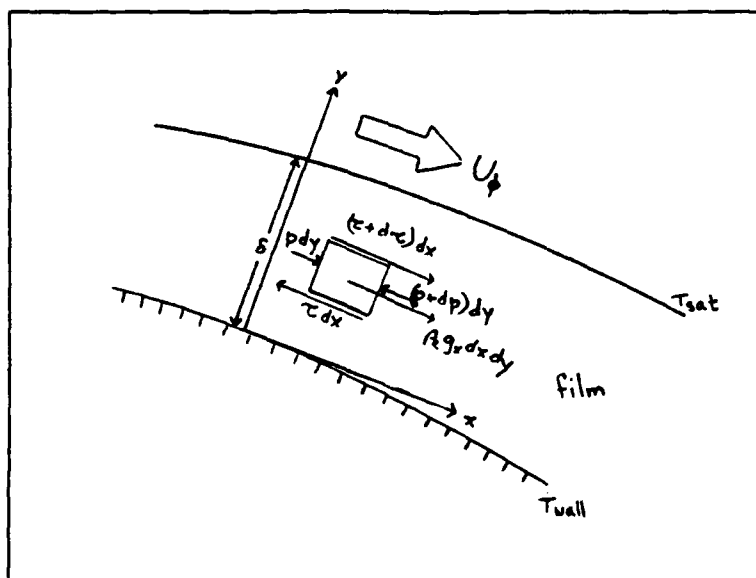
Figure II-5. Condensate Film Element for Mixed Convection with Pressure Gradient.

Conservation of mass and energy are as previously described. Conservation of momentum for the film element is a balance of viscous, pressure and body forces which reduces to

$$\eta_l \frac{d^2u}{dy^2} + \rho_l \, g \, f_1(\phi) - \frac{dp}{dx} = 0 \qquad (II-71)$$

with boundary conditions

$$u_{y=0} = 0$$

$$\left(\frac{du}{dy}\right)_{y=\delta} = \frac{m \, U_\phi}{\eta_l} \qquad (II-72)$$

As previously stated, the film pressure is a combination of the pressure due to potential flow, p_ϕ, and the pressure due to surface tension, p_σ. Thus the total pressure gradient is given by

$$\frac{dp}{dx} = \frac{dp_\phi}{dx} + \frac{dp_\sigma}{dx} \quad . \tag{II-73}$$

The pressure gradient due to potential flow is given by

$$\frac{dp_\phi}{dx} = -\rho_v \, U_\phi \frac{dU_\phi}{dx} = \frac{-\rho_v U_\phi}{\chi(\phi)} \frac{dU_\phi}{d\phi} \quad . \tag{II-74}$$

Substituting the expressions for potential flow and $\chi(\phi)$ (Equation (II-22) and (II-15)), into Equation (II-74) results in

$$\frac{dp_\phi}{dx} = -\frac{\rho_v \, U_\infty^2}{2a} f_3(\phi) \tag{II-75}$$

where

$$f_3(\phi) = \frac{(1+k)^2 \, k^2 \, \sin 2\phi}{\left[\sin^2\phi + k^2\cos^2\phi \right]^2} \sqrt{\frac{\cos^2\phi + k^2\sin^2\phi}{k^2 + \frac{1}{4}(k^2-1)^2 \, \sin^2 2\phi}} \quad . \tag{II-76}$$

The pressure due to surface tension is given by

$$P_\sigma = \frac{\sigma}{R(\phi)} \quad . \tag{II-77}$$

It is assumed that $\delta \ll R$. Thus, the pressure gradient is given by

$$\frac{dp_\sigma}{dx} = -\frac{\sigma}{R^2} \frac{dR}{dx} = -\frac{\sigma}{R^2 \, \chi(\phi)} \frac{dR}{d\phi} \quad . \tag{II-78}$$

Substituting Equations (II-9) and (II-15) into Equation (II-78) results in

$$\frac{dp_\sigma}{dx} = -\frac{3}{2} \frac{\sigma}{a^2} f_4(\phi) \tag{II-79}$$

41

where

$$f_4(\phi) = \frac{k\,(1-k^2)\,\sin2\phi}{\left[\,\sin^2\phi + k^2\cos^2\phi\,\right]^{5/2}}\sqrt{\frac{\cos^2\phi + k^2\sin^2\phi}{k^2 + \frac{1}{4}\,(k^2-1)^2\,\sin^22\phi}} \quad . \qquad (\text{II-80})$$

Integrating the momentum equation, subject to the boundary conditions results in a local film velocity of

$$u(y) = \left[\frac{\rho_l\,g}{\eta_l}\,f_1(\phi) + \frac{\rho_v\,U_\infty^2}{2a\,\eta_l}\,f_3(\phi) + \frac{3}{2}\,\frac{\sigma}{\eta_l a^2}\,f_4(\phi)\right]\left(\delta y - \frac{y^2}{2}\right) + \frac{m\,U_\infty}{\eta_l}\,f_2(\phi)\,y \qquad (\text{II-81})$$

and a mean film velocity,

$$u_m = \left[\frac{\rho_l\,g}{\eta_l}\,f_1(\phi) + \frac{\rho_v\,U_\infty^2}{2a\,\eta_l}\,f_3(\phi) + \frac{3}{2}\,\frac{\sigma}{\eta_l\,a^2}\,f_4(\phi)\right]\frac{\delta^2}{3} + \frac{m\,U_\infty}{2\eta_l}\,f_2(\phi)\,\delta \quad . \qquad (\text{II-82})$$

Combining the continuity equation, energy equation and expression for mean film velocity (Equations (II-25), (II-28) and (II-82)), results in

$$\frac{\lambda_l\,\Delta T}{h_{fg}}\frac{1}{\delta} = \frac{d}{dx}\left\{\left[\frac{\rho_l^2\,g}{\eta_l}\,f_1(\phi) + \frac{\rho_l\,\rho_v\,U_\infty^2}{2a\,\eta_l}\,f_3(\phi) + \frac{3}{2}\,\frac{\rho_l\,\sigma}{\eta_l\,a^2}\,f_4(\phi)\right]\frac{\delta^3}{3}\right.$$
$$\left. + \frac{\rho_l\,\lambda_l\,\Delta T\,U_\infty}{2\,h_{fg}\,\eta_l}\,f_2(\phi)\,\delta\right\} \quad . \qquad (\text{II-83})$$

Using the relationship between dx and $d\phi$, and algebraically manipulating Equation (II-83) gives

$$\frac{1}{\delta^*} = \frac{D_e}{\chi(\phi)}\frac{d}{d\phi}\left\{\left[F\,f_1(\phi) + \frac{D_e}{2a}\,P\,f_3(\phi) + \frac{3}{2}\left(\frac{D_e}{a}\right)^2\frac{F}{Bo}\,f_4(\phi)\right]\frac{\delta^{*3}}{3}\right.$$
$$\left. + \frac{1}{2}\,f_2(\phi)\,\delta^*\right\} \qquad (\text{II-84})$$

where F and δ^* are as previously defined in Equation (II-64). P and Bo are

42

dimensionless parameters defined by:

$$P = \frac{\rho_v \, h_{fg} \, \eta_l}{\rho_l \, \lambda_l \, \Delta T}$$

$$Bo = \frac{\rho_l \, g \, D_e^2}{\sigma} \; .$$

(II-85)

P is related to the pressure gradient and Bo, the Bond number, relates the inertia effects to surface tension effects. Differentiating Equation (II-84) results in the following first order ordinary differential equation:

$$\frac{2\,\chi(\phi)}{D_e} = \left\{ \left[2\,F\,f_1(\phi) + \frac{D_e}{a}\,P\,f_3(\phi) + 3\left(\frac{D_e}{a}\right)^2 \frac{F}{Bo}\,f_4(\phi) \right] \delta^{*3} \right.$$

$$+ f_2(\phi)\,\delta^*\right\}\frac{d\delta^*}{d\phi} + \left\{ \left[2\,F\,f_1'(\phi) + \frac{D_e}{a}\,P\,f_3'(\phi) \right. \right.$$

(II-86)

$$\left. \left. + 3\left(\frac{D_e}{a}\right)\frac{F}{Bo}\,f_4'(\phi) \right] \frac{\delta^{*4}}{3} + f_2'(\phi)\,\delta^{*2} \right\}$$

In the previous development, film separation and instability were not applicable since no effects were considered which could retard the film flow and $(d\delta^*/d\phi)\to\infty$ only at $\phi_c = \pi$. However, in the present analysis, the decreasing potential flow and increasing radius of curvature of the elliptical cylinder causes the pressure gradient to have a retarding effect on the condensate film over the back half of the tube. At the point of condensate film separation from the tube wall, the film shear stress at the wall is negative which implies flow reversal ($du/dy \le 0$ at $y = 0$). Differentiating Equation (II-81) and solving for the film separation criteria ($du/dy = 0$ at $y = 0$) results in the following condition for separation to occur:

$$\left[2F\,f_1(\phi) + \frac{D_e}{a}\,P\,f_3(\phi) + 3\left(\frac{D_e}{a}\right)^2 \frac{F}{Bo}\,f_4(\phi) \right] \delta^{*3} + 2\,f_2(\phi)\,\delta^* \le 0 \; .$$

(II-87)

43

Condensate film instability occurs when the rate of change of film thickness is infinite. From Equation (II-86), this condition occurs when

$$\left[2F\, f_1(\phi) \;+\; \frac{D_e}{a}\, P\, f_3(\phi) \;+\; 3 \left(\frac{D_e}{a}\right)^2 \frac{F}{Bo}\, f_4(\phi) \right] \delta^{*3} \;+\; f_2(\phi)\, \delta^* = 0 \;. \qquad \text{(II-88)}$$

From a comparison of Equations (II-87) and (II-88), it is evident that the condition of film instability will occur first (has a smaller magnitude than the film separation criteria for all conditions) and is therefore the limiting condition. Rose [28] suggests that this instability may manifest itself in wavy or turbulent flow, or may signify the detachment of the liquid film from the tube surface. For the case where $1/Bo = 0$ (surface tension neglected), and using Equations (II-21),(II-47) and (II-76) for $f_1(\phi), f_2(\phi)$ and $f_3(\phi)$ in Equation (II-88), it can be seen that the condition for which solutions can be determined over the entire tube surface occurs when

$$P < \frac{a}{D_e} \left(\frac{k}{1+k}\right)^2 F \qquad \text{(II-89)}$$

For a circular tube ($k=1$), Equation (II-89) reduces to $P < F/8$, which was that found by Rose [28]. If the opposite of Equation (II-89) is true, then the pressure gradient effect is dominant enough to significantly retard the flow over the back half of the tube and result in a rapid thickening of the condensate film. Note that the condition for condensate film instability is a function of vapor velocity (F) since the pressure gradient due to potential flow is velocity dependent.

For the case where $P = 0$, and using Equation (II-88), the condition which allows solution of the momentum equation over the entire tube is now given by

$$\frac{1}{Bo} < \frac{1}{3} \left(\frac{a}{D_e}\right)^2 \frac{k^4}{1-k^2} \;. \qquad \text{(II-9?)}$$

44

Note here that the condition for film instability is only a function of geometry. Therefore, for small values of eccentricity (approaching a vertical flat plate), the retarding effect of surface tension on the condensate film over the back half of the tube is significant and can result in a rapid thickening of the condensate film at ϕ_C.

The initial condition for this problem is again based on symmetry, which requires that $(d\delta^*/d\phi)_{\phi=0} = 0$. Combining this condition with Equation (II-86) results in a fourth order expression for δ^*:

$$\left[2 F f_1'(0) + \frac{D_e}{2a} P f_3'(0) + 3 \left(\frac{D_e}{a} \right) \frac{F}{Bo} f_4'(0) \right] \frac{\delta^{*4}}{3} + f_2'(0) \delta^{*2} - \frac{2 \chi(0)}{D_e} = 0 \quad \text{(II-91)}$$

whose root of interest is determined by

$$A = \frac{1}{3} \left[2F f_1'(0) + \frac{D_e}{a} P f_3'(0) + 3 \left(\frac{D_e}{a} \right)^2 \frac{F}{Bo} f_4'(0) \right]$$

$$B = f_2'(0)$$

$$C = -\frac{2\chi(0)}{D_e} \quad \text{(II-92)}$$

$$\delta^*(0) = \sqrt{\frac{\sqrt{B^2 - 4 A C} - B}{2A}} \quad .$$

Equation (II-86) can be solved numerically to obtain the condensate film thickness. The other heat transfer parameters are determined as before (Equations (II-39) and (II-56)).

It can be shown that this formulation reduces to the models developed for circular tubes. Consider the case where $k=1$ and $1/Bo=0$ (circular tube with no surface tension); Equation (II-84) reduces to:

$$\frac{1}{\delta^*} = \frac{d}{d\phi} \left\{ [2 F \sin\phi + 8 P \sin2\phi] \frac{\delta^{*3}}{3} + 2 \delta^* \sin\phi \right\} \quad . \quad \text{(II-93)}$$

which is identical to that developed by Rose [28] where

$$\delta^{\bullet} = \delta \left(\frac{U_{\infty} \rho_l}{2a\ \eta_l} \right) = \frac{1}{\sqrt{2}}\ \delta^{\bullet}_{Rose} \quad . \tag{II-94}$$

For the case where $k=1$, $P=0$ and $1/Bo=0$ (circular tube, no surface tension and no pressure gradient), Equation (II-84) reduces to the Shekriladze-Gomelauri [21] model.

F. MIXED CONVECTION CONDENSATION ON AN ELLIPTICAL CYLINDER WITH VAPOR BOUNDARY LAYER SEPARATION (FUJII ET AL. [22] TYPE ANALYSIS)

The mixed convection model developed by Shekriladze and Gomelauri [21] has been used because of its simplicity and ease of solution. However, since the interfacial shear is approximated by an asymptotic expression based on an infinite condensation rate and uses potential flow outside the vapor boundary-layer (which is always positive), vapor boundary-layer separation does not occur. As described in Chapter I, Fujii et al. [22] modified the interfacial shear stress expression by simultaneously solving the boundary-layer equations for the condensate and vapor ensuring compatibility at the condensate/vapor interface. This technique allows for a more precise description of the condensation problem under forced convection conditions and includes vapor boundary-layer separation.

Consider a pure saturated vapor at temperature T_{sat}, flowing downward over a horizontal elliptical cylinder with free stream velocity, U_{∞}. The elliptical cylinder is oriented such that its major axis is aligned with the direction of gravity and vap flow. Due to the complexities of solving the two-phase boundary-layer equation, it is as ied that the only forces acting on the condensate film element are gravity and v. s forces. Surface tension and pressure gradient are neglected which is reasonable s e they were found to have negligible influence under most conditions (discusse n

46

Chapter IV). Other assumptions are the same as in Section II.E. The vapor is assumed to be in thermal equilibrium such that the energy equation for the vapor need not be considered in the analysis. The only forces acting on an element in the vapor boundary-layer (see Figure II-6) are inertia, viscosity and pressure gradient, which is impressed upon the element by potential flow outside the vapor boundary-layer. The tangential
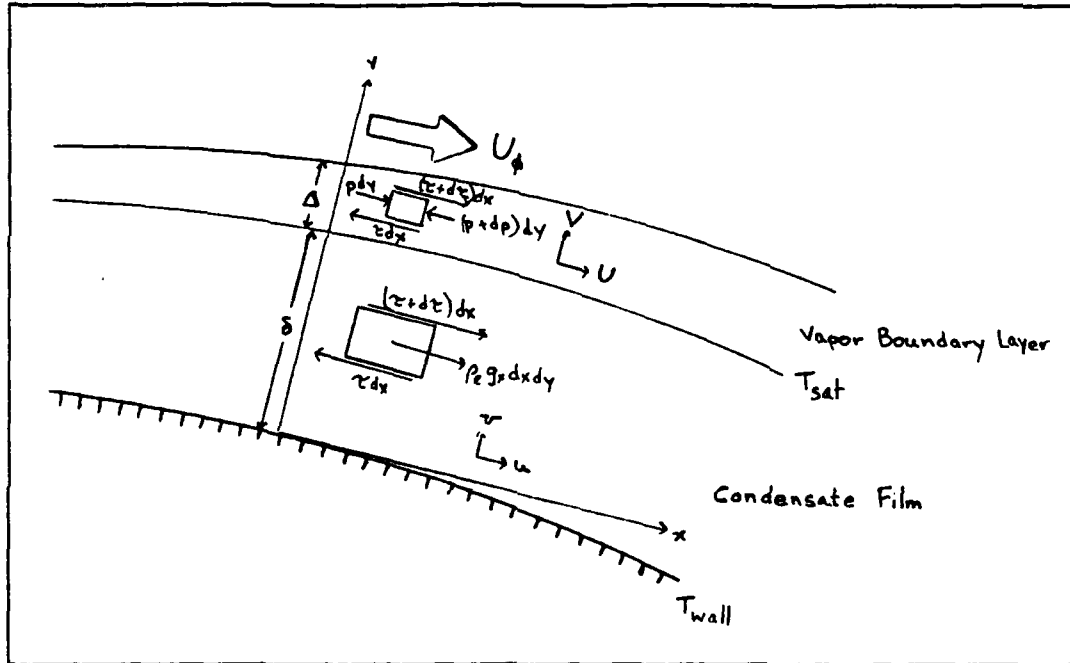
Figure II-6. Condensate Film and Vapor Elements for Mixed Convection using Fujii et al. [22] Type Model.

velocity at the vapor/condensate interface is much smaller than the potential velocity outside the vapor boundary-layer and can therefore be assumed to be negligible. Based on the above assumptions, conservation of mass and momentum for the vapor boundary-layer are given by

$$\frac{\partial U}{\partial x} + \frac{\partial V}{\partial y} = 0 \quad (continuity) \ (a)$$

$$U \frac{\partial U}{\partial x} + V \frac{\partial U}{\partial y} = U_\phi \frac{dU_\phi}{dx} + \frac{\eta_v}{\rho_v} \frac{\partial^2 U}{\partial y^2} \quad (momentum) \ (b)$$

(II-95)

47

For the condensate film, conservation of mass, momentum and energy are given by

$$\frac{\eta_l}{\rho_l} \frac{\partial^2 u}{\partial y^2} + g f_1(\phi) = 0 \qquad (momentum) \ (a)$$

(II-96)

$$m = \frac{d}{dx}\{\rho_l u_m \delta\} = \frac{\lambda_l (T_{sat}-T_{wall})}{h_{fg} \delta} \qquad (energy \ and \ mass) \ (b) \quad .$$

where conservation of mass and energy have been combined as in previous sections. Boundary conditions for this system of equations are given by

$$u_{y=0} = v_{y=0} = 0$$

(II-97)

$$U_{y=\delta+\Delta} = U_\phi , \qquad \left(\frac{\partial U}{\partial y}\right)_{y=\delta+\Delta} = 0 \quad .$$

where Δ is the vapor boundary-layer thickness. The compatibility conditions at the interface require that

$$U_{y=\delta} = u_{y=\delta} = 0 , \qquad \eta_l \left(\frac{\partial u}{\partial y}\right)_{y=\delta} = \eta_v \left(\frac{\partial U}{\partial y}\right)_{y=\delta} = \tau_\delta$$

(II-98)

$$and \quad -\rho_v V_{y=\delta} = \frac{\lambda_l (T_{sat}-T_{wall})}{h_{fg} \delta} \quad ,$$

where the last compatibility relation is the condensation mass flux rate (i.e. for a given surface area, the amount of vapor condensed must equal the increase in the mass of the film).

The technique for solving the vapor boundary-layer momentum equation involves an approximate integral technique developed by Truckenbrodt [23]. The initial problem development follows the method of Pohlhausen [36]. The continuity and momentum equations (Equations (II-95a) and (II-95b)), are integrated over the thickness of the boundary layer from $y = \delta$ to $y = \delta+\Delta$ and then combined to eliminate the normal component of vapor velocity, V, resulting in a momentum integral equation

$$\frac{1}{U_\phi^2} \frac{d}{dx}\{U_\phi^2 \Delta_2\} + \frac{\Delta_1}{U_\phi} \frac{dU_\phi}{dx} = \frac{V_\delta}{U_\phi} + \frac{\tau_\delta}{\rho_v U_\phi^2}$$

(II-99)

48

where Δ_1 and Δ_2 are the vapor boundary layer displacement and momentum thicknesses given respectively by

$$\Delta_1 = \int_\delta^{\delta+\Delta} \left(1 - \frac{U}{U_\phi}\right) dy$$

$$\text{and} \quad \Delta_2 = \int_\delta^{\delta+\Delta} \frac{U}{U_\phi} \left(1 - \frac{U}{U_\phi}\right) dy \quad , \tag{II-100}$$

V_δ is the normal component of vapor velocity at the vapor/condensate interface due to the condensation process itself and is sometimes called the vapor boundary-layer suction velocity. Differentiating the Δ_2 term in Equation (II-99) and rearranging the equation results in:

$$\frac{d\Delta_2}{dx} + \frac{\Delta_2}{U_\phi} \frac{dU_\phi}{dx} \left(2 + \frac{\Delta_1}{\Delta_2}\right) = \frac{V_\delta}{U_\phi} + \frac{\tau_\delta}{\rho_v U_\phi^2} \quad . \tag{II-101}$$

With some further algebraic manipulation this yields

$$\frac{d}{dx}\left\{\frac{\Delta_2^2 \rho_v}{\eta_v}\right\} = \frac{2}{U_\phi}\left[\frac{\tau_\delta \Delta_2}{\eta_v U_\phi} - \left(2 + \frac{\Delta_1}{\Delta_2}\right)\frac{\Delta_2^2 \rho_v}{\eta_v}\frac{dU_\phi}{dx} + \frac{V_\delta \Delta_2 \rho_v}{\eta_v}\right] \quad . \tag{II-102}$$

To solve this expression, the vapor velocity distribution across the boundary-layer thickness must be determined. This distribution is a function of a pressure gradient parameter, κ, and a suction parameter, κ_1, given by Tuckenbrodt [23] as

$$\kappa = \frac{\Delta_2^2 \rho_v}{\eta_v}\frac{dU_\phi}{dx} \quad \text{and} \quad \kappa_1 = -\frac{V_\delta \Delta_2 \rho_v}{\eta_v} \quad . \tag{II-103}$$

Truckenbrodt [23] defined a shear function $f(\kappa,\kappa_1)$ and a shape function $H(\kappa,\kappa_1)$ as:

$$f(\kappa,\kappa_1) = \frac{\tau_\delta \Delta_2}{\eta_v U_\phi} \quad \text{and} \quad H(\kappa,\kappa_1) = \frac{\Delta_1}{\Delta_2} \tag{II-104}$$

and a dimensionless function, Z, given by

$$Z = Re_v \left(\frac{\Delta_2}{D_e}\right)^2 \tag{II-105}$$

49

Equation (II-102) becomes

$$D_e \frac{dZ}{dx} = 2\frac{U_\infty}{U_\phi} \left[f - (2+H) \kappa - \kappa_1 \right] \quad . \tag{II-106}$$

Based on existing theoretical data (Schlicting [37] and Torda [38]), Truckenbrodt [23] proposed a simple linear approximation for Equation (II-106) given by

$$D_e \frac{dZ}{dx} = \frac{U_\infty}{U_\phi} \left[0.441(1-2\kappa_1) - 6\kappa \right] \quad . \tag{II-107}$$

Substituting Equations (II-103), (II-105) and (II-106) into Equation (II-107) and defining dimensionless velocities by

$$\bar{U}_\phi = \frac{U_\phi}{U_\infty} \quad and \quad \bar{V}_\delta = \frac{V_\delta}{U_\infty} \quad , \tag{II-108}$$

results in

$$\frac{dZ}{d\phi} = \frac{1}{\bar{U}_\phi} \frac{\chi(\phi)}{D_e} \left\{ 0.441 \left[1 + 2\bar{V}_\delta \sqrt{Re_v}\, Z \right] - 6 \frac{D_e}{\chi(\phi)} \frac{d\bar{U}_\phi}{d\phi} Z \right\} \quad . \tag{II-109}$$

The dimensionless suction velocity, V_δ, is determined by transforming the compatibility relation involving the condensate mass flux rate in Equation (II-98) and is given by

$$-\bar{V}_\delta \sqrt{Re_v} = \frac{G}{\delta^*} \tag{II-110}$$

where G is a dimensionless parameter which is proportional to the condensation rate and is defined by

$$G = \frac{\lambda_l (T_{sat} - T_{wall})}{\eta_l h_{fg}} \sqrt{\frac{\rho_l \eta_l}{\rho_v \eta_v}} \quad . \tag{II-111}$$

Combining Equations (II-109) and (II-110), the governing equation for the vapor-boundary layer becomes

$$\frac{dZ}{d\phi} = \frac{1}{\bar{U}_\phi} \frac{\chi(\phi)}{D_e} \left\{ 0.441 \left[1 - 2\frac{G}{\delta^*}\sqrt{Z} \right] - 6 \frac{D_e}{\chi(\phi)} \frac{d\bar{U}_\phi}{d\phi} Z \right\} \quad . \tag{II-112}$$

The initial condition for Equation (II-112) comes from symmetry and is given by

$$\left(\frac{dZ}{d\phi}\right)_{\phi=0} = 0 \quad .$$

(II-113)

Combining Equations (II-112) and (II-113) results in

$$6 \frac{D_e}{\chi(0)} \left(\frac{d\bar{U}_\phi}{d\phi}\right)_{\phi=0} (\sqrt{Z(0)})^2 + 0.882 \; G \frac{1}{\delta^*}(0) \sqrt{Z(0)} - 0.441 = 0 \quad .$$

(II-114)

This is a quadratic equation from which $Z(0)$ is determined to be,

$$Z(0) = \left[-0.0735 \; G \frac{\chi(0)}{D_e} \left(\frac{d\bar{U}_\phi}{d\phi}\right)_{\phi=0}^{-1} \frac{1}{\delta^*(0)} \right.$$

$$\left. + \sqrt{\left(0.0735 \; G \frac{\chi(0)}{D_e} \left(\frac{d\bar{U}_\phi}{d\phi}\right)_{\phi=0}^{-1} \frac{1}{\delta^*(0)}\right)^2 + 0.0735 \frac{\chi(0)}{D_e} \left(\frac{d\bar{U}_\phi}{d\phi}\right)_{\phi=0}^{-1}} \right]^2 .$$

(II-115)

The interfacial shear is determined from Equation (II-104). Truckenbrodt [23] provides a simple approximation for the shear function, $f(\kappa,\kappa_1)$, given by

$$f(\kappa,\kappa_1) = 3.22 \sqrt{\kappa_a (\kappa_a + \kappa)}$$

(II-116)

where

$$\kappa_a = 0.0682 + 0.174 \; \kappa_1 \quad .$$

(II-117)

κ and κ_1 are modified by combining Equations (II-103) and (II-105):

$$\kappa = \frac{D_e}{\chi(\phi)} \frac{d\bar{U}_\phi}{d\phi} Z \quad and \quad \kappa_1 = \frac{G}{\delta^*}\sqrt{Z} \quad .$$

(II-118)

Dimensionless interfacial shear is defined by:

$$\bar{\tau}_\delta = \frac{2\sqrt{Re_\nu} \; \tau_\delta}{\rho_\nu \; U_\infty^2} \quad .$$

(II-119)

An expression for dimensionless shear can then be obtained by combining Equations (II-104), (II-105) and (II-116):

$$\bar{\tau}_\delta = 6.44 \frac{\bar{U}_\phi}{\sqrt{Z}} \sqrt{\kappa_a (\kappa_a + \kappa)} \quad .$$

(II-120)

51

The governing equations for the condensate film are solved in the usual manner. The momentum equation (Equation (II-96a)), is integrated to solve for condensate film velocity,

$$u = \frac{\rho_l \, g}{\eta_l} f_1(\phi) \left(\delta y - \frac{y^2}{2} \right) + \frac{\tau_\delta}{\eta_l} y \quad . \tag{II-121}$$

The mean velocity is determined from Equation (II-24):

$$u_m = \frac{\rho_l \, g}{\eta_l} f_1(\phi) \frac{\delta^2}{3} + \frac{\tau_\delta}{2\eta_l} \delta \quad . \tag{II-122}$$

Substituting Equation (II-122) into the energy/continuity equation (Equation (II-96b)) and multiplying both sides of the equation by

$$\frac{\eta_l^2 \, D_e^2 \, h_{fg}}{\rho_l^2 \, U_\infty^2 \, \lambda_l \, (T_{sat} - T_{wall})} \tag{II-123}$$

results in

$$\frac{1}{\delta^*} - \frac{D_e}{\chi(\phi)} \frac{d}{d\phi} \left\{ F \, f_1(\phi) \, \frac{\delta^{*3}}{3} + \frac{1}{4} \frac{1}{G} \, \bar{\tau}_\delta \, \delta^{*2} \right\} \quad . \tag{II-124}$$

Carrying out the differentiation of Equation (II-124) and rearranging results in the ordinary differential equation,

$$\frac{d\delta^*}{d\phi} = \frac{\dfrac{\chi(\phi)}{D_e} - \dfrac{F}{3} \dfrac{d f_1}{d\phi} \delta^{*4} - \dfrac{1}{4} \dfrac{1}{G} \dfrac{d \bar{\tau}_\delta}{d\phi} \delta^{*3}}{F \, f_1(\phi) \, \delta^{*3} + \dfrac{1}{2} \dfrac{1}{G} \bar{\tau}_\delta \, \delta^{*2}} \quad , \tag{II-125}$$

which, due to the symmetry of the problem, has the initial condition,

$$\left(\frac{d\delta^*}{d\phi} \right)_{\phi=0} = 0 \quad . \tag{II-126}$$

Combining Equations (II-125) and (II-126) results in

$$\frac{\chi(0)}{D_e} - \frac{F}{3}\left(\frac{df_1}{d\phi}\right)_{\phi=0} \delta^{*4}(0) - \frac{1}{4}\frac{1}{G}\left(\frac{d\bar{\tau}_\delta}{d\phi}\right)_{\phi=0} \delta^{*3}(0) = 0 \qquad (II-127)$$

from which $\delta^*(0)$ can be determined by numerical methods.

For the case of $k = 1$ (circular tube), Equation (II-125) reduces to the analysis of Fujii et al. [22] as corrected by Lee and Rose [25]. The differential equation for the vapor boundary-layer (Equation (II-112)) and for the condensate film (Equation (II-125)) are solved simultaneously using the compatibility relations of Equations (II-117), (II-118) and (II-120). At the point of vapor boundary-layer separation, the interfacial shear stress becomes negative. Downstream of this point, it is assumed that the shear stress at the vapor/condensate interface is negligible and a simple Nusselt type analysis is used for the remainder of the elliptical surface. The heat transfer parameters are determined as before (Equations (II-39) and (II-56)).

53

III. NUMERICAL METHOD

In the theoretical development, the governing equations for each model were either reduced to a single first order ordinary differential equation (ODE) or to a simultaneous solution of a system of first order ODEs of the form

$$\frac{dy}{dx} = fn(x,y) \quad . \tag{III-1}$$

Initial conditions were determined from the symmetry of the problem which required that both the slopes of the condensate film and vapor boundary-layer were zero at $\phi = 0$. These systems of equations are solved using one of the forward stepping numerical methods.

A. SOLUTION TECHNIQUE FOR THE NUSSELT [5] AND SHEKRILADZE-GOMELAURI [21] ANALYSIS METHODS

Each analysis method resulted in a single first order ODE of the form given by Equation (III-1). The solution of this equation provides the condensate film thickness along the elliptical tube surface. Many numerical methods are available to solve this type of problem, each with its own advantages and disadvantages. For this study, a fifth order Adams method predictor-corrector algorithm was developed from Crandall [39]. The Adams methods are multi-step techniques which use finite difference type operators incorporating previously determined points (hence the term multi-step) to determine the value corresponding to the next step. These methods provide the same accuracy and are more efficient than the Runge-Kutta (single step) methods but re restricted to a fixed step size. The Adams method employed in this study uses an Adams-Bashforth explicit method [39] to predict the value of the dependent variable at the next step and then an Adams-Moulton implicit method [39] to correct this predicted

54

value. This method is not self starting and requires determination of the first four points. To start-up the algorithm, lower order Adams methods were used to obtain these four points. The recurrence formulae for this algorithm are given by

$$y_s = y_{s-1} + h \sum_k \beta_k fn(x_k, y_k) \tag{III-2}$$

where x is the independent variable, y is the dependent variable, h is the step size, s is the step number for which y is to be determined, k are the points determined in previous steps and β_k are the coefficients provided in Table III-1 and III-2.

TABLE III-1. RECURRENCE COEFFICIENTS FOR PREDICTOR FORMULA

FORMULA	β_k					TRUNCA-TION ERROR
	s-5	s-4	s-3	s-2	s-1	
(1)					1	$O(h^2)$
(2)				-1/2	3/2	$O(h^3)$
(3)			5/12	-16/12	23/12	$O(h^4)$
(4)		-9/24	37/24	-59/24	55/24	$O(h^5)$

TABLE III-2. RECURRENCE COEFFICIENTS FOR CORRECTOR FORMULA

FORMULA	β_k					TRUNCA-TION ERROR
	s-4	s-3	s-2	s-1	s	
(1)				1/2	1/2	$O(h^3)$
(2)			-1/12	8/12	5/12	$O(h^4)$
(3)		1/24	-5/24	19/24	9/24	$O(h^5)$
(4)	-19/720	106/720	-264/720	646/720	251/720	$O(h^6)$

The algorithm used in the solution for mixed convection condensation with surface tension and pressure gradient (Section II.E) is provided in Appendix (B).

For many applications, this type of start-up routine would normally not provide sufficient accuracy. However, no difficulties were encountered using this numerical procedure for solving the asymptotic interfacial shear stress models. Solution convergence was obtained for an angle step size of 0.1°. The difference between an angle step size of 1.0° and 0.1° was less than 1%.

B. SOLUTION TECHNIQUE FOR THE FUJII ET AL. [22] ANALYSIS METHOD

Reduction of the governing equations resulted in a system of two simultaneous ODEs, one for the momentum thickness of the vapor boundary-layer and one for the condensate film thickness. The Adams method previously described did not provide sufficient accuracy to solve this two-phase boundary layer problem. In particular, the system of equations exhibited a stiffness problem, i.e., the numerical method could not accurately solve the vapor boundary-layer ODE over the first several steps even with an angle step size of 0.001°. To obtain sufficient accuracy, a much smaller step size would be required which would significantly reduce the efficiency of the computer algorithm. Lee [40] indicated that similar difficulties had been encountered when Lee and Rose [25] solved the same equations for a horizontal circular cylinder. Lee and Rose [25] used a Runge-Kutta method which permitted variable step size. Thus, the step size could be reduced sufficiently to obtain the required accuracy for the vapor boundary-layer ODE over the front of the tube and then increased over the remainder of the tube to improve the efficiency of the algorithm. Utilizing this numerical procedure, they were able to solve the system of equations over most of the range of dimensionless parameters (F and G). However, in some cases (specifically large values of F and G), the system of equations were still too stiff for solution.

To overcome the problem of stiffness, a numerical problem solver (IVPAG) from the International Mathematical and Statistical Library (IMSL) [41] was used. This

algorithm uses Gear's stiff method [42] to efficiently solve systems in which stiffness is a problem. However, as in the study of Lee and Rose [25], this method could still not solve the two-phase boundary-layer equations over the entire range of dimensionless parameters considered, but did cover the practical ranges of the parameters.

It was originally conceived that the computer algorithm would progress around the tube surface until the criteria for vapor boundary-layer separation was reached $(d\tau_\delta/d\phi < 0)$. At this point, the model would shift from solution of the two-phase boundary-layer equations to the simple Nusselt model. However, the numerical solver encountered difficulties in solving the system of equations as it approached the point of vapor boundary-layer separation. Therefore, the solution method was changed to a two step procedure. In the first step, the system of equations were solved until the computer algorithm indicated a problem had been reached (usually the algorithm indicated a stiffness problem had been encountered). The interfacial shear stress data was analyzed to verify that this problem was the result of rapidly changing conditions associated with vapor boundary-layer separation. Therefore, to facilitate the solution, vapor boundary-layer separation was assumed to have occurred if the interfacial shear stress at the last point obtainable was less than ten percent of the maximum interfacial shear stress observed over the surface. At this point, the problem solver was within one to two step sizes of the actual separation point (for a step size of 0.1°, the computed separation point was therefore within 0.2° of the actual separation point). The second step involved re-running the analysis using the computed separation point calculated in the first step as the point at which the two-phase model was switched to the simple Nusselt model. A converged solution was obtained for an angle step size of 0.1°. The algorithm for solving the two-phase model is provided in Appendix (C).

IV. RESULTS AND DISCUSSION

When comparing solutions for an elliptical tube with those of a circular tube, equivalent surface areas have been used. The effective diameter of the equivalent circular cylinder is given by Equation (II-16). The dimensionless streamwise length x^*, defined as the ratio of the streamwise length, x, to the half perimeter length and given by

$$x^* = \frac{2\,x}{\pi\,D_e} \quad , \tag{IV-1}$$

is used when comparing local values of film thickness and heat-transfer coefficients. Its use enables direct comparison between elliptical and circular tubes since it represents an equivalent fraction of the total perimeter from the top of the tube to the dimensionless point.

A practical range of eccentricities for an elliptical tube with major axis aligned vertically is $0.3 < k < 0.6$. The lower limit of 0.3 is based on discussions with a tube manufacturer (Reference [43]) in which the elliptical tube is formed by pressing a circular tube with a roller assembly to obtain the proper major and minor axis dimensions. Roller contact points would be evenly spaced to maintain the elliptical curvature and to prevent an overly flat surface. The upper limit is chosen as the eccentricity in which noticeable effects were observed in the heat transfer characteristics (as discussed in this chapter).

A. EFFECT OF GRAVITY

As previously noted (Section I.A), some improvement in condensation heat transfer is expected for an elliptical tube in quiescent vapor compared to a circular one since more of the surface is aligned with gravity. By increasing the "effect" of gravity on the

58

condensate film, the mean condensate velocity at a given streamwise location is increased which results in a thinning of the condensate film and increased heat transfer. The gravity function, $f_1(\phi)$, defined in Equation (II-21) is shown in Figure IV-1.
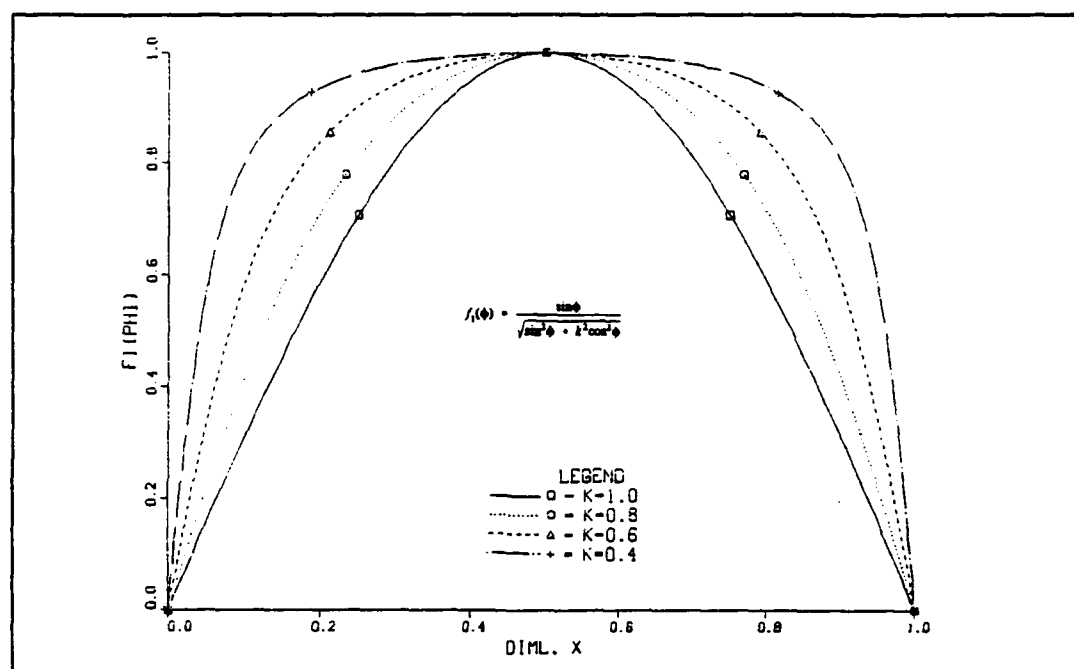
Figure IV-1. Gravity Function, $f_1(\phi)$ vs. Streamwise Length, x^*.

As the elliptical tube approaches a flat plate configuration $(k \to 0)$, the effect of gravity increases to sweep the condensate film along the tube surface. The effect of gravity on the local film thickness is shown in Figure IV-2 for two eccentricities. As can be seen, the condensate film is thinned over the front and rear portion of the tube compared to a circular tube but is slightly thicker in the middle region. The thickness of the film is controlled by the rate of condensation (which is dependent on condensate film thickness) and the condensate velocity (which is also dependent on condensate film thickness and gravity). Near the top of the elliptical tube, the larger gravity component

increases the condensate velocity relative to that of a circular tube resulting in a thinner condensate film. This thinner film, however, results in an increased condensation rate which tends to thicken the film further downstream. Since the elliptical tube has a greater condensation rate near the top of the tube, the film thickens
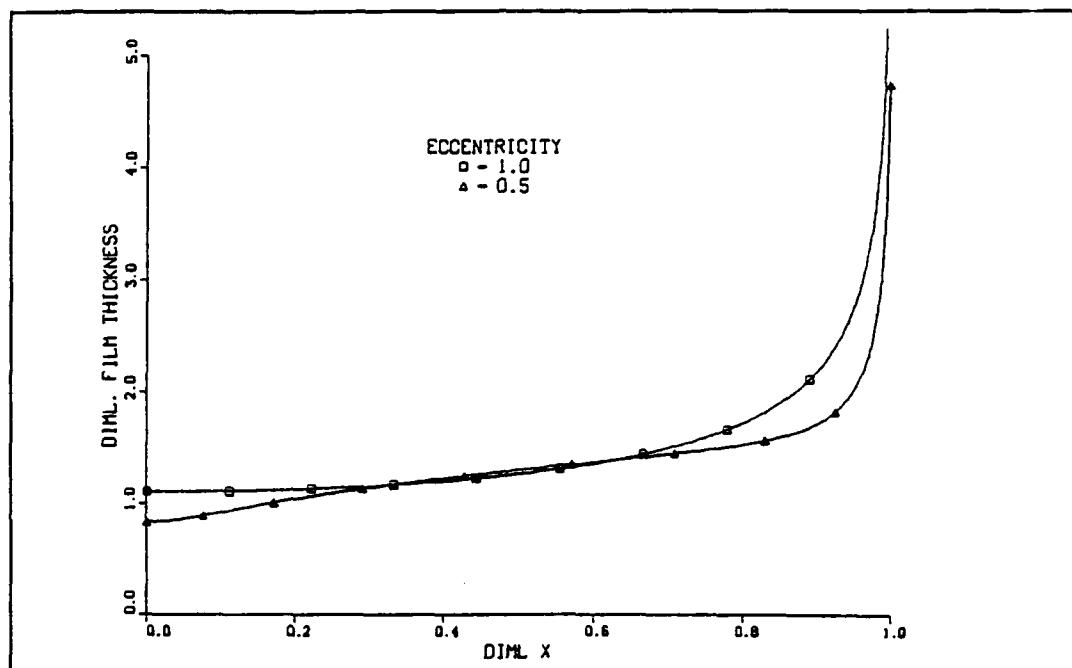
Figure IV-2. Local Film Thickness for Varying Eccentricity (k).

more rapidly compared to that on a circular tube causing the relatively thicker film in the middle region as seen in the figure. At 90°, the gravity component is the same as on a circular tube and so has no relative thinning effect. Over the rear half of the tube, the reduced condensation rate (as a result of this thicker condensate film) and increased velocity due to the larger gravity component relative to a circular tube results in continued thickening of the film on the elliptical tube, but at a slower rate than that on a circular tube. Eventually, the elliptical tube film thickness is again thinner than on a circular tube for the same dimensionless streamwise length. The condensate film

thickness is therefore determined by a balance of the effects of two effects: increased condensate velocity (which tends to thin the film) and increased condensation rate (which tends to thicken the film).

The overall effect on the mean heat-transfer coefficient (given as a mean Nusselt number) is shown in Figure IV-3. To compare the elliptical tube with a circular tube, the leading coefficient of the Nusselt solution (Equation I-3b) is plotted against
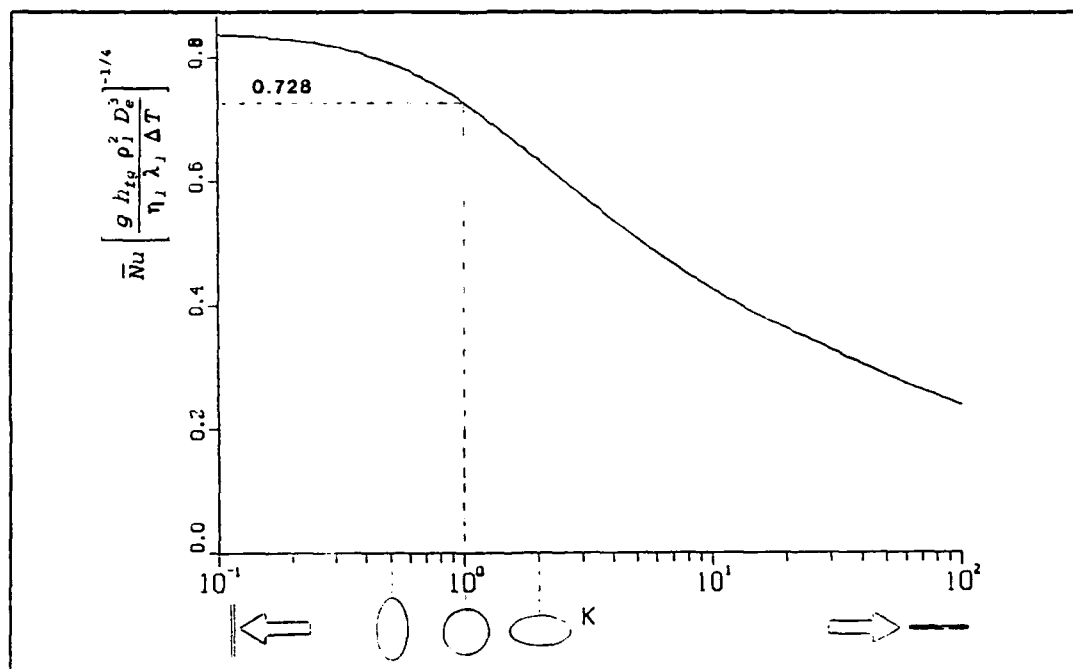
Figure IV-3. Mean Nu Leading Coefficient for Varying k.

eccentricity. Solutions for a circular cylinder ($k = 1.0$) and a vertical flat plate ($k \rightarrow 0$, $L \doteq 2a$) agree well with the results of Nusselt [5]. For the horizontal flat plate ($k \rightarrow \infty$), the heat-transfer coefficient approaches zero as would be predicted by the Nusselt model. For the practical range of eccentricities ($0.3 < k < 0.6$), it can be seen that the effect of placing more of the tube surface in the direction of gravity is to increase the mean heat-transfer coefficient by 7% for $k = 0.6$ and 13% for $k = 0.3$. Conversely, by

placing more of the tube surface perpendicular to the direction of gravity (i.e., approaching a horizontal flat plate), the mean heat-transfer coefficient decreases as expected. These results are in agreement with earlier elliptical tube studies [32,33].

B.   EFFECT OF VAPOR VELOCITY

1.   Asymptotic Interfacial Shear Stress Approximation

The streamlined shape of the elliptical tube has an effect on the vapor flow over the tube. The vapor velocity function, $f_2(\phi)$, defined by Equation (II-47) is shown in Figure IV-4 versus dimensionless streamwise length x^*. As seen in the figure, the elliptical tube experiences higher vapor velocities than a circular tube at the front and rear of the tube but a lower vapor velocity in the central region. Using a balance of the
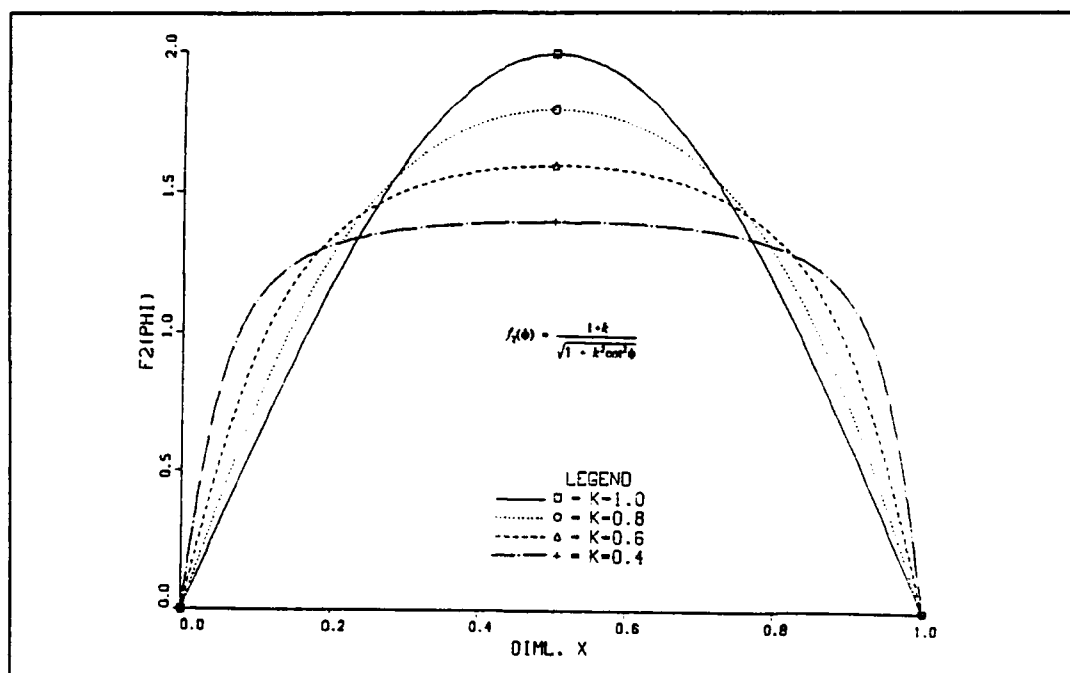
Figure IV-4. Vapor Velocity Function, $f_2(\phi)$, for Varying k.

factors which thicken and thin the condensate film. for the case of pure forced convection ($F \rightarrow 0$, no gravity effect), the higher relative vapor velocity at the top of the elliptical tube results in a larger interfacial shear stress and hence a thinner condensate film and larger condensation rate compared to a circular tube. With more condensate flowing into the middle section of the elliptical tube and a lower relative vapor velocity, the condensate film thickens more rapidly than in the case of a circular tube. As the condensate flows over the rear of the tube, the decreased condensation rate (due to the thicker film in the middle region) and increased vapor shear results in thinner film compared to the circular tube. Figure IV-5 shows these effects in detail for a
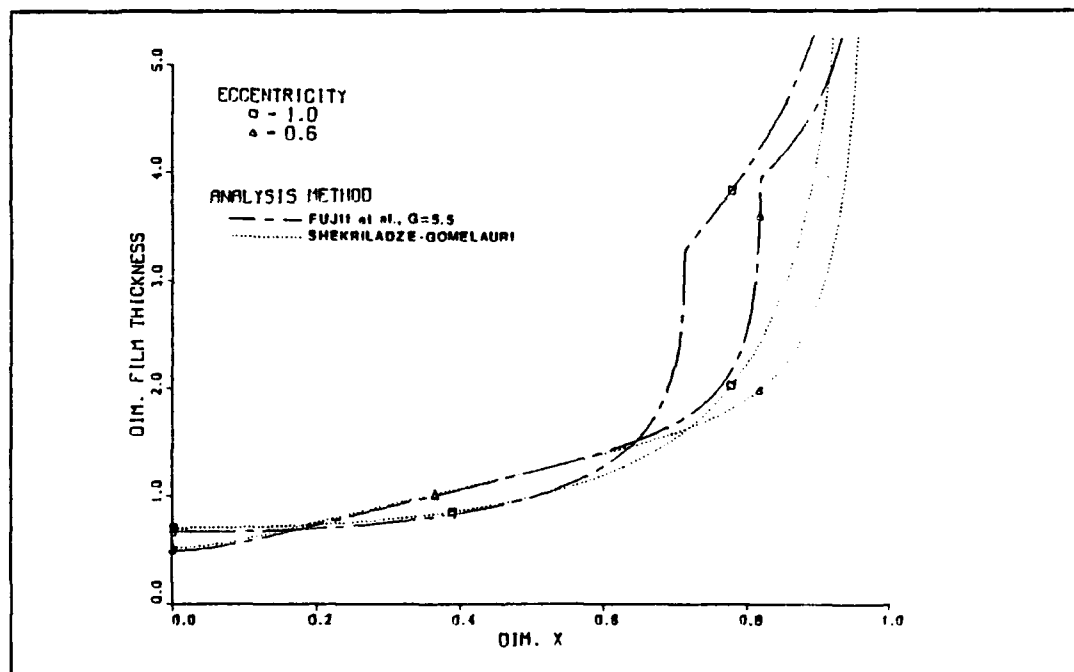
Figure IV-5. Effect of Vapor Velocity on Local Film Thickness for a Circular Tube and Elliptical Tube ($k = 0.6$).

circular tube ($k = 1$) and an elliptical tube ($k = 0.6$) using the asymptotic interfacial shear stress (Shekriladze-Gomelauri) approximation and the two-phase boundary layer

shear stress (Fujii et al.) approximation (to be discussed later). Whereas the gravity effect ($f_1(\phi)$) described in Section IV.A was always larger for the elliptical tube (see Figure IV-1), the vapor shear effect $f_2(\phi)$ is larger or smaller depending on the section of the tube to be analyzed (see Figure IV-4). The overall effect of vapor shear using the Shekriladze-Gomelauri [21] model is to reduce (by about 2% in the practical range of eccentricities) the elliptical tube mean heat-transfer coefficient relative to an equivalent circular tube.

In the mixed convection region, the mean heat-transfer coefficient of an elliptical tube is increased or decreased compared to a circular tube depending on the relative magnitudes of the vapor shear and gravity effects. This relative magnitude is measured by dimensionless parameter, F. For large F, gravity is dominant and the heat-transfer coefficient trend is described in Section IV.A . For small F, vapor shear is dominant and the trends described in this section determine the heat transfer. Figure IV-6 shows
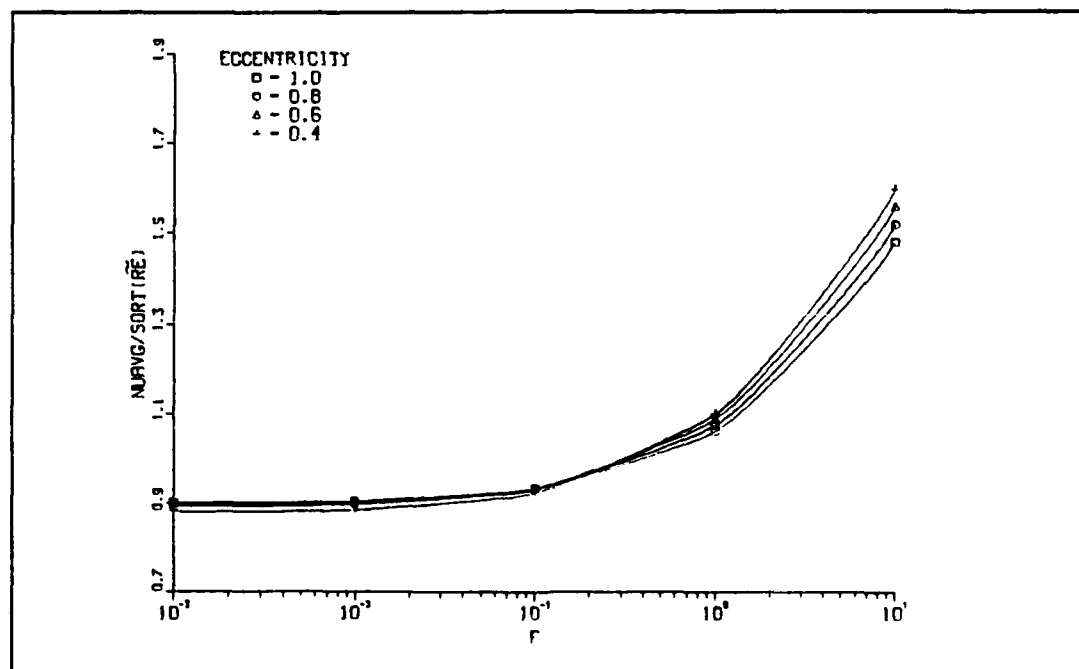
Figure IV-6. Effects of Vapor Velocity on Mean Nu Using the Asymptotic Interfacial Shear Stress Approximation Analysis Method.

64

the effect of F on the mean heat-transfer coefficient for varying eccentricity. As $F \to \infty$, corresponding to free convection condensation, solutions for elliptical and circular tubes match those reported in Section IV.A. For the case of a circular tube for all values of F, the present numerical solutions are within 0.4% of an equation by Rose [28]:

$$\overline{Nu} \ \tilde{Re}^{-1/2} = \frac{0.9 + 0.728 \ F^{1/2}}{(1 + 3.44 \ F^{1/2} + F)^{1/4}} \ . \tag{IV-2}$$

2.   Two-Phase Boundary-Layer Shear Stress Approximation

Vapor boundary-layer separation is not predicted by the asymptotic shear stress approximation since the interfacial shear is based on potential flow outside the vapor boundary-layer which is always positive. Solution of the two-phase boundary-layer equations for the condensate and vapor, with matched shear stress at the interface, allows determination of the vapor boundary-layer separation point and its effect on the condensation heat transfer. The analysis also introduces a dimensionless parameter G which is proportional to the condensation rate. Figure IV-5 compares the asymptotic shear stress approximation with the two-phase boundary layer shear stress approxima-tion for a large condensation rate (large G) for a circular and elliptical tube ($k = 0.6$). Over the forward and middle sections of the tube, the general trends are as described in Section IV.B.1 for the asymptotic shear stress approximation. Over the rear of the tube, however, as the separation point is approached, the condensate film thickens more rapidly due to the reduced vapor shear effect ($\tau \to 0$). It can be seen that for the elliptical tube, the separation point occurs further downstream than for the circular tube and thus this rapid thickening is delayed. By delaying separation, more of the tube surface has a thinner film. This serves to increase the heat-transfer coefficient for an elliptical tube compared to a circular tube if it were the only effect considered.

In total, however, the mean heat-transfer coefficient is affected by a combination of gravity, vapor shear and boundary-layer separation. Figure IV-7 shows the effect of F, G and k on the vapor boundary-layer separation point $(x_S^{\bullet})$. As previously explained (Chapter III), solutions could not be obtained for all possible F and G combinations (particularly large F and G). In general, as F and G increase (less vapor shear and higher condensation rate), or k decreases (more elliptical), the vapor separation point shifts toward the rear of the tube. For low condensation rates (small G) corresponding to low vapor suction, vapor separation occurs near the positions obtained for single phase separation without suction. Little change occurs in the separation point location as vapor velocity is varied. For large condensation rates (large G), the vapor boundary-layer experiences high suction which shifts the separation point downstream (i.e., as G increases, $x_S^{\bullet}$ increases). As vapor velocity is decreased (increasing F), the separation point shifts further downstream. As k decreases (more elliptical), the vapor boundary-layer separation point moves further downstream when compared to a circular tube under all conditions of F and G. At high F and G, the vapor boundary-layer separation points come together at the rear of the tube for both the elliptical and circular tube.

Figure IV-8 shows the influence that the above effects (vapor shear, gravity, condensation rate and eccentricity) have on the mean heat-transfer coefficient. The solutions for $k = 1$ agree with the results of Fujii et al. [22] as corrected by Lee and Rose [25]. Similar trends were obtained for the elliptical tubes. For large values of condensation rate (large G), the two-phase boundary-layer shear stress analysis agrees closely with the asymptotic shear stress analysis method as expected since the latter assumes an infinite condensation rate. For decreasing k, the results for an elliptical tube tend to show a reduction in heat transfer at low F (compared to a circular tube)
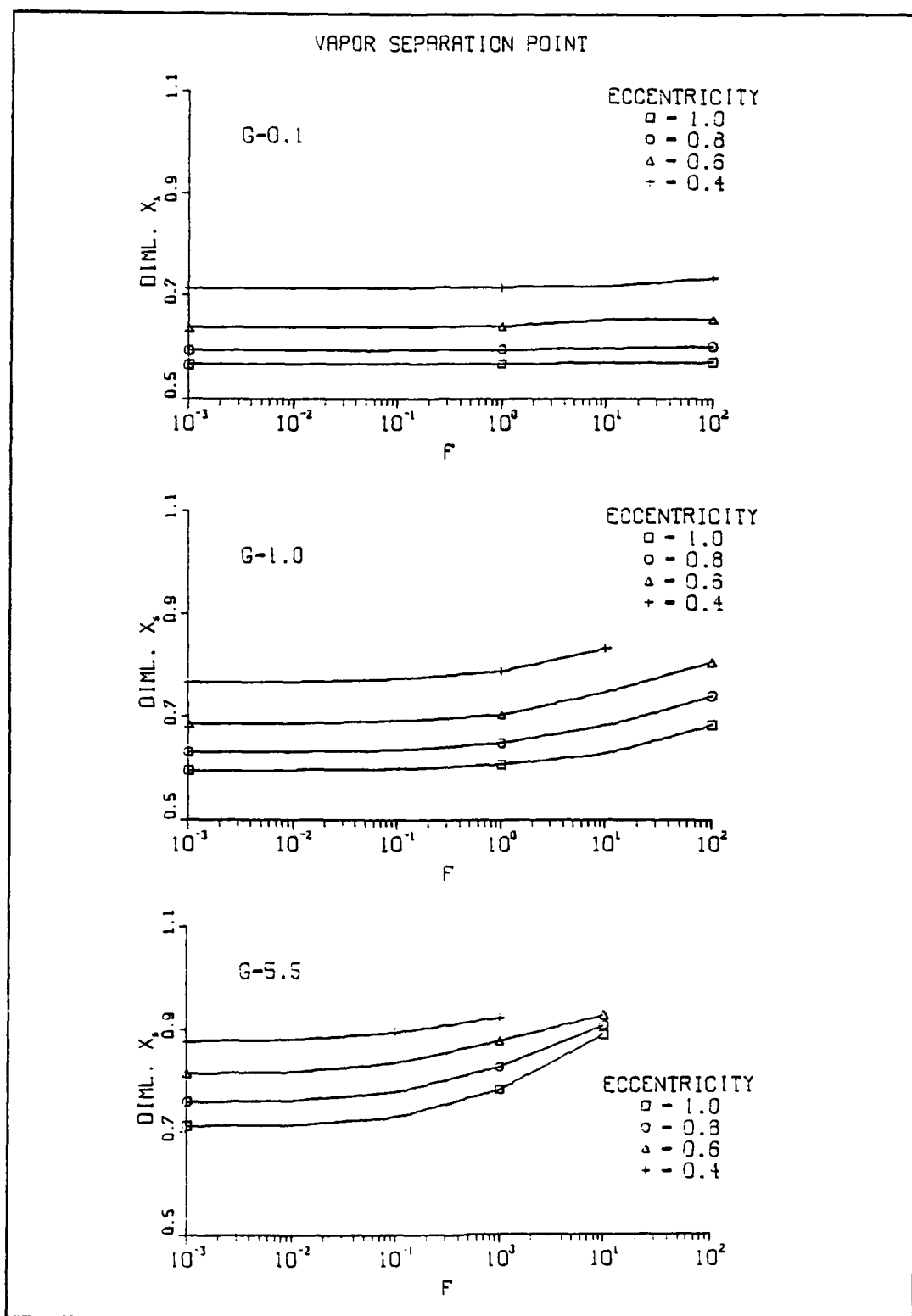
Figure IV-7. Vapor Separation Point Location with Varying F, G and k.
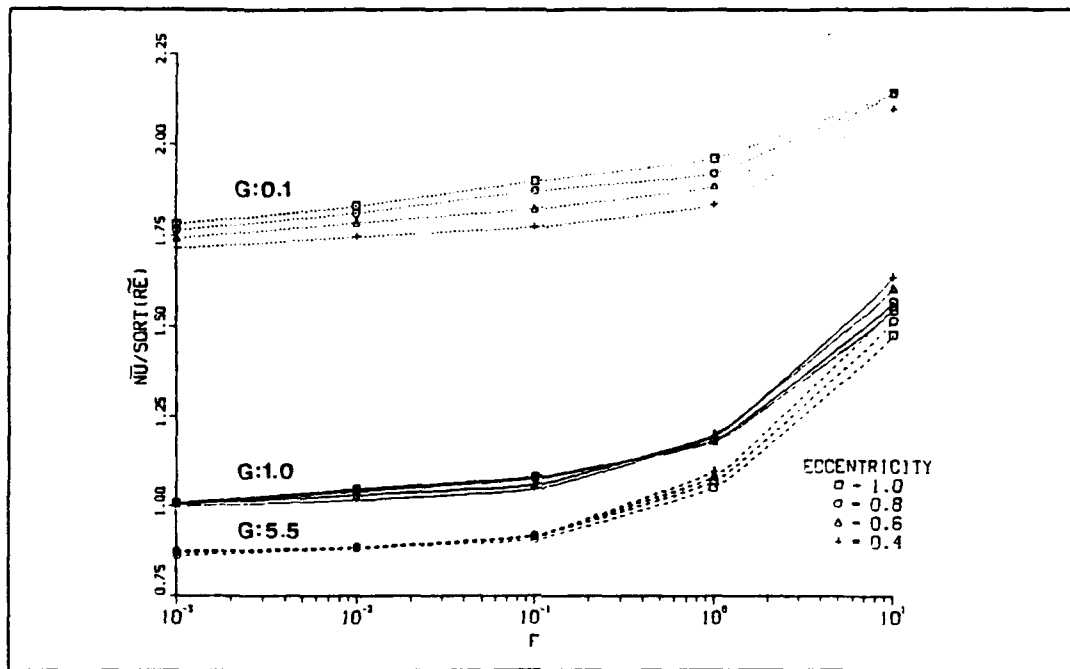
Figure IV-8. Effects of Vapor Velocity and Vapor Separation on Mean Nu using the Two-Phase Boundary-Layer Approximation Analysis Method.

and an increase in heat transfer at high F, as previously mentioned. The cross-over point from reduction to improvement occurs at increasing values of F as G decreases. For large values of F, the results converge to the Nusselt analysis. This shift in the cross-over point is attributed to the change in the vapor boundary-layer separation point with varying condensation and vapor velocity (varying G and F). As seen in Figure IV-7, for large condensation rate ($G = 5.5$) and low vapor velocity (large F), the large vapor suction causes a delay in vapor boundary-layer separation such that it occurs at essentially the same streamwise location for all eccentricities. As velocity increases (F becomes smaller) the separation point shifts forward at different rates dependent on eccentricity which is evidenced by the diverging curves in Figure IV-7c. Since early vapor boundary-layer separation results in a reduction in heat transfer due to rapid thickening of the condensate film, the circular tube ($k = 1$) experiences more of a

reduction in heat transfer compared to an elliptical tube. The effect of delaying separation is to cause a thinning in the mean film thickness for the tube. In the balance, where the streamwise component of gravity and the shift in vapor boundary-layer separation are positive effects (i.e., both contribute to a relative thinning of the elliptical tube condensate film compared to a circular tube) and vapor shear is a negative effect (i.e., lower shear contributes to a relative thickening of the elliptical tube condensate film compared to a circular tube), delays in vapor separation move the cross-over point from gravity dominant to shear dominant heat transfer. For the case of low G in Figure IV-7a, there is no noticeable shifting of the vapor boundary-layer separation point as F is varied. Thus the vapor boundary-layer separation point contribution does not change with vapor velocity (F) to the balance and the cross-over point occurs at lower velocities (larger F). The overall effect of vapor shear using this analysis is typically a slight reduction ($< 2\%$) in the heat-transfer coefficient for an elliptical tube compared to an equivalent surface area circular tube, dependent on the magnitude of the condensation rate parameter, G.

Figures IV-9 and IV-10 show the effects of vapor boundary-layer separation on the local film thickness and heat-transfer coefficient for a given dimensionless streamwise distance. For low F and G, the separation point occurs relatively early, but is significantly delayed when using an elliptical tube. As F increases (vapor velocity decreases), the separation points remain at their same respective streamwise locations. The areas under the curves in Figure IV-10 represent the total heat transfer. Bearing this in mind, the comparison between elliptical and circular tubes is made a little easier. At high F (for given G), the area under the curve for an elliptical tube exceeds that for a circular tube while at low F, the opposite is true. However, for a given eccentricity, the values of x_s^* are the same for varying F (as noted earlier).

As G increases (increasing condensation rate and suction), vapor boundary-layer separation is further delayed (compared to low G) and is virtually eliminated at high F. Separation is always delayed for an elliptical tube compared to a circular tube.

LOCAL FILM THICKNESS
F-0.01, G-0.1

LOCAL FILM THICKNESS
F-10.0, G-0.1
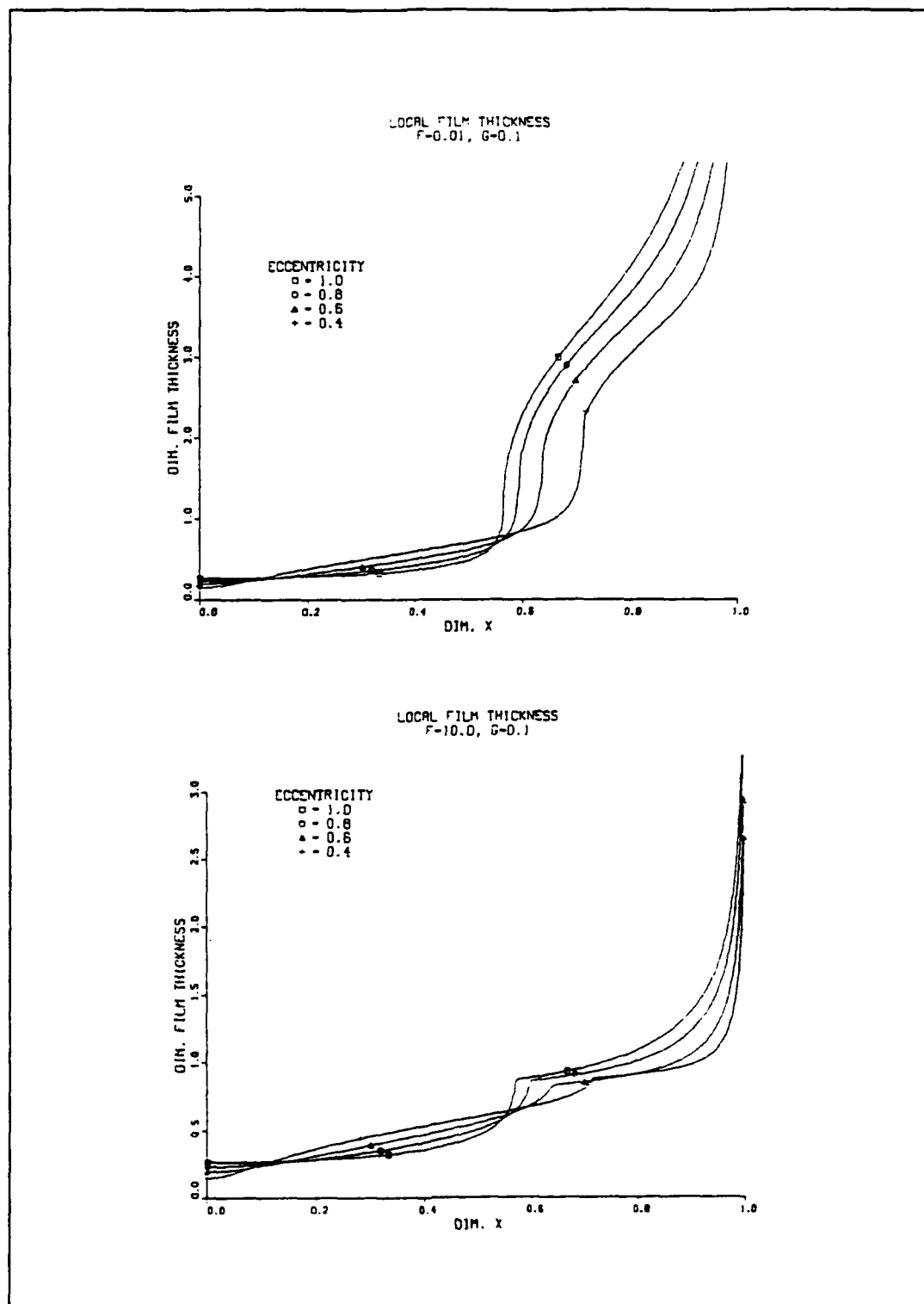
Figure IV-9 a and b. Dimensionless Local Film Thickness for Varying G, F and k from the Two-Phase Boundary Layer Shear Stress Method of Analysis.

71

LOCAL FILM THICKNESS
F=0.01, G=5.5

LOCAL FILM THICKNESS
F=10.0, G=5.5
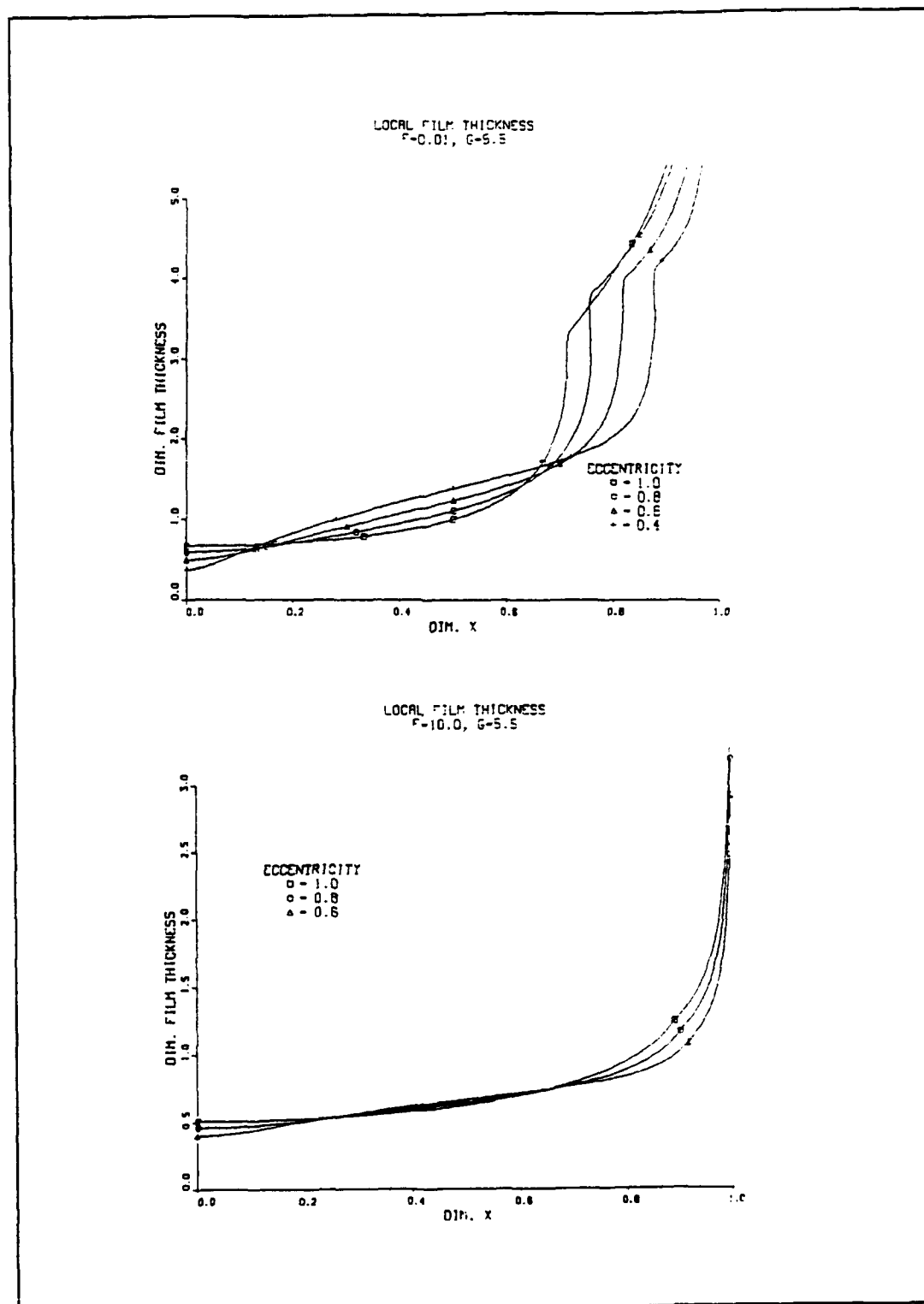
Figure IV-9 c and d. Dimensionless Local Film Thickness for Varying G, F and k from the Two-Phase Boundary Layer Shear Stress Method of Analysis.
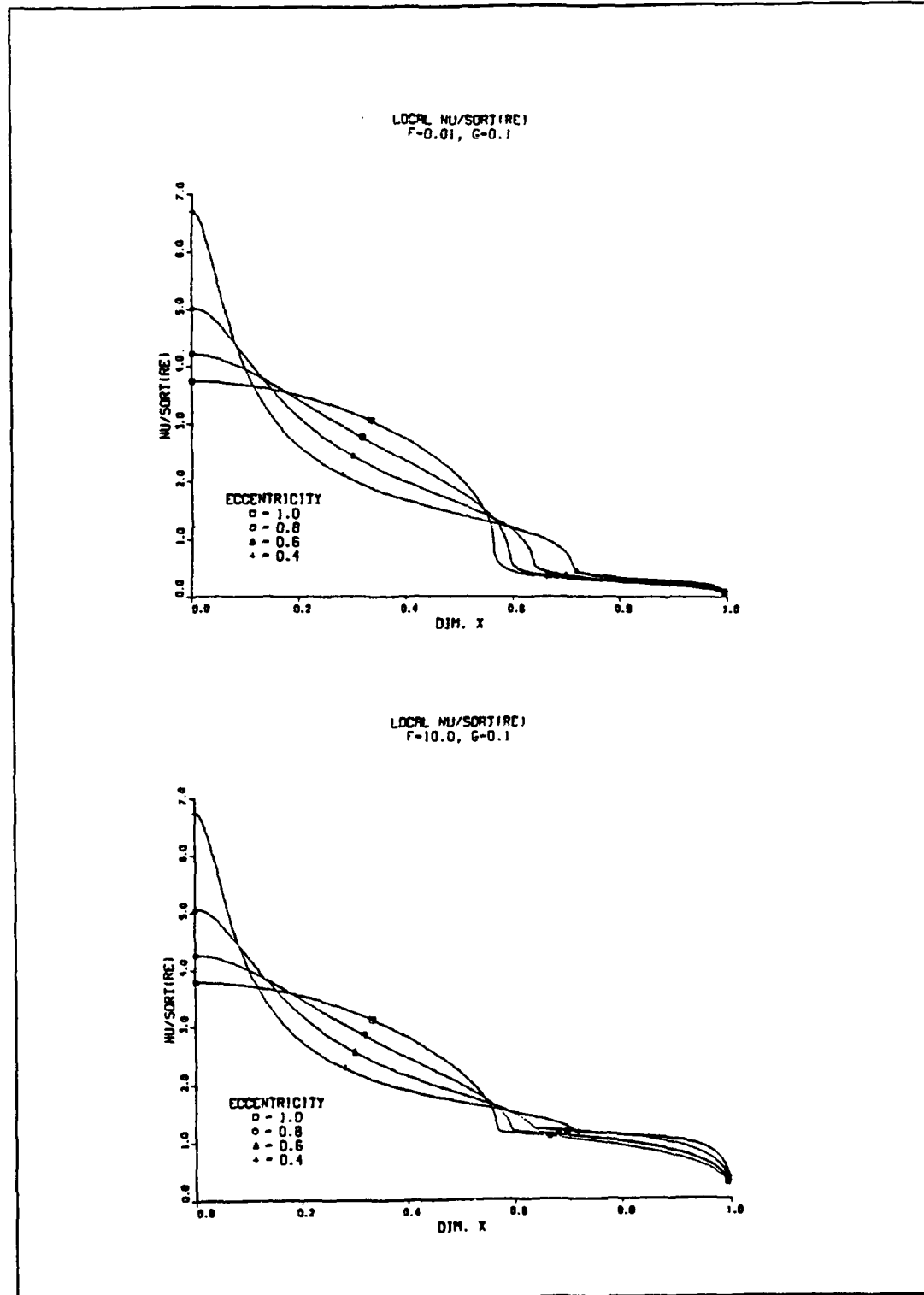
Figure 10 a and b. Local Nu for Varying G, F and k from the Two-Phase Boundary Layer Shear Stress Analysis Method.
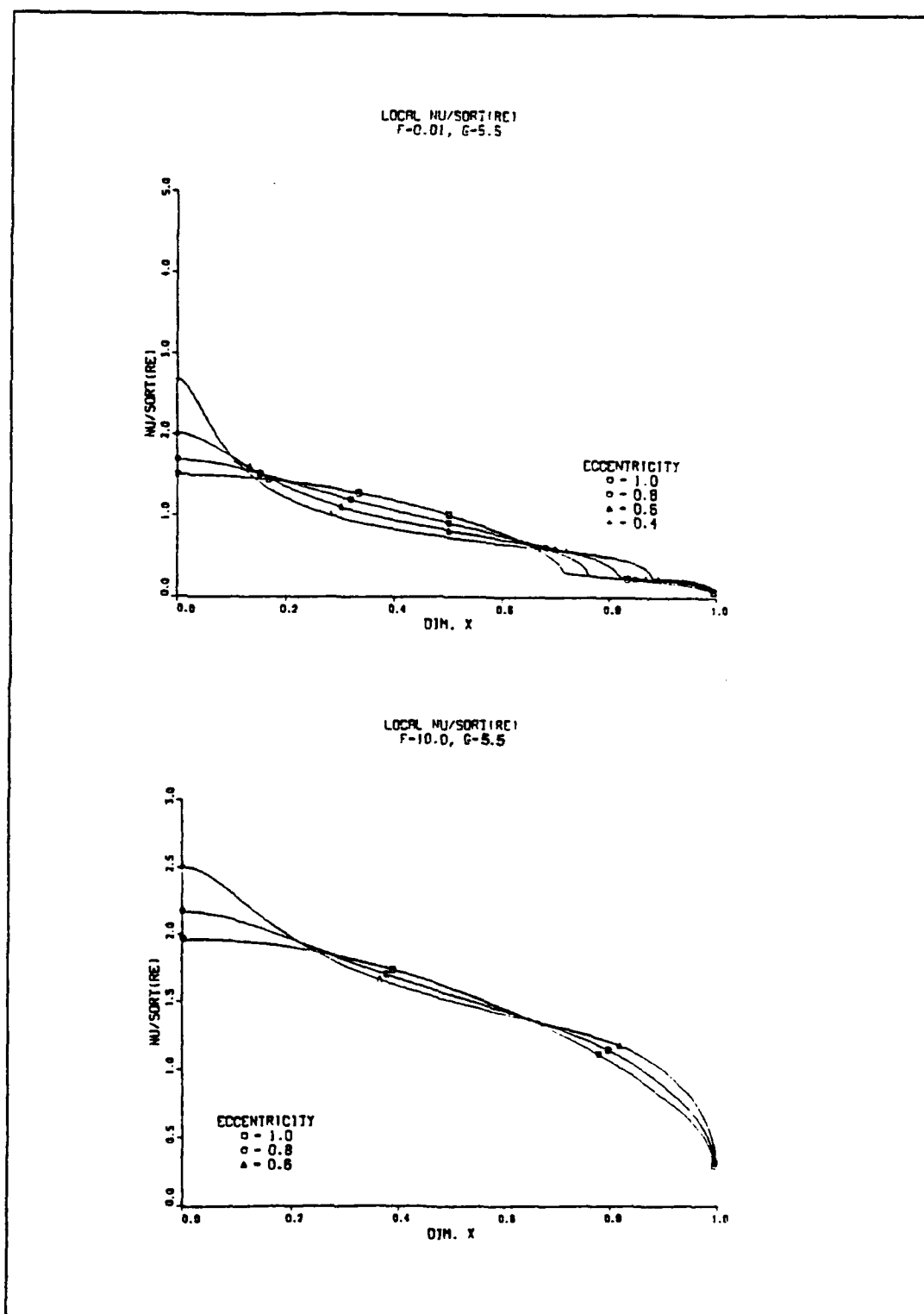
Figure 10 c and d. Local Nu for Varying G, F and k from the Two-Phase Boundary Layer Shear Stress Analysis Method.

74

C. EFFECT OF SURFACE TENSION

As noted in Section II.E, a condition exists for which $d\delta^*/d\phi$ becomes infinite at some critical angle ϕ_C. What is actually happening can be discerned from Figure IV-11 which shows the surface tension function $f_4(\phi)$ versus x^* for varying eccentricity. Surface tension causes a favorable pressure gradient over the front half of the elliptical tube and an adverse pressure gradient over the back half. The severity of the pressure gradient is localized to small regions at the top and bottom of the elliptical tube where
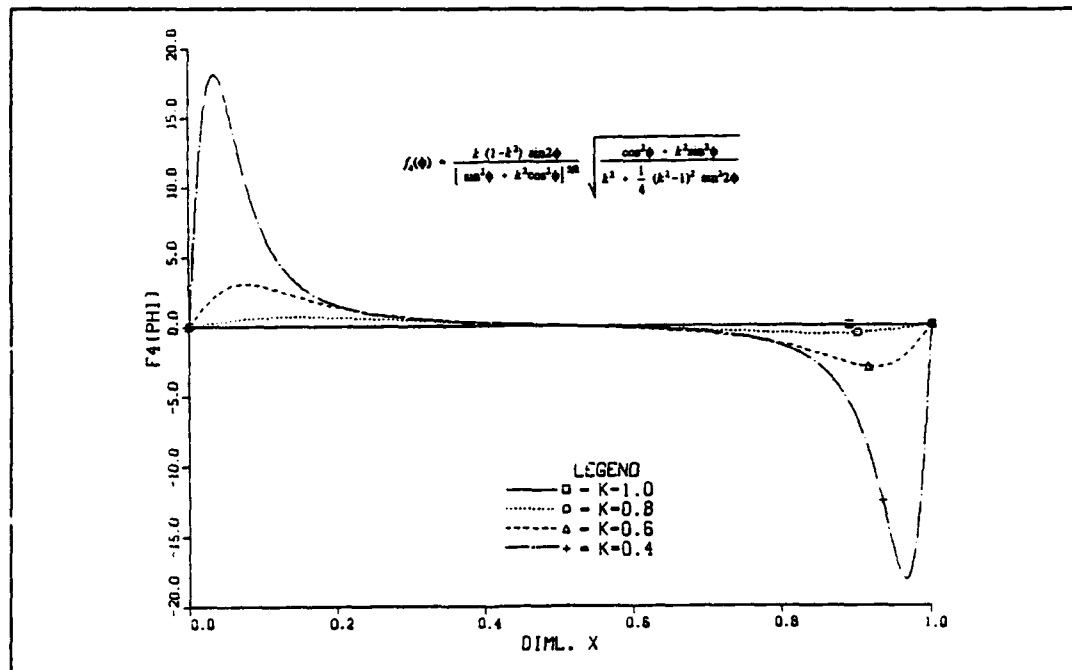
Figure IV-11. Surface Tension Function, $f_4(\phi)$ for Varying Eccentricity.

change in surface curvature is most severe. Therefore, it is most significant for small values of eccentricity. The above analysis explains the reason for condensate flow instability discussed in Section II.E and predicted by Equation (II-90).

Further discussion of surface tension is restricted to those cases in which a solution could be obtained over at least 90% of the tube surface. This restriction was arbitrarily chosen based on the small amount of heat transfer which occurs on the lower part of the tube and would therefore have minimal impact on the accuracy of the results. Figure IV-12 shows the effects of surface tension on the mean heat-transfer coefficient for $k = 0.6$ and 0.4. The Bond number, Bo, gives the relative effect of inertia to surface tension. Values of $1/Bo$ of 0.01 (typical for steam) and 0.001 (typical for refrigerants) as well as $1/Bo = 0$ have been shown on the figure. A number of interesting points can be highlighted. Firstly, the surface tension effect is much smaller for highly wetting refrigerants, as expected. Secondly, inclusion of surface tension leads to a small decrease in the mean heat-transfer coefficient ($< 2\%$) over the whole range of F for the practical range of eccentricities, suggesting that any thinning of the condensate film over the top half of the tube is more than offset by a thickening over the lower half. As eccentricity decreases, this discrepancy is accentuated. Finally, surface tension effects are felt more in the free convection region (high F) than in the forced convection region (low F) as film thickness becomes dominated by vapor shear.

Krupiczka [29] used the curvature of the condensate film surface to analyze surface tension on a horizontal circular cylinder. He determined that the effect of surface tension was only significant over the bottom portion of the tube. This fact implies that since the film is very thin over the top of the tube, its curvature is very close to that of the tube surface itself, which, for a circular tube results in no surface tension effect (constant radius of curvature). As the condensate flows around the lower half of the circular tube, the film curvature no longer follows the tube surface. Rather, the radius of curvature is increasing resulting in a small improvement in the heat-transfer coefficient. A similar analysis can be applied to the elliptical tube. Over the
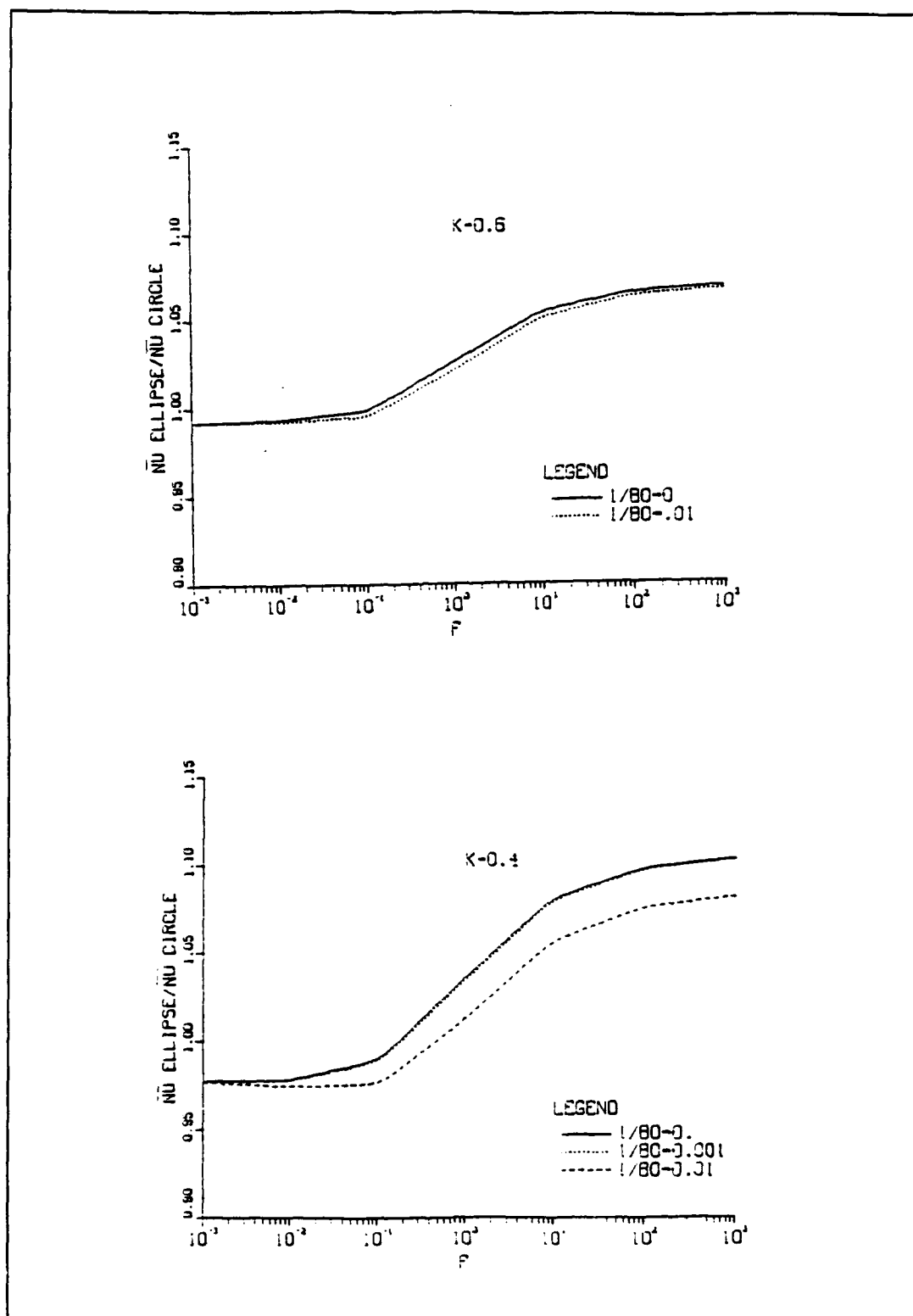
Figure IV-12. Effect of Surface Tension on the Mean Nu for $k = 0.4$ and 0.6 .

77

top half of the tube where the condensate film is thinnest, modeling the surface tension effect using the curvature of the tube surface is valid. However, the adverse pressure gradient over the lower half of the tube is probably not as severe as seen in Figure IV-11. Over this portion of the tube, the film is thicker and its decreasing surface curvature is not as severe as the tube surface curvature. The conclusion drawn from this analysis is that surface tension does not have a significant effect on the mean heat-transfer coefficient for an elliptical tube.

D.   EFFECT OF PRESSURE GRADIENT

The effect of pressure gradient was analyzed using the asymptotic shear stress approximation (similar to Rose [28] for a circular tube). In this analysis, the pressure gradient in the condensate film was assumed to be due to the pressure gradient impressed on the condensate by vapor potential flow. As in the case of surface tension, there is a relationship between parameters P and F (Equation II-89) for which a solution could not be obtained for the entire tube. Figure IV-13 shows the pressure gradient function versus x^* for varying k which sets up a favorable pressure gradient over the top of the tube and an adverse pressure gradient over the lower half of the tube. The effect of eccentricity is to shift the point of maximum pressure gradient to the front and rear of the tube. Thus, ϕ_C shifts downstream for an elliptical tube compared to a circular tube for similar P and F. This is a result of the more streamlined shape and the smaller resultant pressure drop over the streamwise length of an elliptical tube.

As in the analysis of surface tension, discussion is limited to those cases for which solutions could be obtained over the entire tube. When pressure gradient was included in the momentum equation of the condensate film, solutions agreed with the results of Rose [28] for a circular tube, yielding a maximum 5% decrease in the heat-transfer coefficient over the entire range of F compared to the case with pressure gradient

78

$$f_3(\phi) = \frac{(1+k)^2\, k^2\, \sin 2\phi}{[\sin^2\phi + k^2\cos^2\phi]^2} \sqrt{\frac{\cos^2\phi + k^2\sin^2\phi}{k^2 + \frac{1}{4}(k^2-1)^2\sin^2 2\phi}}$$
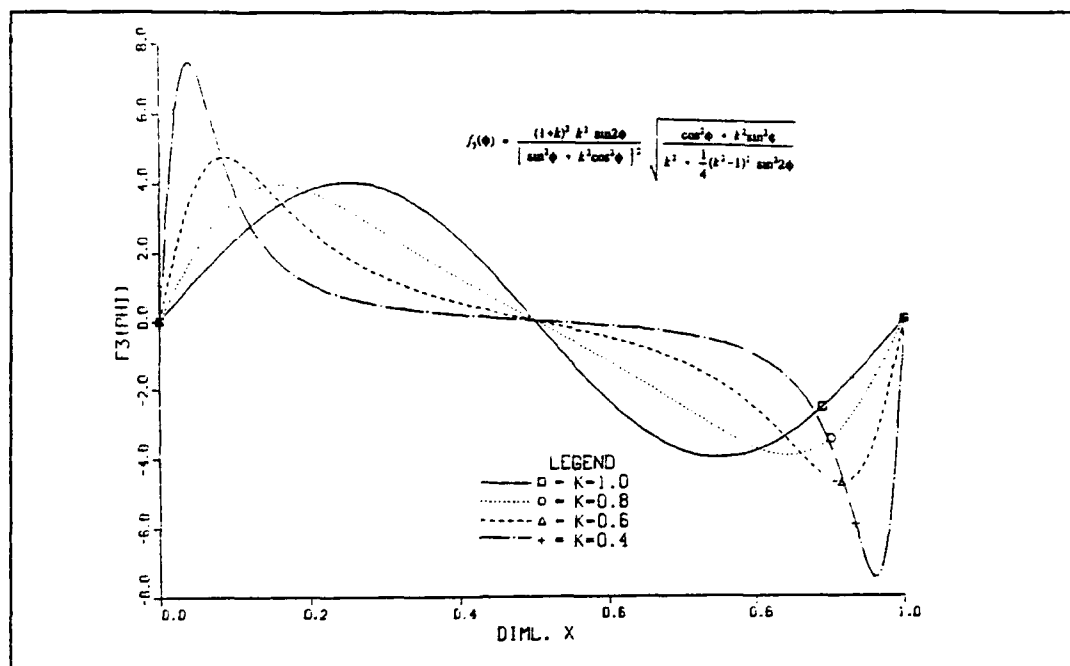
Figure IV-13. Pressure Gradient Function, $f_3(\phi)$, for Varying Eccentricity.

neglected. Figure IV-14 shows the mean heat-transfer coefficient for a circular tube ($k = 1$) for varying F and P. The favorable pressure gradient increases the mean condensate velocity resulting in a thinner film and an increased mean heat-transfer coefficient over the top of the tube. This increase is offset by the adverse pressure gradient which slows the condensate film velocity over the lower half of the tube, thickens the film and decreases the mean heat-transfer coefficient. For an eccentricity of 0.6, Figure IV-15 compares the effect of pressure gradient for an elliptical tube with those for a circular tube for varying F and P. For both the circular and elliptical tubes, the effect of pressure gradient provides a slight reduction in condensation heat transfer. Figure IV-15 indicates that the reduction in heat transfer was less for the elliptical tube compared to the circular tube as a result of the more favorable potential velocity distribution around the ellipse.

79
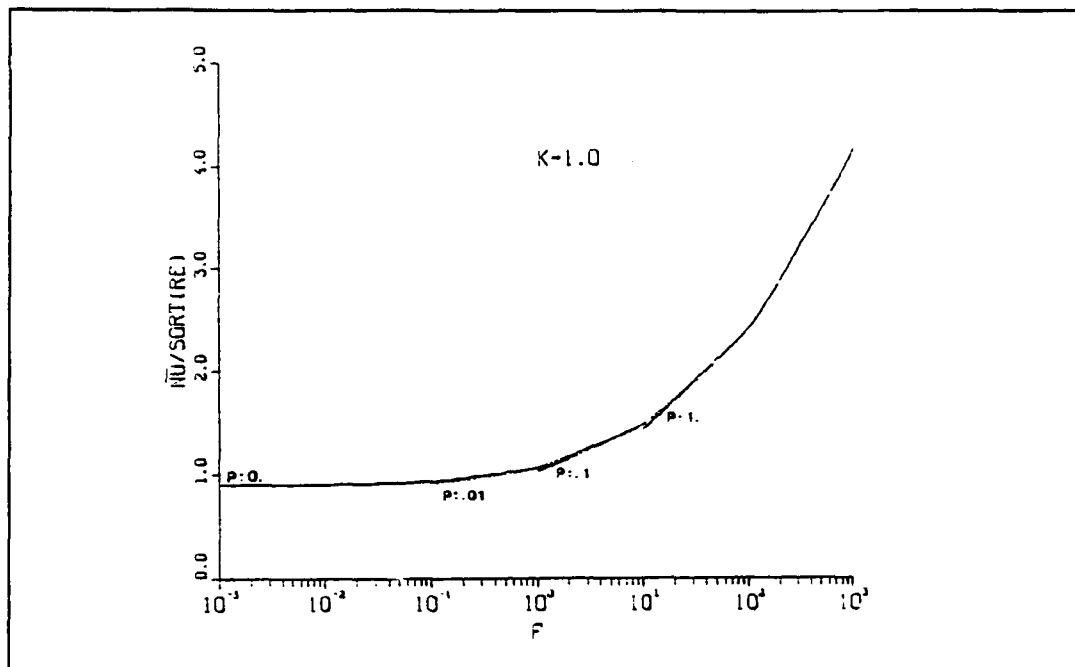
Figure IV-14. Effect of Pressure Gradient on the Mean Nu for a Circular Tube (*k*=1).
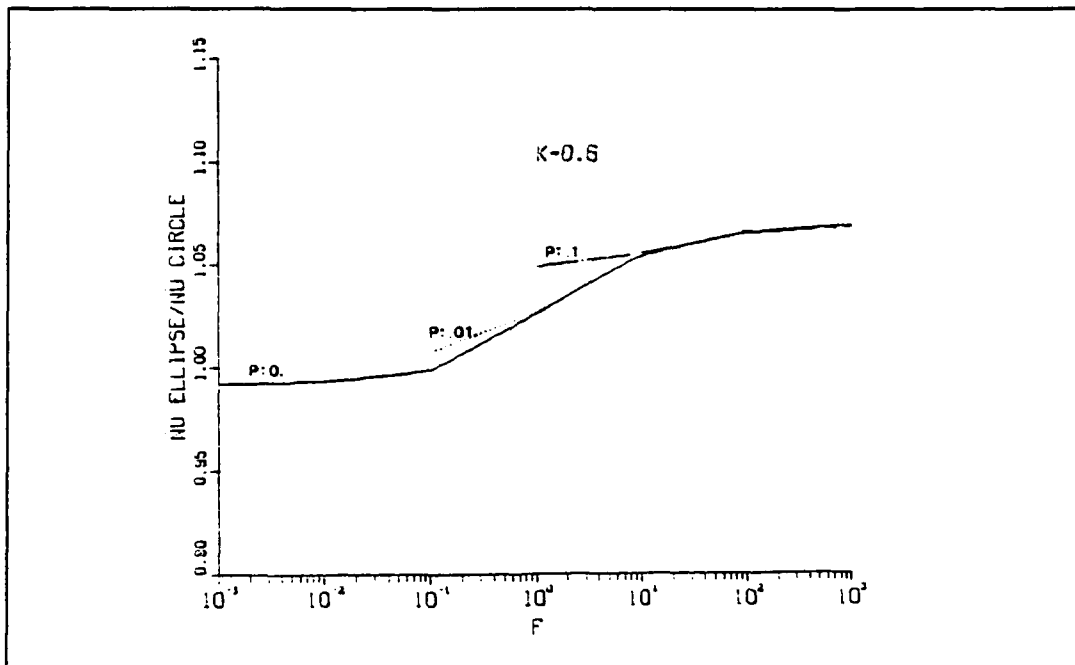
Figure IV-15. Effect of Pressure Gradient on Mean Nu, *k* = 0.6, Relative to a Circular Cylinder.

80

E.   EFFECT OF VAPOR PRESSURE DROP

The previous results indicate that vapor shear decreases the heat-transfer coefficient for an elliptical tube when compared to a circular tube. However, a consideration not yet discussed is that the vapor pressure drop across an elliptical tube is significantly smaller than a circular tube for the same free-stream velocity. Alternatively, for a given pressure drop, the free-stream velocity is greater for the elliptical tube. Since very little data is available for two-phase drag coefficients around tubes, single-phase data was used where the drag coefficient for the tube is due entirely to form drag. Values of C_D for a circular ($k = 1$) and an elliptical tube ($k = 0.5$) were estimated to be approximately 1.2 and 0.6 respectively (White [44]). For steam with T_{sat}= 60°C condensing on a horizontal tube with T_{wall}= 40°C and U_∞= 25 m/s for the circular tube, the corresponding vapor velocity for the elliptical tube, for the same pressure drop, was calculated to be U_∞= 35 m/s. The resulting values of F are therefore 0.0257 and 0.0132 for the circular and elliptical tubes respectively. Using the asymptotic shear stress assumption for both values of F gives an increase in the heat transfer for an elliptical tube of 16.3% when compared to a circular tube. Using the two-phase boundary-layer shear stress assumption gives a corresponding increase of 17.1%. Therefore, though the effect of vapor shear alone results in a reduction of the heat-transfer coefficient (as discussed in Section IV.B), when the streamlined shape of the elliptical tube and its effect on the vapor pressure drop is taken into account (allowing for higher U_∞ for a given pressure drop), there is an increase in the heat-transfer coefficient when compared to a circular cylinder.

81

F.   INSIDE HEAT TRANSFER COEFFICIENT

So far only the outside heat-transfer coefficient has been discussed. In real condensers, it is the overall heat-transfer coefficient which is important and so consideration must also be given to the single-phase convective heat transfer occurring inside the elliptical tube. A preliminary survey of the literature (Incropera and Dewitt [45]) shows that for turbulent flow conditions where the Prandtl number is greater than 0.5 (which is true for most practical condensers), correlations developed for circular tubes may be used with good accuracy to approximate the inside heat-transfer coefficient for an elliptical tube if the hydraulic diameter is used in place of the circular diameter. The hydraulic diameter is given by

$$D_h = \frac{4 A_c}{\wp} \qquad (IV-3)$$

where A_C is the cross-sectional area of the tube and $\wp$ is the inside perimeter of the tube. The perimeter for an elliptical tube and an equivalent surface area circular tube is the same. The cross-sectional area of an elliptical tube is given by

$$A_c = \pi \, a \, b \qquad (IV-4)$$

and is smaller than an equivalent surface area circular tube. Inside heat transfer correlations for turbulent flow heat transfer inside a circular tube are typically of the form [45]

$$Nu \left(= \frac{\alpha \, D_h}{\lambda} \right) \propto Re^{0.8} \left(= \left[\frac{\rho \, U \, D_h}{\eta} \right]^{0.8} \right) \qquad (IV-5)$$

Thus, the inside heat-transfer coefficient is related to the hydraulic diameter by

$$\alpha \propto D_h^{-0.2} \qquad (IV-6)$$

As an example, consider an elliptical tube with $k = 0.5$ and a major axis with $a = 0.01$ m. The equivalent circular tube would have a diameter of 0.0154 m. The ratio of the heat transfer coefficient of the elliptical tube to the circular tube is given by

$$\frac{\alpha_{elliptical}}{\alpha_{circle}} = \left[\frac{(D_h)_{elliptical}}{(D_h)_{circle}} \right]^{-0.2} = \left[\frac{(A_C)_{elliptical}}{(A_C)_{circle}} \right]^{-0.2} \quad , \tag{IV-7}$$

thus,

$$\frac{\alpha_{elliptical}}{\alpha_{circle}} = \left[\frac{ab}{(D_e/2)^2} \right]^{-0.2} = 1.035 \quad . \tag{IV-8}$$

For this simple analysis, it can be seen that the inside heat-transfer coefficient of the elliptical tube is 3.5% greater than the equivalent surface area circular tube. This result, when added to the increase in the outside heat-transfer coefficient (for a given pressure drop), would increase the overall heat-transfer coefficient of the condenser.

V. CONCLUSIONS

Analyses of laminar film condensation on a horizontal elliptical tube were conducted under conditions of free and forced convection, the latter using both an asymptotic interfacial shear stress approximation as well as solution of the two-phase boundary-layer equations. For the asymptotic shear stress approximation, the effects of surface tension and pressure gradient were also included. Where possible, these analyses have been validated against existing solutions for laminar film condensation on a horizontal circular tube and a vertical flat plate.

Whether or not condensation heat transfer is improved for an elliptical tube compared to an equivalent surface area circular tube is dependent on a balance of the effects of gravity, vapor shear and vapor boundary-layer separation and the influence these have on the thickness of the condensate film. Under quiescent vapor conditions (no vapor shear or boundary-layer separation), gravity causes an increase (~10%) in the heat transfer on an elliptical tube compared to a circular tube of the same surface area due to an increase in "effective" gravity. Under conditions of forced convection, both shear stress approximations indicate a small decrease (< 2%) in performance due to the reduction in interfacial shear as a result of the better streamlined shape of the elliptical tube when compared to the circular tube in the same free stream vapor flow. However, when pressure drop effects are also considered, the higher allowable vapor velocity over an elliptical tube (for the same pressure drop as a circular tube) results in an increase in the mean heat-transfer coefficient of 15-20%. For conditions of mixed convection, the condensate film thickness is controlled by both gravity and vapor shear effects. The cross-over between heat transfer improvement (gravity dominant flow) and heat

84

transfer reduction (vapor shear dominant flow) for the elliptical tube is dependent on the vapor boundary-layer separation point. For large condensation rates (high vapor suction), vapor boundary-layer separation is delayed and the cross-over point shifts to higher velocities (smaller F). For low condensation rates (low vapor suction), movement of the vapor boundary-layer separation point is minimal, resulting in a minor effect on heat transfer and a cross-over point that shifts toward lower velocities (large F). Pressure gradient and surface tension each lead to a small decrease in the mean heat-transfer coefficient ($< 2\%$) for an elliptical tube.

In general, therefore, the outside heat-transfer coefficient of a condenser tube is improved by using an elliptical tube geometry. Approximation of the single-phase inside heat-transfer coefficient using a hydraulic diameter and a Seider-Tate type correlation indicates that the elliptical tube also has better inside heat transfer performance compared to an equivalent surface area circular tube. Thus, the overall heat-transfer coefficient should be improved.

VI. RECOMMENDATIONS

This study represents an initial step in determining if a shell-and-tube condenser using horizontal elliptical tubes has better heat transfer than a comparable circular tube bundle. The effects of multi-tube arrangements (i.e., the influence of adjacent tubes and the spacing between tubes) on vapor flow characteristics needs to be evaluated to determine if further improvements in the overall heat-transfer coefficient can be achieved. It is suspected that the interfacial shear of the condensate film on elliptical tubes will be further reduced but the corresponding reduction in vapor pressure drop across the condenser will result in a net gain in heat transfer compared to a circular tube bundle. An analysis similar to that conducted by Aoune and Burnside [46, 47] can be used to evaluate multi-tube arrangements.

Further studies should be conducted on a single elliptical tube to better determine the effect of surface tension on heat transfer. The surface tension model used in this study was based only on the curvature of the tube surface and does not take into account the relatively thicker film over the lower half of the tube. The curvature of the actual condensate film surface should be analyzed in a manner similar to Krupiczka [29]. This analysis, together with the asymptotic shear stress assumption, would involve the solution of a second order ODE.

Analysis of the effect of offsetting the elliptical tube at an angle, α, with respect to vapor flow and gravity must be conducted to determine its effect on the heat-transfer performance of the tube. This is important since in real condensers, vapor will approach the tube at various angles. Additionally, since the elliptical tube is a streamlined body, vapor flow in a direction other than the direction of the major axis

86

may result in a lifting force on the tube which may result in tube vibration and wear. These effects would have to be studied and methods to minimize any resultant vibration must found. The problems associated with joining elliptical tubes to the condenser tube sheet and baffle plates also needs to be addressed.

Finally, experiments must be conducted on elliptical tubes to validate the predictions of these theoretical models.

APPENDIX A - DERIVATION OF TANGENTIAL VAPOR VELOCITY OVER AN ELLIPTICAL TUBE FROM POTENTIAL FLOW THEORY

The basic technique used to determine fluid flow velocity over a body is to employ a conformal transformation to translate the body from one complex plane into another complex plane. From this, the velocity of the transformed body can be readily computed using potential theory. For this particular application, the fluid velocity along the surface of a circular cylinder is determined and then transformed into the complex plane in which the cylinder has an elliptical shape.

Consider a circular cylinder in the complex plane, z_1, as shown in Figure A-1. The surface of the circle is defined by

$$z_1 = c\, e^{i\theta} \qquad (a)$$

$$x_1^2 + y_1^2 = c^2 \qquad (b)$$

(A-1)

The conformal transform to translate the circular body from the z_1 plane to an elliptical body in the z_2 plane is given by

$$z_2 = z_1 - \frac{1}{z_1} \quad , \qquad\qquad\qquad (A-2)$$

thus

$$z_2 = (x_1 + iy_1) - \frac{1}{x_1 + iy_1} = x_1\left(1 - \frac{1}{c^2}\right) + iy_1\left(1 + \frac{1}{c^2}\right) \quad . \qquad (A-3)$$

The real and imaginary coordinates in the z_2 plane are given by

$$x_2 = x_1\left(1 - \frac{1}{c^2}\right) \quad and \quad y_2 = y_1\left(1 + \frac{1}{c^2}\right) \quad . \qquad (A-4)$$

88
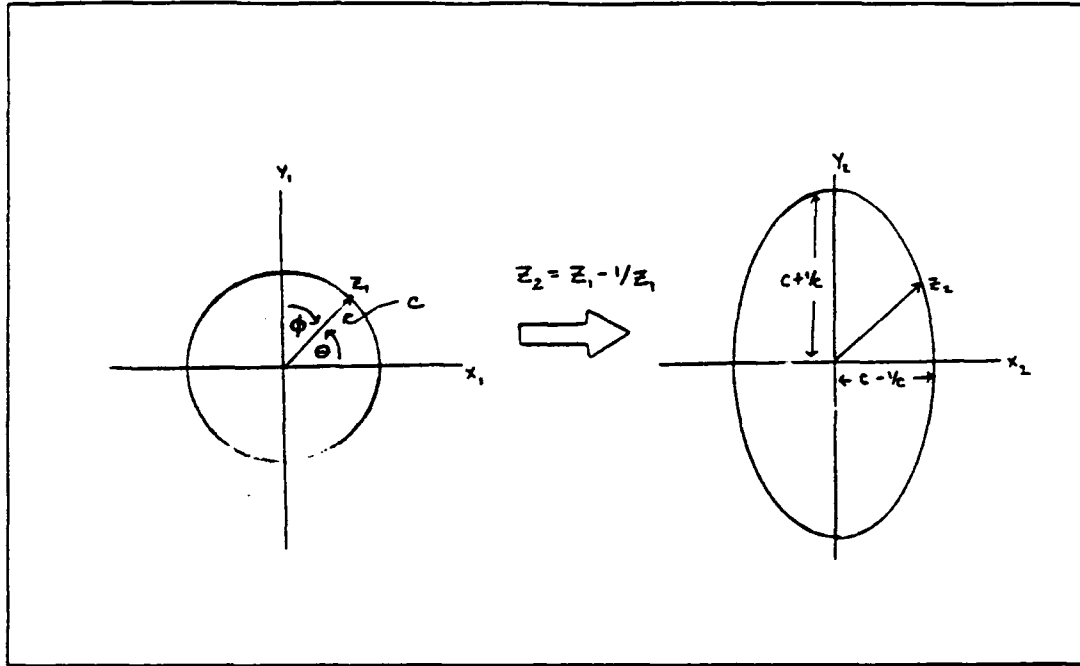
Figure A-1. Circular Cylinder in z_1 Plane, Elliptical Cylinder in z_2 Plane.

Substituting Equation (A-4) into Equation (A-1b) results in

$$\frac{x_2^2}{\left(c - \dfrac{1}{c}\right)^2} + \frac{y_2^2}{\left(c + \dfrac{1}{c}\right)^2} = 1 \quad , \tag{A-5}$$

which is the expression for an ellipse in cartesian coordinates where the semi-major axis, a, is given by $c + (1/c)$ and the semi-minor axis, b, by $c - (1/c)$. The complex potential function in the z_1 plane for the circle is given by

$$w(z_1) = U_\infty z_1 e^{-i\frac{\pi}{2}} + \frac{U_\infty c^2 e^{i\frac{\pi}{2}}}{z_1} = \Phi + i\psi \quad , \tag{A-6}$$

where Φ is the velocity field potential function and ψ is the stream function. The fluid velocity in the z_1 plane is determined from the complex derivative,

$$\frac{dw}{dz_1} = U_\infty e^{-i\frac{\pi}{2}} - \frac{U_\infty c^2 e^{i\frac{\pi}{2}}}{z_1^2} = u_1 - iv_1 \quad , \tag{A-7}$$

89

where u_1 and v_1 are the fluid velocity components in cartesian coordinates. The fluid velocity in the z_2 plane (for the ellipse) is found by the chain rule, thus,

$$\frac{dw}{dz_2} = \frac{dw}{dz_1}\frac{dz_1}{dz_2} = u_2 - iv_2 \quad .$$

(A-8)

Combining Equations (A-1a),(A-2) and (A-7) results in

$$\frac{dw}{dz_2} = \frac{U_\infty c^2 \left(e^{i\,(2\theta\,-\,\pi/2)} - e^{i\pi/2}\right)}{c^2 e^{i\,2\theta} + 1}$$

(A-9)

The magnitude of the fluid velocity is found by multiplying the complex velocity by its conjugate. Using Euler's formula,

$$e^{i\theta} = \cos\theta + i\,\sin\theta \quad ,$$

(A-10)

and with some algebraic manipulation, the potential velocity of the fluid at the surface of the ellipse is given by

$$U_\theta^2 = \frac{dw}{dz_2}\frac{\overline{dw}}{\overline{dz_2}} = \frac{U_\infty^2 c^4 \,(2 + 2\cos2\theta)}{c^4 + 1 + 2c^2 \cos2\theta} \quad ,$$

(A-11)

where the bar denotes the complex conjugate. Equation (A-11) is further simplified using the trigonometric identities

$$\cos2\theta = \cos^2\theta - \sin^2\theta$$
$$\cos2\theta = 2\cos^2\theta - 1 \quad .$$

(A-12)

and the relationship between c, a and b,

$$4c^2 = (a+b)^2 \quad .$$

(A-13)

Thus the potential velocity is given by

$$U_\theta = U_\infty \frac{(1+k)\,\cos\theta}{\sqrt{\cos^2\theta + k^2\sin^2\theta}} \quad .$$

(A-14)

The angle, θ, is measured from the x_1 (horizontal) axis. The relationship between θ and

ϕ, the angle measured from the y_1 (vertical) axis, is given by

$$\theta = \frac{\pi}{2} - \phi \quad .$$ (A-15)

Note that ϕ is an angle defined in the z_1 plane for the circle and is the parametric angle defined in Section II.A . The potential velocity is thus given by

$$U_\phi = U_\infty \frac{(1+k)\ \sin\phi}{\sqrt{\sin^2\phi + k^2\cos^2\phi}} = U_\infty \frac{(1+k)}{\sqrt{1 + k^2\cot^2\phi}} \quad .$$ (A-16)

APPENDIX B - COMPUTER CODE FOR ASYMPTOTIC SHEAR STRESS MODEL

```
*     PROGRAM MIXED1

*******************************************************************
*
*     THIS PROGRAM NUMERICALLY SOLVES THE PROBLEM OF MIXED
*     CONVECTION CONDENSATION WITH SURFACE TENSION ON AN ELLIPTICAL
*     CYLINDER.  THE PROBLEM FORMULATION USES THE ASYMPTOTIC SHEAR
*     STRESS APPROXIMATION ANALYSIS METHOD.
*
*     THE PROGRAM USES AN AUTHOR DEVELOPED FORWARD STEPPING
*     ALGORITHM BASED ON A 4TH ORDER ADAMS PREDICTOR-CORRECTOR
*     METHOD TO SOLVE A 1ST ORDER ORDINARY DIFFERENTIAL EQUATION.
*
*     THIS PROGRAM CAN BE RUN WITH DIMENSIONLESS PARAMETERS
*     (F,G,P, BO) SPECIFIED OR WHERE THE PARAMETERS ARE CALCULATED
*     BASED ON SPECIFIED FLUID PROPERTIES.  MODIFICATIONS TO THE
*     PROGRAM (REMOVAL OF UNNECCESSARY STEPS BY "COMMENTING" THE
*     STATEMENT OUT OF THE PROGRAM) IS REQUIRED.   SPECIFIED FLUID
*     PROPERTIES INCLUDE T SAT, T WALL, AND UINF.
*
*     NUMERICAL RESULTS ARE DIRECTED TO AN EXTERNAL DATA FILE.
*
*     MAJOR VARIABLES USED ARE:
*
*         THETA       PARAMETRIC ANGLE
*         X           STREAMWISE LENGTH
*         DEFF        EFFECTIVE DIAMETER
*         DEL         CONDENSATE FILM THICKNESS
*         DELND,Z     DIMENSIONLESS FILM THICKNESS
*         F,P,BO,     DIMENSIONLESS PARAMETERS
*         JARPRL
*         UINF        VAPOR FREE STREAM VELOCITY
*         TS          VAPOR SATURATION TEMPERATURE
*         TW          WALL SURFACE TEMPERATURE
*         DENSL       CONDENSATE DENSITY
*         DENSV       VAPOR DENSITY
*         CONDL       CONDENSATE THERMAL CONDUCTIVITY
*         VISL        CONDENSATE VISCOSITY
*         HFG         LATENT HEAT OF VAPORIZATION
*         NU          NUSSELT NUMBER
*         NUAVG       MEAN NU NUMBER
*         ALPHA       HEAT TRANSFER COEFFICIENT
*         QFLUX       HEAT FLUX
*         A           SEMI-MAJOR AXIS
*         :           ECCENTRICITY
*         XFN         PARAMETRIC RADIUS
*         G           GRAVITY FUNCTION
*         F1          VELOCITY FUNCTION
*         F11         DERIVATIVE, VELOCITY FUNCTION
*         F2          PRESSURE GRADIENT FUNCTION
*         F3          SURFACE TENSION FUNCTION
*
*******************************************************************
      PARAMETER(PI=3.141592654,GRAV=9.807)

      REAL Z(0:180000),THETA(0:180000),X(0:180000),H,DEFF,X1,X2,X3,
     +NUAVG,NU,NUORE,UINF,TS,TW,TL,DENSL,VISL,TG,CONDL,HFG,B2,DELND,
     +DEL,QFLUX,A,K,RE,SUM,XFN,ALPHA,ALPHA0,DQFLUX,F,PHI,
     +A1,A2,A3,A4,A5,A6,A7,A8,A9,A10,A11,TF,PSAT,TB,TC,TD,R,TE,DENSV,
     +SIGML,FCN,P,C1,C2,C3,FC0,FC1,FC2,FC3,ZP1,ZP2,ZP3,ZP4,BO,
     +C4,C5,F21,F31,NUCOEFF

      INTEGER N,J,JJ,IC

      COMMON /GEOM/A,K,DEFF/PARAM/F,BO,P

      EXTERNAL FCN,XFN,G,G1,F1,F11,F2,F3

      OPEN(20,FILE='/MIXED1 OUTPUT A1',STATUS='OLD')
      OPEN(30,FILE='/DEL2 DATA A1',STATUS='OLD')
```

```
***     INPUT FLUID PARAMETERS    ***

        PRINT*,'ELLIPSE OF THE FORM (X/B)**2+(Y/A)**2=1'
        PRINT*,'INPUT "A" DIMENSION (M)?'
        READ*,A
        PRINT*,'INPUT T SAT AND T WALL (K)?'
        READ*,TS,TW
        PRINT*,'INPUT ANGLE STEP SIZE (DEGREES)?'
        READ*,H
        PRINT*,'STEP SIZE, H = ',H
C       PRINT*,'INPUT UINF?'
C       READ*,UINF
        PRINT*,'INPUT K?'
        READ*,K
        PRINT*,'INPUT F?'
        READ*,F

        N=180/H+1
        H=PI/180.*H
        BO=0.
        P=0.

***     DETERMINE FLUID PROPERTIES    ********

        A1=15.49217901
        A2=-5.6783717693
        A3=1.4597584637
        A4=13.877000608
        .5=-80.887673591
        A6=123.56883468
        A7=-188.321212064
        A8=660.91763485
        A9=-1382.4740091
        A10=1300.1040184
        A11=-449.39571976
        TF=TS/1000.
        PSAT=1.E+6*EXP(A1+A2/TF+A3*LOG(TF)+TF*A4+A5*TF**2+A6*TF**3+A7*
       +TF**4+A8*TF**5+A9*TF**6+A10*TF**7+A11*TF**8)
        TB=1500./TS
        TC=2.5*LOG(1.-EXP(-TB))
        TD=.0015/(1.+.0001*TS)-.000942*EXP(TB+TC)*SQRT(1./TB)-.0004882*TB
        R=461.51
        TE=2.*PSAT/(R*TS)
        DENSV=TE/(1.+SQRT(1.+2.*TD*TE))
        TL=(2.*TW+TS)/3.
        DENSL=1./(.0012674-TL*(2.02915E-6-TL*3.8333E-9))
        VISL=2.414E-5*10**(247.8/(TL-140.))
        TG=TL/273.15
        CONDL=-.92407+TG*(2.8395-TG*(1.8007-TG*(.52577-TG*.07344)))
        HFG=3468920.-TS*(5707.4-TS*(11.5562-TS*.0133103))
        SIGML=(-.0003*(TL-273.15)**2-.138*(TL-273.15)+75.6)/1000.

***     DETERMINE THETA(I),X(I),DEFF    ********
***     USE SIMPSON'S RULE TO NUMERICALLY INTEGRATE ALONG SURFACE   ***

        THETA(0)=0.
        X(0)=0.

        DO 10, I=1,N
            THETA(I)=THETA(I-1)+H
            X1=A*XFN(THETA(I-1))
            X2=A*XFN((THETA(I-1)+THETA(I))*.5)
            X3=A*XFN(THETA(I))
            X(I)=X(I-1)+H/6.*(X1+4.*X2+X3)
10      CONTINUE

        DEFF=2.*X(N)/PI

***     DETERMINE DIMENSIONLESS PARAMETERS AS REQUIRED    ****

C       F=VISL*DEFF*HFG*GRAV/(UINF**2*CONDL*(TS-TW))
        UINF=SQRT(VISL*HFG*GRAV/(F*CONDL*(TS-TW)))
```

```
FILE: MIXED1    FORTRAN  A


C       P=DENSV*HFG*VISL/(DENSL*CONDL*(TS-TW))
C       BO=SIGML/(DENSL*GRAV*DEFF**2)
        RE=DENSL*DEFF*UINF/VISL

        PRINT*,'COMPLETED THETA,X,DEFF'

        WRITE(20,5000) 'SAT. TEMP. (K) = ',TS,'WALL TEMP. = ',TW,
       +'1/BO = ',BO,'P = ',P,'F = ',F,'UINF (M/S) = ',UINF,'REL = ',RE
        WRITE(20,5010) '"A" LENGTH (M) = ',A,'"K" ECCENTRICITY = ',K,
       +'DEFF (M) = ',DEFF
        WRITE(20,5020)

***     DETERMINE INITIAL CONDITION, Z0   ********

        B2=SQRT(UINF*DENSL/(DEFF*VISL))
        THETA(0)=1.E-9
        X(0)=1.E-9
        CALL DRV(F2,0.,F21)
        CALL DRV(F3,0.,F31)
        C1=(2*F*G1(0.)+DEFF/A*P*F21+3*(DEFF/A)**2*F*BO*F31)/3.
        C2=F11(0.)
        C3=-2.*A*XFN(0.)/DEFF
        Z(0)=SQRT((SQRT(C2**2-4*C1*C3)-C2)/(2.*C1))
        ALPHA0=CONDL*B2/Z(0)
        SUM=0.

***     DETERMINE DIMENSIONLESS FILM THICKNESS, Z    ****
***     ADAMS-MOULTON PREDICTOR/CORRECTOR ALGORITHM     ****

        FC0=FCN(THETA(0),Z(0))
        ZP1=Z(0)+H*FC0
        Z(1)=Z(0)+H/2.*(FC0+FCN(THETA(1),ZP1))
        FC1=FCN(THETA(1),Z(1))
        ZP2=Z(1)+H/2.*(3.*FC1-FC0)
        Z(2)=Z(1)+H/12.*(5*FCN(THETA(2),ZP2)+8.*FC1-FC0)
        FC2=FCN(THETA(2),Z(2))
        ZP3=Z(2)+H/12.*(23.*FC2-16.*FC1+5.*FC0)
        Z(3)=Z(2)+H/24.*(9.*FCN(THETA(3),ZP3)+19.*FC2-5.*FC1+FC0)
        FC3=FCN(THETA(3),Z(3))

        DO 50,I=4,N
            ZP4=Z(I-1)+H/24.*(55.*FC3-59.*FC2+37.*FC1-9.*FC0)
            Z(I)=Z(I-1)+H/720.*(251.*FCN(THETA(I),ZP4)+646.*FC3-264.*
       +    FC2+106.*FC1-19.*FC0)
            FC0=FC1
            FC1=FC2
            FC2=FC3
            FC3=FCN(THETA(I),Z(I))
            C4=(2.*F*G(THETA(I))+DEFF/A*P*F2(THETA(I))+3.*(DEFF/A)**2*F
       +    *BO*F3(THETA(I)))*Z(I)**3+F1(THETA(I))*Z(I)
            C5=C4+F1(THETA(I))*Z(I)
            IF(C4.LE.0.) THEN
                    PRINT*,'C4 LIMIT'
                    IC=I
                    GO TO 60
            ENDIF
            IF(C5.LE.0.) THEN
                    PRINT*,'C5 LIMIT'
                    IC=I
                    GO TO 60
            ENDIF
50      CONTINUE
        IC=N-1

60      PRINT*,'COMPLETED Z DETERMINATION'

***     DETERMINE HEAT TRANSFER PROPERTIES    *********

        J=0
        JJ=0
        DO 100,I=1,IC
            DELND=Z(I)
```

94

```
            DEL=DELND/B2
            ALPHA=CONDL/DEL
            SUM=SUM+(ALPHA0*A*XFN(THETA(I-1))+ALPHA*A*XFN(THETA(I)))*H*.5
            ALPHA0=ALPHA
            IF(JJ.EQ.J) THEN
                  QFLUX=ALPHA*(TS-TW)
                  NU=DEFF/DEL
                  DQFLUX=1./DELND
                  WRITE(20,5030) THETA(I)*180./PI,X(I)*2./(DEFF*PI),
      +           DEL*1000.,QFLUX/1000.,DELND,DQFLUX,NU
                  WRITE(30,*) X(I)*2./(DEFF*PI),DELND
                  J=J+1./180.*N+1
            ENDIF
            JJ=I+1
100     CONTINUE

      WRITE(20,5030) THETA(IC)*180./PI,X(IC)*2./(DEFF*PI),DEL*1000.,
     +QFLUX/1000.,DELND,DQFLUX,DEFF/DEL
      WRITE(30,*) X(IC)*2./(DEFF*PI),DELND

      NUAVG=SUM*2/(PI*CONDL)

      WRITE(20,5040) 'NU/SQRT(RE) = ',NUAVG/SQRT(RE),'NUAVG = ',NUAVG

5000  FORMAT(1X,T5,70('*') // 1X,T5,'HEAT TRANSFER PROPERTIES' // 2(1X,
     +T10,A17,F6.2 / ),4(1X,T10,A17,E9.3 /))
5010  FORMAT( / 1X,T5,'ELLIPSE GEOMETRY' // 3(1X,T10,A19,F6.4 / ))
5020  FORMAT( / 1X,T7,'THETA',T15,'DIM X',T25,'DEL',T32,'HT FLUX',
     +T41,'DIM DEL',T52,'DIM',T58,'NUSS #' / T7,'(DEG)',T25,'(MM)',T32,
     +'(KW/M2)',T50,'HT FLUX' / T6,7('='),T15,6('='),T23,7('='),T32,
     +7('='),T41,7('='),T50,7('='),T58,6('=') /)
5030  FORMAT(1X,F6.3,F7.3,T15,F6.4,T23,F7.4,T32,E8.2,T41,F7.4,T50,F7.4,
     +T58,E9.3 )
5040  FORMAT( // 3(1X,T5,A17,F8.4 /))
6000  FORMAT(1X,F4.1,F10.3,F7.3)

      END

****************************************************************************

      FUNCTION XFN(PHI)

****************************************************************************
*
*     THIS FUNCTION SUBPROGRAM IS USED TO DETERMINE STREAMWISE LENGTH
*     AS A FUNCTION OF THETA.  XFN REPRESENTS PARAMETRIC RADIUS.
*
****************************************************************************

      REAL XFN,PHI,A,K,DEFF
      COMMON /GEOM/A,K,DEFF
      XFN=SQRT((K**2+.25*((K**2-1.)*SIN(2*PHI))**2/((COS(PHI))**2
     ++(K*SIN(PHI))**2))
      END

****************************************************************************

      FUNCTION G(PHI)

****************************************************************************
*
*     THIS FUNCTION SUBPROGRAM REPRESENTS THE GRAVITY FUNCTION.
*
****************************************************************************

      REAL G,PHI,A,K,DEFF
      COMMON /GEOM/A,K,DEFF
      G=SIN(PHI)/SQRT((SIN(PHI))**2+(K*COS(PHI))**2)
      END

****************************************************************************
```

```
      FUNCTION G1(PHI)

************************************************************************
*
*     THIS FUNCTION SUBPROGRAM REPRESENTS THE STREAMWISE DERIVATIVE
*     OF THE GRAVITY FUNCTION.
*
************************************************************************
      REAL G1,PHI,A,K,DEFF
      COMMON/GEOM/A,K,DEFF
      G1=K**2*COS(PHI)/SQRT(((SIN(PHI))**2+(K*COS(PHI))**2)**3)
      END


************************************************************************

      FUNCTION F1(PHI)

************************************************************************
*
*     THIS FUNCTION SUBPROGRAM REPRESENTS THE VAPOR VELOCITY
*     FUNCTION
*
************************************************************************
      REAL F1,PHI,A,K,DEFF
      COMMON /GEOM/A,K,DEFF
      F1=(1.+K)*SIN(PHI)/SQRT((SIN(PHI))**2+(K*COS(PHI))**2)
      END


************************************************************************

      FUNCTION F11(PHI)

************************************************************************
*
*     THIS FUNCTION SUBPROGRAM REPRESENTS THE STREAMWISE DERIVATIVE
*     OF THE VAPOR VELOCITY FUNCTION.
*
************************************************************************
      REAL F11,PHI,A,K,DEFF
      COMMON/GEOM/A,K,DEFF
      F11=(1.+K)*K**2*COS(PHI)/SQRT(((SIN(PHI))**2+(K*COS(PHI))**2)**3)
      END


************************************************************************

      FUNCTION F2(PHI)

************************************************************************
*
*     THIS FUNCTION SUBPROGRAM REPRESENTS THE PRESSURE GRADIENT
*     FUNCTION.
*
************************************************************************
      REAL F2,PHI,A,K,DEFF
      EXTERNAL XFN
      COMMON/GEOM/A,K,DEFF
      F2=((1.+K)*K)**2*SIN(2*PHI)/((SIN(PHI))**2+(K*COS(PHI))**2)
     +/XFN(PHI)
      END


************************************************************************

      FUNCTION F3(PHI)

************************************************************************
*
*     THIS FUNCTION SUBPROGRAM REPRESENTS THE SURFACE FUNCTION.
*
************************************************************************
```

96

```
      REAL F3,PHI,A,K,DEFF
      EXTERNAL XFN
      COMMON/GEOM/A,K,DEFF
      F3=K*(1.-K**2)*SIN(2*PHI)/SQRT(((SIN(PHI))**2+(K*COS(PHI))**2)
     +**5)/XFN(PHI)
      END
```

****

```
      FUNCTION FCN(PHI,Z)
```

****
```
*
*      THIS FUNCTION SUBPROGRAM IS USED IN A PROBLEM-SOLVER
*      SUBROUTINE TO SOLVE THE O.D.E.
*                  DZ/DX = F(PHI,Z)
*
```
****

```
      REAL F21,F31,PHI,FCN1,FCN2,FCN,A,K,DEFF,F,BO,P

      COMMON /GEOM/A,K,DEFF/PARAM/F,BO,P

      EXTERNAL XFN,G,G1,F1,F11,F2,F3

      CALL DRV(F2,PHI,F21)
      CALL DRV(F3,PHI,F31)

      FCN1=(2.*F*G(PHI)+DEFF/A*P*F2(PHI)+3.*(DEFF/A)**2*F*BO*F3(PHI))
     +*Z**3+F1(PHI)*Z
      FCN2=2.*A*XFN(PHI)/DEFF-(2.*F*G1(PHI)+DEFF/A*P*F21+3.*(DEFF/A)**2
     +*F*BO*F31)*Z**4/3.-F11(PHI)*Z**2
      FCN=FCN2/FCN1

      END
```

****

```
      SUBROUTINE DRV(FN,PHI,FN1)
```

****
```
*
*      THIS SUBROUTINE NUMERICALLY DIFFERENTIATES A FUNCTION.
*
```
****

```
      REAL FN,PHI,FN1,EPS
      FN1=(FN(PHI+1.E-6)-FN(PHI-1.E-6))/2.E-6
      RETURN
      END
```

APPENDIX C - COMPUTER CODE FOR TWO-PHASE BOUNDARY LAYER

MODEL

```
*       PROGRAM VAPBL1

***************************************************************
*
*       THIS PROGRAM NUMERICALLY SOLVES THE PROBLEM OF MIXED
*       CONVECTION CONDENSATION WITH SURFACE TENSION ON AN ELLIPTICAL
*       CYLINDER.  THE PROBLEM FORMULATION USES THE SOLUTION OF THE
*       TWO-PHASE BOUNDARY LAYER EQUATIONS FOR THE CONDENSATE AND VAPOR.
*
*       THE PROGRAM USES AN IMSL NUMERICAL PROBLEM SOLVER, DIVPAG,
*       TO SOLVE A 1ST ORDER ORDINARY DIFFERENTIAL EQUATION.  THE
*       PROBLEM SOLVER IS WRITTEN IN DOUBLE PRECISION WHILE THE MAIN
*       PROGRAM IS IN SINGLE PRECISION.  THE MAIN PROGRAM MUST BE
*       COMPILED IN DOUBLE PRECISION (AUTO DOUBLE).
*
*       THIS PROGRAM CAN BE RUN WITH DIMENSIONLESS PARAMETERS
*       (F,G) SPECIFIED OR WHERE THE PARAMETERS ARE CALCULATED
*       BASED ON SPECIFIED FLUID PROPERTIES.  MODIFICATIONS TO THE
*       PROGRAM (REMOVAL OF UNNECCESSARY STEPS BY "COMMENTING" THE
*       STATEMENT OUT OF THE PROGRAM) IS REQUIRED.   SPECIFIED FLUID
*       PROPERTIES INCLUDE T SAT, T WALL, AND UINF.
*
*       IF THE ALGORITHM HAS DIFFICULTY LOCATING THE VAPOR SEPARATION
*       POINT, THEN THE PROGRAM NEEDS TO BE MODIFIED TO INPUT THE
*       PARAMETRIC AND, PHI, FOR THE SEPARATION POINT.
*
*       NUMERICAL RESULTS ARE DIRECTED TO AN EXTERNAL DATA FILE.
*
*       MAJOR VARIABLES USED ARE:
*
*          PHI         PARAMETRIC ANGLE
*          X           STREAMWISE LENGTH
*          DEFF        EFFECTIVE DIAMETER
*          DEL         CONDENSATE FILM THICKNESS
*          DELND       DIMENSIONLESS FILM THICKNESS
*          Z           DIMENSIONLESS VAPOR MOMENTUM THICKNESS
*          F,JARPRL    DIMENSIONLESS PARAMETERS
*          UINF        VAPOR FREE STREAM VELOCITY
*          TS          VAPOR SATURATION TEMPERATURE
*          TW          WALL SURFACE TEMPERATURE
*          DENSL       CONDENSATE DENSITY
*          DENSV       VAPOR DENSITY
*          CONDL       CONDENSATE THERMAL CONDUCTIVITY
*          VISL        CONDENSATE VISCOSITY
*          VISV        VISCOSITY OF VAPOR
*          HFG         LATENT HEAT OF VAPORIZATION
*          NU          NUSSELT NUMBER
*          REV         VAPOR REYNOLDS NUMBER
*          RE          TWO-PHASE REYNOLDS NUMBER
*          NUAVG       MEAN NU NUMBER
*          ALPHA       HEAT TRANSFER COEFFICIENT
*          QFLUX       HEAT FLUX
*          A           SEMI-MAJOR AXIS
*          K           ECCENTRICITY
*          XFN         PARAMETRIC RADIUS
*          G           GRAVITY FUNCTION
*          F1          VELOCITY FUNCTION
*          F11         DERIVATIVE, VELOCITY FUNCTION
*          F2          PRESSURE GRADIENT FUNCTION
*          F3          SURFACE TENSION FUNCTION
*          TAU         INTERFACIAL SHEAR
*          KAPPA       PRESSURE GRADIENT FORM PARAMETER
*          KAPPAA      SUCTION FORM PARAMETER
*
***************************************************************

        PARAMETER(PI=3.141592654,GRAV=9.807,NEQ=2,NEQ1=1,NPARAM=50)

        REAL PHI(0:180000),DEL(0:180000),X(0:180000),A,TS,TW,
       +H,A1,A2,A3,A4,A5,A6,A7,A8,A9,A10,A11,TF,PSAT,TB,TC,TD,R,TE,DENSV,
       +TL,DENSL,VISL,VISV,TG,CONDL,HFG,SIGML,F,K,X1,X2,X3,DEFF,UINF,
       +REV,RE,JARPRL,DEL00,DEL0,Z0,TAU,DTAU,FDEL0,DFDEL0,DEL1,Z1,ALPHA0,
```

```
        +SUM,AA(1,1),FCN,FCNJ,HINIT,PARAM(NPARAM),KAPPA,KAPPAA,DKAPPA,
        +TOL,XEND,XBEG,Y(2),DDEL,DZ,Y1(1),NU,NUAVG,NUORE,DKAPPAA,X0,DX0,
        +DELND,DELL,ALPHA,QFLUX,DQFLUX,D2UPHI,DUPHI,UPHI

         INTEGER N,JJ,II,IDO,IMETH

         COMMON /GEOM/A,K,DEFF/PARAM/JARPRL,F

         EXTERNAL ZFN,DELFN,XFN,G,G1,F1,F11,NUSSELT,DRV,FCN,FCNJ,IVPAG,
        +SSET

         OPEN(20,FILE='/VAPOR1 OUTPUT A1',STATUS='OLD')
         OPEN(30,FILE='/VAPOR2 OUTPUT A1',STATUS='OLD')

         PRINT*,'ELLIPSE OF THE FORM (X/B)**2+(Y/A)**2=1'
         PRINT*,'INPUT "A" DIMENSION (M)?'
         READ*,A
         PRINT*,'INPUT T SAT AND T WALL (K)?'
         READ*,TS,TW
         PRINT*,'INPUT ANGLE STEP SIZE (DEGREES)?'
         READ*,H
         PRINT*,'STEP SIZE, H = ',H
C        PRINT*,'INPUT PHI AT SEPARATION?'
C        READ*,PHIS
         PRINT*,'INPUT UINF?'
         READ*,UINF
         PRINT*,'INPUT K?'
         READ*,K
C         PRINT*,'INPUT G?'
C         READ*,JARPRL

         N=180/H+1
         PRINT*,'N-1=',N-1
         H=PI/180.*H

***     DETERMINE FLUID PROPERTIES   ********

         A1=15.49217901
         A2=-5.6783717693
         A3=1.4597584637
         A4=13.877000608
         A5=-80.887673591
         A6=123.56883468
         A7=-188.321212064
         A8=660.91763485
         A9=-1382.4740091
         A10=1300.1040184
         A11=-449.39571976
         TF=TS/1000.
         PSAT=1.E+6*EXP(A1+A2/TF+A3*LOG(TF)+TF*A4+A5*TF**2+A6*TF**3+A7*
        +TF**4+A8*TF**5+A9*TF**6+A10*TF**7+A11*TF**8)
         TB=1500./TS
         TC=2.5*LOG(1.-EXP(-TB))
         TD=.0015/(1.+.0001*TS)-.000942*EXP(TB+TC)*SQRT(1./TB)-.0004882*TB
         R=461.51
         TE=2.*PSAT/(R*TS)
         DENSV=TE/(1.+SQRT(1.+2.*TD*TE))
         TL=(2.*TW+TS)/3.
         DENSL=1./(.0012674-TL*(2.02915E-6-TL*3.8333E-9))
         VISL=2.414E-5*10**(247.8/(TL-140.))
         VISV=-4.478415E-6+TS*(5.0216E-8-1.579E-11*TS)
         TG=TL/273.15
         CONDL=-.92407+TG*(2.8395-TG*(1.8007-TG*(.52577-TG*.07344)))
         HFG=3468920.-TS*(5707.4-TS*(11.5562-TS*.0133103))
         SIGML=(-.0003*(TL-273.15)**2-.138*(TL-273.15)+75.6)/1000.

***     DETERMINE PHI(I),X(I),DEFF   ********
***     USES SIMPSON'S RULE TO NUMERICALLY INTEGRATE ALONG SURFACE   ***

         PHI(0)=0.
         X(0)=0.
```

```
        DO 10, I=1,N
            PHI(I)=PHI(I-1)+H
            X1=XFN(PHI(I-1))
            X2=XFN((PHI(I-1)+PHI(I))*.5)
            X3=XFN(PHI(I))
            X(I)=X(I-1)+H/6.*(X1+4.*X2+X3)
10      CONTINUE

        DEFF=2.*X(N)/PI
        PRINT*,'COMPLETED DE DETERMINATION, DE=',DEFF

****    DIMENSIONLESS PARAMETER DETERMINATION    ****

        F=VISL*DEFF*HFG/(CONDL*UINF**2*(TS-TW))
        REV=UINF*DENSV*DEFF/VISV
        RE=UINF*DENSL*DEFF/VISL
        JARPRL=CONDL*(TS-TW)/HFG*SQRT(DENSL/(DENSV*VISL*VISV))
        PRINT*,'COMPLETED PARAMETER DETERMINATION'

        WRITE(20,5000) 'SAT. TEMP. (K) = ',TS,'WALL TEMP. = ',TW,
       +'F = ',F,'UINF (M/S) = ',UINF,'G = ',JARPRL
        WRITE(20,5010) '"A" LENGTH (M) = ',A,'"K" ECCENTRICITY = ',K,
       +'DEFF (M) = ',DEFF

***     DETERMINE INITIAL VALUES OF Z AND DEL            ***
***     USES INTIAL VALUE OF DEL FROM SHEKRILADZE-GOMELAURI   ***
***     FOR MIXED CONVECTION AS STARTING POINT TO FIND Z THEN ***
***     REDETERMINES DEL FOR THE PREDICTED VALUE OF Z USING   ***
***     NEWTON'S METHOD, CHECKS FOR CONVERGENCE AND ITERATES  ***

        DELOO=SQRT(.75*K/F*(SQRT(((1.+K)/K)**2+16.*F*A/(3.*DEFF))
       +-(1.+K)/K))

        DELO=DELOO
        Z0=(-.0735*XFN(0.)*JARPRL/DEFF/F11(0.)/DELO+SQRT((.0735*
       +XFN(0.)*JARPRL/DEFF/F11(0.)/DELO)**2+.0735*XFN(0.)/DEFF/
       +F11(0.)))**2

        UPHI=F1(0.)
        DUPHI=F11(0.)
        CALL DRV(F11,0.,D2UPHI)
        X0=XFN(0.)
        CALL DRV(XFN,0.,DX0)

20      KAPPA=DEFF/X0*DUPHI*Z0
30      KAPPAA=.0682+.174*JARPRL*SQRT(Z0)/DELO

        DKAPPA=DEFF*Z0*D2UPHI/X0-DEFF*DUPHI*Z0*DX0/X0**2
        DTAU=6.44*SQRT(KAPPA*KAPPAA+KAPPAA**2)*DUPHI/SQRT(Z0)+3.22*UPHI
       +*KAPPAA*DKAPPA/SQRT(Z0)/SQRT(KAPPA*KAPPAA+KAPPAA**2)

        FDELO=X0/DEFF-F/3.*G1(0.)*DELO**4-DTAU*DELO**3/(4.*JARPRL)
        DFDELO=-4.*F*G1(0.)*DELO**3/3.-3.*DTAU*DELO**2/(4.*JARPRL)
        DEL1=DELO-FDELO/DFDELO
        IF((ABS(DEL1-DELO).GT.(.001*DELO)).AND.(FDELO.GT.1.E-7)) THEN
            DELO=DEL1
            GO TO 30
        ENDIF

        Z1=(-.0735*XFN(0.)*JARPRL/(DEFF*F11(0.)*DEL1)+SQRT((.0735*
       +XFN(0.)*JARPRL/(DEFF*F11(0.)*DEL1))**2+.0735*XFN(0.)/(DEFF*
       +F11(0.))))**2

        IF ((ABS(DEL1-DELOO).GT.(.001*DELOO)).OR.(ABS(Z1-Z0).GT.(.001*
       +Z0))) THEN
            Z0=Z1
            DELOO=DEL1
            DELO=DEL1
            GO TO 20
        ENDIF

        DEL(0)=DEL1
```

```
        ALPHA0=1./DEL(0)
        SUM=0.
        PRINT*,'COMPLETED Z(0),DEL(0) DETERMINATION',' Z=',Z1,
       +'DEL=',DEL(0)

***     EVALUATION OF Z(I) AND DEL(I)                    ****
***     USES IMSL ROUTINE DIVPAG                         ****

        HINIT=1.E-4
        IMETH=2
        CALL SSET(NPARAM,0.0,PARAM,1)
        PARAM(1)=HINIT
        PARAM(12)=IMETH
        XBEG=PHI(0)
        Y(1)=Z1
        Y(2)=DEL(0)
        TOL=1.E-3
        IDO=1
        DO 100,I=1,N-1
C       IF(PHI(I).GT.PHIS) GO TO 190
        XEND=PHI(I)
        CALL DIVPAG(IDO,NEQ,FCN,FCNJ,AA,XBEG,XEND,TOL,PARAM,Y)
        DEL(I)=Y(2)
        KAPPA=DEFF/XFN(PHI(I))*F11(PHI(I))*Y(1)
        KAPPAA=.0682+.174*JARPRL*SQRT(Y(1))/Y(2)
        TAU=6.44*F1(PHI(I))*SQRT(KAPPA*KAPPAA+KAPPAA**2)/SQRT(Y(1))
        WRITE(30,*) 'PHI=',PHI(I)*180/PI,'TAU=',TAU
        II=I

***     CHECK FOR VAPOR BOUNDARY LAYER SEPARATION       ****

        IF(TAU.LE.0.) GO TO 190
100     CONTINUE

190     PRINT*,'SEPARATION ANGLE AT PHI=',PHI(II)*180./PI
        PRINT*,'TAU=',TAU,'DEL=',DEL(II)

        IDO=3
        CALL DIVPAG(IDO,NEQ,FCN,FCNJ,AA,XBEG,XEND,TOL,PARAM,Y)

***     USES A SIMPLE NUSSELT ANALYSIS TO COMPUTE FILM THICKNESS  ****
***     DOWNSTREAM OF THE SEPARATION POINT.  PROBLEM SOLVER IS    ****
***     IMSL DIVPAG                                               ****

        IF(II.NE.(N-1)) THEN
           XBEG=PHI(II)
           IDO=1
           Y1(1)=DEL(II)
           DO 200, I=II+1,N-1
              XEND=PHI(I)
              CALL DIVPAG(IDO,NEQ1,NUSSELT,FCNJ,AA,XBEG,XEND,TOL,PARAM
      +         ,Y1)
              DEL(I)=Y1(1)
200        CONTINUE
        ENDIF
        IDO=3
        CALL DIVPAG(IDO,NEQ1,NUSSELT,FCNJ,AA,XBEG,XEND,TOL,PARAM,Y1)

        PRINT*,'COMPLETED Z(I), DEL(I) DETERMINATION'
        WRITE(20,5050) PHI(II)*180./PI
        WRITE(20,5020)

***     DETERMINE HEAT TRANSFER PROPERTIES     *********

        JJ=0
        DO 300,I=1,N-1
           DELND=DEL(I)
           DELL=DELND*SQRT(VISL*DEFF/(DENSL*UINF))
           ALPHA=1./DEL(I)
           SUM=SUM+(ALPHA0*XFN(PHI(I-1))+ALPHA*XFN(PHI(I)))*H*.5
           ALPHA0=ALPHA
```

```
          IF((JJ.EQ.I).OR.(JJ.EQ.0)) THEN
               QFLUX=ALPHA*(TS-TW)
               NU=DEFF/DELL
               DQFLUX=1./DELND
               JJ=JJ+10./180.*N+1
                WRITE(20,5030) PHI(I)*180/PI,X(I)*2/(DEFF*PI),DELL
       +            *1000,QFLUX/1000,DELND,DQFLUX,NU
          ENDIF
300    CONTINUE

       WRITE(20,5030) PHI(N-1)*180./PI,X(N-1)*2./(DEFF*PI),DELL*1000.,
      +QFLUX/1000.,DELND,DQFLUX,DEFF/DELL
       WRITE(30,*) X(N-1)*2./(DEFF*PI),DELND

       NUAVG=SUM*2/(PI*DEFF)

       WRITE(20,5040) 'NU/SQRT(RE) = ',NUAVG/SQRT(RE)

5000   FORMAT(1X,T5,70('*') // 1X,T5,'HEAT TRANSFER PROPERTIES' // 2(1X,
      +T10,A17,F6.2 / ),5(1X,T10,A17,E9.3 /))
5010   FORMAT( / 1X,T5,'ELLIPSE GEOMETRY' // 3(1X,T10,A19,F6.4 / ))
5020   FORMAT( / 1X,T7,'THETA',T15,'DIM X',T25,'DEL',T32,'HT FLUX',
      +T41,'DIM DEL',T52,'DIM',T58,'NUSS #' / T7,'(DEG)',T25,'(MM)',T32,
      +'(KW/M2)',T50,'HT FLUX' / T6,7('='),T15,6('='),T23,7('='),T32,
      +7('='),T41,7('='),T50,7('='),T58,6('=') /)
5030   FORMAT(1X,T6,F7.3,T15,F6.4,T23,F7.4,T32,E8.2,T41,F7.4,T50,F7.4,
      +T58,F9.1)
5040   FORMAT( // 3(1X,T5,A17,F8.4 /))
5050   FORMAT(1X,T6,'VAPOR SEPARATION AT PHI = ',F6.2)

       END

*********************************************************************

       FUNCTION XFN(PHI)

*********************************************************************
*
*      THIS FUNCTION SUBPROGRAM IS USED TO DETERMINE STREAMWISE LENGTH
*      AS A FUNCTION OF PHI.
*
*********************************************************************

       REAL XFN,PHI,A,K,DEFF
       COMMON /GEOM/A,K,DEFF
       XFN=A*SQRT((K**2+.25*((K**2-1.)*SIN(2*PHI))**2)/((COS(PHI))**2
      ++(K*SIN(PHI))**2))
       END

*********************************************************************

       FUNCTION G(PHI)

*********************************************************************
*
*      GRAVITY FUNCTION
*
*********************************************************************

       REAL G,PHI,A,K,DEFF
       COMMON /GEOM/A,K,DEFF
       G=SIN(PHI)/SQRT((SIN(PHI))**2+(K*COS(PHI))**2)
       END

*********************************************************************

       FUNCTION G1(PHI)

*********************************************************************
*
*      STREAMWISE DERIVATIVE OF GRAVITY FUNCTION
*
```

102

```
****************************************************************

      REAL G1,PHI,A,K,DEFF
      COMMON/GEOM/A,K,DEFF
      G1=K**2*COS(PHI)/SQRT(((SIN(PHI))**2+(K*COS(PHI))**2)**3)
      END

****************************************************************

      FUNCTION F1(PHI)

****************************************************************
*
*     VAPOR VELOCITY FUNCTION
*
****************************************************************

      REAL F1,PHI,A,K,DEFF
      COMMON /GEOM/A,K,DEFF
      F1=(1.+K)*SIN(PHI)/SQRT((SIN(PHI))**2+(K*COS(PHI))**2)
      END

****************************************************************

      FUNCTION F11(PHI)

****************************************************************
*
*     STREAMWISE DERIVATIVE OF VELOCITY FUNCTION
*
****************************************************************

      REAL F11,PHI,A,K,DEFF
      COMMON/GEOM/A,K,DEFF
      F11=(1.+K)*K**2*COS(PHI)/SQRT(((SIN(PHI))**2+(K*COS(PHI))**2)**3)
      END

****************************************************************

      FUNCTION DELFN(PHI,Z,DEL,DZ)

****************************************************************
*
*     STREAMWISE DERIVATIVE OF CONDENSATE FILM THICKNESS
*
****************************************************************

      REAL DELFN,PHI,Z,DEL,DZ,DELFN1,DELFN2,DELFN3,X,FF1,FF11,FF12,DXFN
     +,A,K,DEFF,JARPRL,F,KAPPA,KAPPAA,XX,FKAPPA

      EXTERNAL XFN,F1,F11,G,G1

      COMMON/GEOM/A,K,DEFF/PARAM/JARPRL,F

      IF(PHI.EQ.0.D+0) THEN
          DELFN=0.D+0
      ELSE
      FF1=F1(PHI)
      FF11=F11(PHI)
      CALL DRV(F11,PHI,FF12)
      X=XFN(PHI)
      CALL DRV(XFN,PHI,DXFN)
      KAPPA=DEFF*FF11*Z/X
      KAPPAA=.0682+.174*JARPRL*SQRT(Z)/DEL
      XX=KAPPAA*KAPPA+KAPPAA**2
      FKAPPA=SQRT(XX)

      DELFN1=.805*KAPPAA*DEFF*FF1*FF11*DEL**3/(JARPRL*FKAPPA*X*SQRT(Z))
     ++(7.0035E-2)*(2.*KAPPAA+KAPPA)*FF1*DEL**2/(FKAPPA*Z)-.805*FKAPPA*
     +FF1*DEL**3/(JARPRL*Z**1.5)
```

```
      DELFN2=F*G(PHI)*DEL**3+3.22*FF1*FKAPPA*DEL**2/(JARPRL*SQRT(Z))
     +-.14007*(2.*KAPPAA+KAPPA)*FF1*DEL/FKAPPA

      DELFN3=X/DEFF-F*G1(PHI)*DEL**4/3.-1.61*FKAPPA*FF11*DEL**3/(JARPRL
     +*SQRT(Z))-.305*KAPPAA*DEFF*FF1*FF12*SQRT(Z)*DEL**3/(JARPRL*FKAPPA*
     +X)+.305*KAPPAA*DEFF*DXFN*FF1*FF11*SQRT(Z)*DEL**3/(JARPRL*FKAPPA*
     +X**2)

      DELFN=(DELFN3-DELFN1*DZ)/DELFN2
      ENDIF
      END

***************************************************************************

      FUNCTION ZFN(PHI,Z,DEL)

***************************************************************************
*
*     STREAMWISE DERIVATIVE OF VAPOR MOMENTUM THICKNESS PARAMETER
*
***************************************************************************

      REAL ZFN,PHI,Z,DEL,DEFF,A,K,JARPRL,F

      EXTERNAL XFN
      EXTERNAL F1
      EXTERNAL F11

      COMMON/GEOM/A,K,DEFF/PARAM/JARPRL,F

      IF(PHI.EQ.0.D+0) THEN
          ZFN=0.D+0
      ELSE
      ZFN=(.441*(1.-2.*JARPRL*SQRT(Z)/DEL)-6.*DEFF*F11(PHI)*Z/XFN(PHI))
     +*XFN(PHI)/F1(PHI)/DEFF
      ENDIF

      END

***************************************************************************

      SUBROUTINE NUSSELT(NEQ,PHI,Y,YPRIME)

***************************************************************************
*
*     STREAMWISE DERIVATIVE OF CONDENSATE FILM THICKNESS USING
*     A NUSSELT ANALYSIS DOWNSTREAM OF VAPOR SEPARATION POINT.
*
***************************************************************************

      INTEGER NEQ
      REAL PHI,Y(NEQ),YPRIME(NEQ),A,K,DEFF,JARPRL,F

      EXTERNAL XFN,G,G1

      COMMON/GEOM/A,K,DEFF/PARAM/JARPRL,F

      YPRIME(1)=(XFN(PHI)/DEFF-F/3.*Y(1)**4*G1(PHI))/(F*G(PHI)*Y(1)**3)

      RETURN
      END

***************************************************************************

      SUBROUTINE DRV(FN,PHI,FN1)

***************************************************************************
*
*     SUBROUTINE TO NUMERICALLY DIFFERENTIATE A FUNCTION
*
***************************************************************************
```

```
      REAL FN,PHI,FN1,EPS
      FN1=(FN(PHI+1.E-6)-FN(PHI-1.E-6))/2.E-6

      RETURN
      END

***************************************************************

      SUBROUTINE TAUFN(PHI,Z,DEL,DZ,DDEL,TAU,DTAU)

***************************************************************
*
*     SUBROUTINE TO DETERMINE THE INTERFACIAL SHEAR STRESS AND
*     ITS STREAMWISE DERIVATIVE.
*
***************************************************************

      REAL PHI,Z,DEL,DXFN,DZ,DDEL,KAPPA,KAPPA1,KAPPAA,DKAPPA,
     +DKAPPA1,DKAPPAA,TAU,DTAU,A,K,DEFF,JARPRL,F

      EXTERNAL XFN,F1,F11

      COMMON/GEOM/A,K,DEFF/PARAM/JARPRL,F

      CALL DRV(F11,PHI,F12)
      CALL DRV(XFN,PHI,DXFN)

      KAPPA=DEFF*F11(PHI)*Z/XFN(PHI)
      KAPPA1=JARPRL*SQRT(Z)/DEL
      KAPPAA=.0682+.174*KAPPA1
      DKAPPA=DEFF/XFN(PHI)*(Z*F12+F11(PHI)*DZ)-DEFF/(XFN(PHI))**2*
     +F11(PHI)*Z*DXFN
      DKAPPA1=JARPRL*(.5*DEL*DZ-Z*DDEL)/(SQRT(Z)*DEL**2)
      DKAPPAA=.174*DKAPPA1

      TAU=6.44*F11(PHI)*SQRT((KAPPAA*KAPPA+KAPPAA**2)/Z)
      DTAU=6.44*(((KAPPAA*KAPPA+KAPPAA**2)*F11(PHI)+.5*F1(PHI)*
     +(KAPPAA*DKAPPA+(2.*KAPPAA+KAPPA)*DKAPPAA))/SQRT(Z*(KAPPAA*
     +KAPPA+KAPPAA**2))-.5*(KAPPAA*KAPPA+KAPPAA**2)*F1(PHI)*DZ/
     +SQRT(Z**3*(KAPPAA*KAPPA+KAPPAA**2)))

      RETURN
      END

***************************************************************

      SUBROUTINE FCN(NEQ,X,Y,YPRIME)

***************************************************************
*
*     SUBROUTINE TO INPUT DIFFERENTIAL EQUATION TO BE SOLVED
*     BY THE PROBLEM SOLVER.
*
***************************************************************

      INTEGER NEQ

      REAL X,Y(NEQ),YPRIME(NEQ)

      EXTERNAL ZFN,DELFN

      YPRIME(1)=ZFN(X,Y(1),Y(2))
      YPRIME(2)=DELFN(X,Y(1),Y(2),YPRIME(1))

      RETURN
      END

***************************************************************

      SUBROUTINE FCNJ(NEQ,X,Y,DYPDY)

***************************************************************
```

105

FILE: VAPBL   FORTRAN   A

```
*
*      SUBROUTINE REQUIRED BY PROBLEM SOLVER, NO FUNCTION IN ANALYSIS
*
*****************************************************************
       INTEGER NEQ

       REAL X,Y(NEQ),DYPDY(*)

       RETURN
       END
```

LIST OF REFERENCES

1. *Standards for Steam Surface Condensers*, 6th ed., Heat Exchange Institute, 1970.

2. *Standards of Tubular Exchanger Manufacturers Association*, 4th ed., Tubular Exchanger Manufacturers Association, Inc., 1959.

3. Walker, G., *Industrial Heat Exchangers*, McGraw-Hill, New York, 1982.

4. Marto, P.J., "Heat Transfer and Two-Phase Flow during Shell-side Condensation", *Heat Transfr Engng*, vol. 5, No. 1-2: 31-61, 1984.

5. Nusselt, W., "Des Oberflächenkondensation des Wasserdampfes", *Zeit. Ver. Deutsch. Ing.*, vol. 60: 569-575, 1916.

6. Rose, J.W., "Fundamentals of Condensation Heat Transfer: Laminar Film Condensation, *Trans. JSME*, vol. 31: 357-375, 1988.

7. Marto, P.J., "Recent Progress in Enhancing Film Condensation Heat Transfer in Horizontal Tubes", *Heat Transfer Eng.*, vol. 7, No. 3-4: 53-63, 1986.

8. Bergles, A.E., Webb, R.L. and Junkan, G.H., "Energy Conservation via Heat Transfer Enhancement", *Energy*, vol. 4: 193-200, 1979.

9. Webb, R.L., "The Use of Enhanced Surface Geometries in Condensers: An Overview", *Power Condenser Heat Transfer Technology*, Marto, P.J. and Nunn, R.H. eds., pp. 287-324, Hemisphere Publishing Corp., New York, 1981.

10. Dhir, V. and Lienhard, J., "Laminar Film Condensation on Plane and Axisymetric Bodies in Non-uniform Gravity", *Trans. ASME J. Heat Transfer*, vol. 93: 97-100, 1971.

11. Shklover, G.G., Semenov, V.P., Pryakhin, V.V. and Usachev, A.M., "Heat Transfer with Steam Condensing on a Horizontal Tube with a Profile of Variable Curvature", *Therm. Engng*, vol. 32: 125-127, 1985.

12. Semenov, V.P., Shklover, G.G., Usachev, A.M. and Semenova, T.P., "Enhancement of Heat Transfer in Condensation of Steam on a Horizontal Noncircular Pipe", *Heat Transfer - Soviet Research*, 22: 15-20, 1990.

13. Wallis, R.P., "Photographic Study of Fluid Flow Between Banks of Tubes", *Engineering*, vol. 148: 423-425, 1939.

14. Joyner, V.T. and Palmer, C.B., "An Experimental Survey of Flow Across Banks of Elliptical and Pointed Tubes", *NACA WRL-609*, 1943.

15. Ota, T. and Nishiyama, H., "Heat Transfer and Flow Around an Elliptic Cylinder", *Int. J. Heat Mass Transf.*, vol. **27**: 1771-1779, 1984.

16. Moalem, D and Sideman, S., "Theoretical Analysis of a Horizontal Condenser-Evaporato' Elliptical Tube", *Trans. ASME J. Heat Transf.*, vol. **97**: 352-359, 1975.

17. Huang, S.Y. and Mayinger, F., "Wärmeübergang bei freier Konvektion um elliptische Rohre", *Wärme and Stoffübertragung*, vol. **18**: 175-183, 1984. ("Heat Transfer with Natural Convection Around Elliptical Tubes")

18. Merker, G.P. and Bähr, M., "Stoffübergang und Druckverlust in quer angeström ten Rohrbündeln mit versetzt angeordneten Profilrohren", *Wärme und Stoffübertragung*, vol. **27**: 187-194, 1992. ("Mass Transfer and Pressure Drop in Cross Flow Tube Banks with Staggered Profile Tubes")

19. Sparrow, E.M. and Gregg, J.L., "A Boundary Layer Treatment of Laminar Film Condensation", *Trans. ASME J. Heat Transf.*, vol. **81C**: 13-18, 1959.

20. Sparrow, E.M. and Gregg, J.L., "Laminar Condensation Heat Transfer on a Horizontal Cylinder", *Trans. ASME J. Heat Transf.*, vol. **81C**: 291-296, 1959.

21. Shekriladze, I.G. and Gomelauri, V.I., "Theoretical Study of Laminar Film Condensation of Flowing Vapour", *Int. J. Heat Mass Transf.*, vol. **9**: 581-591, 1966.

22. Fujii, T., Honda, H. and Oda, K., "Condensation of Steam on a Horizontal Tube - The Influence of Oncoming Velocity and Thermal Condition at the Tube Wall", *Condensation Heat Transfer*, pp. 35-43, ASME, New York, 1979.

23. Truckenbrodt, E., "Ein einfaches Näherungsverfahren zum Berechnen der laminaren Reibungsverfahren mit Absaugung", *Forschung*, **22**: 147-157, 1956. ("A Simple Approximation Method for Calculating a Viscous Laminar Boundary Layer with Suction")

24. Terril, R.M., "Laminar Boundary - Layer Flow Near Separation with and without Suction", *Phil. Trans. Roy. Soc. London*, Ser. A., vol. **253**: 55-100, 1960.

25. Lee, W.C. and Rose, J.W., "Film Condensation on a Horizontal Tube - Effect of Vapour Velocity", *Proc. 7th Int. Heat Transf. Conf., Munich*, vol. **5**: 101-106, 1982.

26. Gaddis, E.S., "Solution of the Two Phase Boundary-Layer Equations for Laminar Film Condensation of Vapour Flowing Perpendicular to a Horizontal Cylinder", *Int. J. Heat Mass Transf.*, vol. **22**: 371-382, 1979.

27. di Marzo, M. and Casarella, M.J., "Film Condensation over a Horizontal Cylinder for Combined Gravity and Forced Flow", *Trans. ASME J. Heat Transf.*, vol. **107**: 687-695, 1985.

28. Rose, J.W., "Effect of Pressure Gradient in Forced Convection Film Condensation on a Horizontal Tube", *Int. J. Heat Mass Transfer*, vol. **27**: 39-47, 1984.

29. Krupiczka, R., "Effect of Surface Tension on Laminar Film Condensation on a Horizontal Cylinder", *Chem. Eng. Process.*, vol. **19**: 199-203, 1985.

30. Cheng, S. and Tao, J., "Study of Condensation Heat Transfer for Elliptical Pipes in Stationary Saturated Vapor", *ASME, Proc. of 1988 Nat. Heat Transf. Conf.*, Vol. 2: 405-408, 1988.

31. Ali, A.F.M. and McDonald, T.W., "Laminar Film Condensation on Horizontal Cylinder: A First Approximation for Condensation on Inclined Tubes", *ASHRAE Trans.*, vol. **83**, part 2: 242-249, 1977.

32. Wang, J.C.Y., Jiang, Z., Yiwei, M. and Yi, F., "Laminar Film Condensation of Pure Saturated Vapors on Horizontal Elliptical Tubes", *Proc. Int. Symp. on Phase Change Heat Transf.*, p. 307-311, 1988.

33. Sheng, A.Y. and Cha'o, K.C., "Effect of Surface Tension Upon Laminar Film Condensation on a Horizontal Elliptical Tube with Variable Wall Temperature", To be published, 1992.

34. Memory, S.B. and Rose, J.W., "Free Convection Laminar Film Condensation on a Horizontal Tube with Variable Wall Temperature", *Int. J. Heat Mass Transf.*, vol. **34**: 2775-2778, 1991.

35. Panday, P.K., "Laminar Film Condensation of Downward Flowing Vapour on a Horizontal Elliptic Cylinder - A Numerical Solution", *Int. Comm. Heat Mass Transf.*, vol. **14**: 33-43, 1987.

36. Pohlhausen, K., "Zur näherungsweisen Integration der Differentialgleichung der laminaren Reibungsschicht", *ZAMM*, vol. **1**: 252-268, 1921.

37. Schlicting, H., "Ein Näherungsverfahren zur Berechnung der laminaren Reibungsschicht mit Absaugung", *Ing.-Arch.*, vol. **16**: 201-220, 1948.

38. Torda, T.P., "Boundary Layer Control by Continuous Surface Suction or Injection", *J. Math. Phys.*, vol. **31**: 206-213, 1952.

39. Crandall, S.H., *Engineering Analysis, A Survey of Numerical Procedures*, pp. 174-187, Robert E. Krieger Publishing Co., 1986.

40. Lee, W.C., private communication, 1993.

41. *International Mathematical and Statistical Library (IMSL)*, IMSL, Inc., Houston, TX.

42. Gear, C.W., *Numerical Initial Value Problems in Ordinary Differential Equations*, pp. 209-229, Prentice-Hall, Inc., 1971.

43. Lewis, D., A.T. Wall, Co., Warwick, RI, private communication, 1992.

44. White, F.M., *Fluid Mechanics*, 2nd Edition, McGraw-Hill, New York, 1986.

45. Incropera, F.P. and Dewitt, D.P., *Introduction to Heat Transfer*, 2nd Ed., John Wiley and Sons, New York, 1990.

46. Aoune, A. and Burnside, B.M., "Vapour Shear Effects on Tubes in a Horizontal Row in Downward Condensing Flow", *Proc. 2nd Int. Symp. on Condensers and Condensation*, Univ. of Bath: 461-472, 1990.

47. Aoune, A. and Burnside, B.M., "The Influence of Tube Spacing on Vapour Shear in Condensation of Downward Flowing Vapour on a Row of Horizontal Tubes", *Proc. 9th Int. Heat Transfer Conf., Jerusalem*, vol. 3: 27-31, 1990.

INITIAL DISTRIBUTION LIST

	No. Copies
1. Defense Technical Information Center Cameron Station Alexander, VA 22304-6145	2
2. Library, Code 52 Naval Postgraduate School Monterey, CA 93943-5002	2
3. Department Chairman, Code ME/Kk Department of Mechanical Engineering Naval Postgraduate School Monterey, CA 93943-5004	1
4. Naval Engineering Curricular Officer, Code 34 Department of Mechanical Engineering Naval Postgraduate School Monterey, CA 93943-5004	1
5. Professor Paul J. Marto, Code 34/Mx Department of Mechanical Engineering Naval Postgraduate School Monterey, CA 93943-5004	3
6. Professor Steve B. Memory Department of Mechanical Engineering University of Miami P.O. Box 248294 Coral Gables, FL 33124	1
7. Professor David Salinas, Code ME/Sa Department of Mechanical Engineering Naval Postgraduate School Monterey, CA 93943-5004	1
8. Professor John W. Rose Department of Mechanical Engineering (QMW) University of London Miles End Road London, E1 4NS ENGLAND	1
9. Mr. David Brown David W. Taylor Naval Ship Research and Development Center Annapolis, MD 21402	1
10. LCDR Vance H. Adams 924 Priscilla Lane Chesapeake, VA 23320	2